Chapter 7
Intense Laser–Atom Interaction

In this chapter we shall introduce the fundamental effects that occur when intense laser light interacts with isolated atoms, that is, ionization by the laser field, laser-assisted recombination (i.e., harmonic generation), and laser-assisted collisional ionization (nonsequential ionization). The focus of this chapter is on a self-contained but concise account of these most fundamental effects and the common theory behind them. Readers interested in more details on particular subjects (or subjects not covered at all in this chapter) may find the following (incomplete) list of reviews and monographs useful: [1–4] (general), [5] (tunneling ionization), [6] (intense-field S-matrix theory), [7] (few-cycle laser pulses), [8, 9] (above-threshold ionization), [10] (harmonic generation), [11] (stabilization), [12] (multiple ionization), [13–15] (attosecond physics), [16] ("double-slit in time"), [17] (two-electron atoms in laser fields), [18] (Floquet method and beyond), [19, 20] (relativistic laser-atom interaction), [21, 22] (time-dependent density functional theory), [23–25] (molecules in intense laser fields), and [24–27] (laser–cluster interaction).

7.1 Atomic Units

We use atomic units (a.u.) in this chapter, not only because they greatly simplify actual calculations but also give a feeling for whether an entity has to be considered large or small on the atomic scale. For instance, the laser frequency of 800 nm laser light is $\omega = 0.057$ a.u., telling us immediately that the laser period is large compared to the period of an electron on, e.g., the first Bohr orbit in a hydrogen atom.

We will introduce the atomic units in a somewhat formal way. For beginners, the use of atomic units is sometimes confusing because dimensional checks are not possible in a straightforward way once $\hbar$, m_e, e have been set "equal to unity". Another practical problem for beginners is to convert the result of a calculation performed using atomic units back to SI units. If one sticks to SI units and the result of a calculation is, say, 42, one knows that the result is dimensionless. If in atomic units the result is 42 it could be as well $42\,\hbar$, $42\,e$, $42\,m_e$, $42\cdot 4\pi\varepsilon_0$, $42\,\hbar m_e/e$, ... A good example is the expression for the nonrelativistic eigenenergies of hydrogen-like ions, which in atomic units is simply given by

P. Mulser, D. Bauer, *High Power Laser–Matter Interaction*, STMP 238, 267–330,
DOI 10.1007/978-3-540-46065-7_7, © Springer-Verlag Berlin Heidelberg 2010

$$\mathcal{E}_n = -\frac{Z^2}{2n^2}, \qquad n = 0, 1, 2, \ldots \qquad \text{(atomic units)} \tag{7.1}$$

where Z is the nuclear charge, and n is the principal quantum number. The right-hand side appears to be dimensionless. Hence, without knowing that the left-hand side is an energy, there would be no way back to SI units. If one performs the entire calculation (i.e., the solution of the Schrödinger equation) in SI units, one obtains

$$\mathcal{E}_n = -\frac{Z^2}{2n^2}\frac{m_e e^4}{\hbar^2(4\pi\varepsilon_0)^2}, \qquad n = 0, 1, 2, \ldots \qquad \text{(SI units)}. \tag{7.2}$$

Even without knowing the left-hand side we can recover from the right-hand side alone that the result is an energy, provided we know the SI units of $\hbar$, m_e, e, and ε_0. This seeming asymmetry between the unit systems arise from the fact that "setting $\hbar$, m_e, e, and $4\pi\varepsilon_0$ equal to unity" is more than a change of units. It is like setting kg, m, s, and C to unity. However, if one knows what the dimension of the final result is, the conversion from atomic units back to SI units is unique.

As in Sect. 2.2.3, let us denote mass, length, time, and charge by M, L, T, and C, respectively. In atomic units we wish to use the action $\hbar$, the electron mass m_e, the modulus of the electron charge e, and 4π times the permittivity of vacuum, $4\pi\varepsilon_0$, as the basic units. The relation between both system of units is established by ("[...]" meaning "units of ...", see also Sect. 2.2.3)

$$[\hbar] = \mathrm{M}^{a_{11}}\mathrm{L}^{a_{12}}\mathrm{T}^{a_{13}}\mathrm{C}^{a_{14}}, \tag{7.3}$$
$$[m_e] = \mathrm{M}^{a_{21}}\mathrm{L}^{a_{22}}\mathrm{T}^{a_{23}}\mathrm{C}^{a_{24}}, \tag{7.4}$$
$$[e] = \mathrm{M}^{a_{31}}\mathrm{L}^{a_{32}}\mathrm{T}^{a_{33}}\mathrm{C}^{a_{34}}, \tag{7.5}$$
$$[4\pi\varepsilon_0] = \mathrm{M}^{a_{41}}\mathrm{L}^{a_{42}}\mathrm{T}^{a_{43}}\mathrm{C}^{a_{44}}. \tag{7.6}$$

The exponents $a_{41}, \ldots, a_{44}$, for instance, are determined by noticing that in SI units the dimension of ε_0 is Coulomb per Volt and meter. Volt is a derived unit, $\mathrm{V} = \mathrm{ML}^2/(\mathrm{CT}^2)$, and hence

$$[4\pi\varepsilon_0] = \mathrm{M}^{-1}\mathrm{L}^{-3}\mathrm{T}^2\mathrm{C}^2. \tag{7.7}$$

Similarly, the remainder of the dimensional matrix is easily calculated and reads

$$A = \begin{pmatrix} a_{11} & a_{12} & a_{13} & a_{14} \\ a_{21} & a_{22} & a_{23} & a_{24} \\ a_{31} & a_{32} & a_{33} & a_{34} \\ a_{41} & a_{42} & a_{43} & a_{44} \end{pmatrix} = \begin{pmatrix} 1 & 2 & -1 & 0 \\ 1 & 0 & 0 & 0 \\ 0 & 0 & 0 & 1 \\ -1 & -3 & 2 & 2 \end{pmatrix}. \tag{7.8}$$

The SI values of one atomic mass, length, time, and charge unit, denoted by $\mathcal{M}$, $\mathcal{L}$, $\mathcal{T}$, and $\mathcal{C}$, respectively, are needed for the transformation back to SI units. Mass and charge are trivial: $\mathcal{M} = m_e$, $\mathcal{C} = e$. Let us calculate the value of the atomic length unit:

$$\mathcal{L} = \hbar^{b_{21}} m_e^{b_{22}} e^{b_{23}} (4\pi\varepsilon_0)^{b_{24}}. \tag{7.9}$$

Plugging in (7.3), (7.4), (7.5), and (7.6) and using the values for the a_{ij} in (7.8) lead to

$$\mathcal{L} = \mathrm{M}^{b_{21}+b_{22}-b_{24}} \mathrm{L}^{2b_{21}-3b_{24}} \mathrm{T}^{-b_{21}+2b_{24}} \mathrm{C}^{b_{23}+2b_{24}}, \tag{7.10}$$

giving us four equations for the four b_{2j}. Since $\mathcal{L}$ is a length, $2b_{21} - 3b_{24} = 1$, and the exponents of mass, time, and charge must be zero. One finds $b_{21} = 2$, $b_{22} = -1$, $b_{23} = -2$, $b_{24} = 1$ so that

$$\mathcal{L} = \frac{\hbar^2 4\pi\varepsilon_0}{m_e e^2} = 0.5292 \cdot 10^{-10}\mathrm{m}, \tag{7.11}$$

which is the Bohr radius a_0. The corresponding calculation for $\mathcal{T}$ is left as an exercise. The inverse dimensional matrix is

$$\mathcal{M} = \hbar^{b_{11}} m_e^{b_{12}} e^{b_{13}} (4\pi\varepsilon_0)^{b_{14}}, \tag{7.12}$$

$$\mathcal{L} = \hbar^{b_{21}} m_e^{b_{22}} e^{b_{23}} (4\pi\varepsilon_0)^{b_{24}}, \tag{7.13}$$

$$\mathcal{T} = \hbar^{b_{31}} m_e^{b_{32}} e^{b_{33}} (4\pi\varepsilon_0)^{b_{34}}, \tag{7.14}$$

$$\mathcal{C} = \hbar^{b_{41}} m_e^{b_{42}} e^{b_{43}} (4\pi\varepsilon_0)^{b_{44}} \tag{7.15}$$

with

$$B = \begin{pmatrix} b_{11} & b_{12} & b_{13} & b_{14} \\ b_{21} & b_{22} & b_{23} & b_{24} \\ b_{31} & b_{32} & b_{33} & b_{34} \\ b_{41} & b_{42} & b_{43} & b_{44} \end{pmatrix} = \begin{pmatrix} 0 & 1 & 0 & 0 \\ 2 & -1 & -2 & 1 \\ 3 & -1 & -4 & 2 \\ 0 & 0 & 1 & 0 \end{pmatrix}. \tag{7.16}$$

It is readily checked that $A \cdot B = B \cdot A = 1$.

We conclude this section by giving the explicit expressions and values for frequently occurring entities in laser-atom interaction in Table 7.1. In the entry for the velocity the fine structure constant

$$\alpha = \frac{e^2}{\hbar 4\pi\varepsilon_0 c} = \frac{1}{137.04} \tag{7.17}$$

appears. The value of the light velocity in vacuum in atomic units equals the inverse fine structure constant. Note that with $\hbar$, e, m_e, and ε_0 alone it is not possible to construct a dimensionless entity (as it is impossible with kg, m, s, and C). One needs a fifth building brick, which is c in the case of the fine structure constant. A useful and frequently used formula to convert the field strength E in atomic units to a laser intensity I in the commonly used Wcm^{-2} is

$$(I \text{ in } \mathrm{Wcm}^{-2}) = 3.51 \cdot 10^{16} \times (E^2 \text{ in a.u.}). \tag{7.18}$$

Table 7.1 One atomic unit of frequently occurring entities expressed in SI units

One atomic unit of		Value
Mass	m_e	$9.1094 \cdot 10^{-31}$ kg
Length	$\frac{\hbar^2 4\pi\varepsilon_0}{e^2 m_e} = a_0$	$0.5292 \cdot 10^{-10}$ m
Time	$\frac{\hbar^3 (4\pi\varepsilon_0)^2}{m_e e^4}$	$2.4189 \cdot 10^{-17}$ s
Charge	e	$1.6022 \cdot 10^{-19}$ C
Action	$\hbar$	$1.0546 \cdot 10^{-34}$ J
Permittivity	$4\pi\varepsilon_0$	$4\pi \cdot 8.8542 \cdot 10^{-12}\,\mathrm{CV}^{-1}\,\mathrm{m}^{-1}$
Energy	$\frac{m_e e^4}{\hbar^2 (4\pi\varepsilon_0)^2}$	$4.3598 \cdot 10^{-19}\mathrm{J} = 27.21\,\mathrm{eV}$
Velocity	$\frac{e^2}{\hbar 4\pi\varepsilon_0}$	$2.1877 \cdot 10^6\,\mathrm{ms}^{-1} = \alpha c$
El. field	$\frac{m_e^2 e^5}{\hbar^4 (4\pi\varepsilon_0)^3}$	$5.1422 \cdot 10^{11}\,\mathrm{Vm}^{-1}$
Magn. flux density	$\frac{m_e^2 e^3}{\hbar^3 (4\pi\varepsilon_0)^2}$	$2.3505 \cdot 10^5$ T
Laser intensity	$\frac{e^{12} m_e^4}{8\pi\alpha\hbar^9 (4\pi\varepsilon_0)^6}$	$3.5095 \cdot 10^{20}\,\mathrm{Wm}^{-2}$

7.2 Atoms in Strong Static Electric Fields

Although we assume the external electric field to be static in this section, the following analysis is useful for atoms in laser fields too, as will become clear below. The Hamiltonian governing an electron moving in a Coulomb potential $-Z/r$ and a static electric field $\boldsymbol{E} = E\boldsymbol{e}_z$ reads

$$\hat{H} = \frac{\hat{\boldsymbol{p}}^2}{2} + V_{\mathrm{eff}}, \qquad V_{\mathrm{eff}} = -\frac{Z}{r} + Ez. \tag{7.19}$$

The effective potential V_{eff} describes a tilted Coulomb potential (see Fig. 7.1). A perturbative treatment of the problem can be found in almost all quantum mechanics or atomic physics text books (Stark effect, see, e.g., [28–30]). In first order (linear Stark effect) the degeneracy with respect to the angular quantum number ℓ is removed while the degeneracy in the magnetic quantum number m is maintained. The non-degenerate ground state is only affected in second order (quadratic Stark effect). It is down-shifted in energy since the potential widens in the presence of the field. In the case of the hydrogen atom ($Z = 1$) this down-shift is given by $\Delta\mathcal{E} = -9E^2/4$.

Let us first point out that, strictly speaking, there exist no discrete, bound states anymore even for the tiniest electric field. This is because even a very small field gives rise to a potential barrier (see Fig. 7.1) through which the initially bound electron may tunnel. The electric field couples all bound states to the continuum and thus all discrete states become resonances with a finite line width. Mathematically speaking, the Hamiltonian (7.19) has only a continuous spectrum, and the eigenfunctions are no longer square-integrable. However, since the barrier for small fields is far out, the probability for tunneling is extremely low (note that the

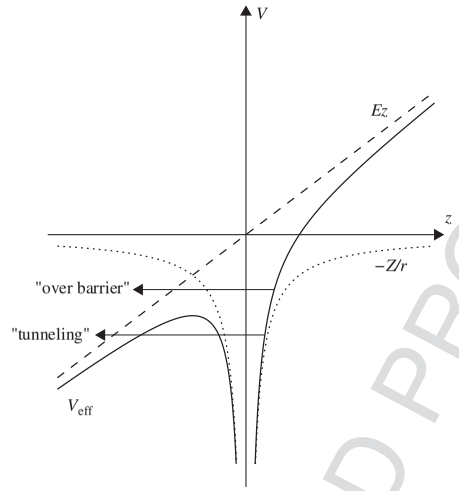

Fig. 7.1 Effective potential V_{eff} in field direction. The unperturbed Coulomb potential and the field potential are also shown separately. Depending on the initial (and possibly Stark-shifted) state, the electron may either escape via tunneling or classically via "over-barrier" ionization

tunneling probability decreases exponentially with the distance to be tunneled, as will be shown in Sect. 7.2.2) and the states are "quasi-discrete".

A strong increase in the ionization probability is expected when the electron can even escape classically, that is, when the distance to be tunneled shrinks to zero. In a crude approximation (which, in fact, is wrong for hydrogen-like ions, as will be discussed in the subsequent section) this so-called "critical field" E_{crit} may be estimated as follows: neglecting the Stark effect, classical over-barrier ionization sets in when the barrier maximum coincides with the energy level of the electron. The position of the barrier is (for $E > 0$) located at

$$z_{\text{barr}} = -\sqrt{\frac{Z}{E}} \tag{7.20}$$

and the energy at the barrier maximum is

$$V_{\text{barr}} = -2\sqrt{ZE}. \tag{7.21}$$

Hence, if we restrict ourselves to the ground state of hydrogen-like ions, we require that

$$\mathcal{E} = -\frac{Z^2}{2} \stackrel{!}{=} -2\sqrt{ZE_{\text{crit}}} \tag{7.22}$$

so that

$$E_{\text{crit}} = \frac{Z^3}{16}. \tag{7.23}$$

Because of the strong Z-dependence of the critical field even with the most intense lasers available today it is not possible to fully strip heavy elements. For hydrogen-like ions (7.23) even underestimates the critical field by more than a factor of two, as will be shown now.

7.2.1 Separation of the Schrödinger Equation

The Schrödinger equation with the Hamiltonian (7.19) separates in parabolic coordinates (ξ, η, φ) (see, e.g., [28–30]),

$$\xi = r+z, \quad \eta = r-z, \qquad r = \frac{1}{2}(\xi+\eta), \quad z = \frac{1}{2}(\xi-\eta), \qquad 0 \le \xi, \eta. \tag{7.24}$$

Here, r is the radial coordinate, and φ is the azimuthal angle (as in spherical, polar or cylindrical coordinates). Cuts of contours of constant ξ and η in the xz-plane are shown in Fig. 7.2. The Hamiltonian in parabolic coordinates reads

$$\hat{H} = -\frac{2}{\xi+\eta}\left[\partial_\xi(\xi\partial_\xi) + \partial_\eta(\eta\partial_\eta)\right] - \frac{1}{2\xi\eta}\partial_\varphi^2 - \frac{2Z}{\xi+\eta} + E\frac{\xi-\eta}{2}. \tag{7.25}$$

Plugging the ansatz

$$\Psi = f_1(\xi) f_2(\eta) \mathrm{e}^{\mathrm{i}m\varphi} \tag{7.26}$$

into the Schrödinger equation $\mathcal{E}\Psi = \hat{H}\Psi$ and multiplying by $(\xi+\eta)/2$ leads to an equation that can be decoupled into

$$\frac{d}{d\xi}\left(\xi\frac{df_1}{d\xi}\right) + \left(\frac{\mathcal{E}}{2}\xi - \frac{m^2}{4\xi} - \frac{E}{4}\xi^2\right) f_1 + Z_1 f_1 = 0, \tag{7.27}$$

$$\frac{d}{d\eta}\left(\eta\frac{df_2}{d\eta}\right) + \left(\frac{\mathcal{E}}{2}\eta - \frac{m^2}{4\eta} + \frac{E}{4}\eta^2\right) f_2 + Z_2 f_2 = 0 \tag{7.28}$$

where Z_1, Z_2 are separation constants fulfilling

$$Z_1 + Z_2 = Z. \tag{7.29}$$

Division by 2ξ and 2η, respectively, yields the two Schrödinger equations

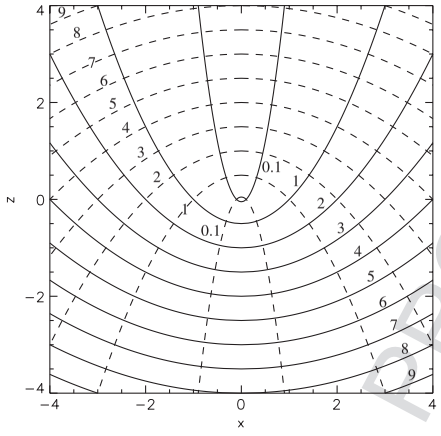

Fig. 7.2 Illustration of parabolic coordinates. Cuts of contours $\xi = \text{const}$ (*dashed*, values given next to the lines) and $\eta = \text{const}$ (*solid*) in the xz-plane (azimuthal symmetry with respect to the z-axis)

$$\left[-\frac{1}{2}\left(\frac{d^2}{d\xi^2}+\frac{1}{\xi}\frac{d}{d\xi}-\frac{m^2}{4\xi^2}\right)-\frac{Z_1}{2\xi}+\frac{E}{8}\xi\right]f_1=\frac{\mathcal{E}}{4}f_1, \tag{7.30}$$

$$\left[-\frac{1}{2}\left(\frac{d^2}{d\eta^2}+\frac{1}{\eta}\frac{d}{d\eta}-\frac{m^2}{4\eta^2}\right)-\frac{Z_2}{2\eta}-\frac{E}{8}\eta\right]f_2=\frac{\mathcal{E}}{4}f_2 \tag{7.31}$$

which have the same shape as two Schrödinger equations in cylindrical coordinates for the potentials

$$V_\xi=-\frac{Z_1}{2\xi}+\frac{E}{8}\xi, \qquad V_\eta=-\frac{Z_2}{2\eta}-\frac{E}{8}\eta. \tag{7.32}$$

Both potentials have a Coulombic part and a linear contribution, like V_{eff} in (7.19). However, because $\xi, \eta \geq 0$, the potential V_ξ has only bound states (we assume without loss of generality $E > 0$). The potential V_η instead displays a barrier. Hence, in parabolic coordinates ionization happens with respect to the η coordinate while the electron remains confined in ξ. The consequences of this in Cartesian coordinates can be understood with the help of Fig. 7.2: confinement to a region $\xi < \xi_{\max}$ implies preferred electron emission towards negative z with a lateral spread that can be estimated by the confining contour $\xi_{\max}$. The potentials V_ξ and V_η are called "uphill" and "downhill potential," respectively. They are illustrated in Fig. 7.3. Given an energy $\mathcal{E}$ one finds a sequence of Z_1 for which the solution of the Schrödinger equation in ξ, (7.30), leads to normalizable bound states. This sequence can be labeled by the number of nodes in f_1 for $\xi > 0$, $n_1 = 0, 1, 2, \ldots$ (note that $Z_1 < 0$ is also possible). The second equation (7.31) has to be solved for

$Z_2 = Z - Z_1$ and the same energy $\mathcal{E}$. This is possible because the corresponding Hamiltonian $\hat{H}_\eta$ [i.e., the square bracket in (7.31)] has a continuous spectrum and is neither bound from below nor from above.

In the field-free case $E = 0$ the two Schrödinger equations (7.30) and (7.31) are identical, and the relation between the "usual" principal quantum number n and the parabolic quantum numbers n_1, n_2 is given by

$$n_i+\frac{|m|+1}{2}=n\frac{Z_i}{Z}, \qquad n_1+n_2+|m|+1=n, \qquad i=1,2. \tag{7.33}$$

Instead of working directly with the parabolic coordinates ξ and η, one can perform an additional, simple coordinate transformation

$$u=\sqrt{2\xi}, \qquad v=\sqrt{2\eta} \tag{7.34}$$

which, after multiplication of the new Schrödinger equation by $(u^2+v^2)/4$, and with the ansatz $\Psi = \Phi_u(u)\Phi_v(v)e^{im\varphi}$ yields

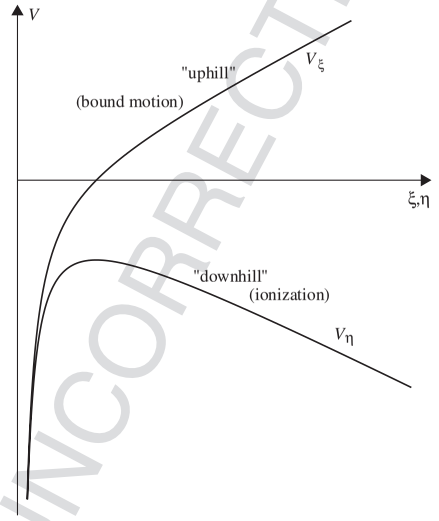

Fig. 7.3 Illustration of the potentials V_ξ and V_η (7.32). The "uphill potential" V_ξ (for $E > 0$) supports only bound states while the "downhill potential" V_η displays a barrier through which the electron may tunnel

$$\left[-\frac{1}{2}\left(\frac{1}{u}\partial_u(u\partial_u)-\frac{m^2}{u^2}\right)+\frac{1}{2}\Omega^2u^2-\frac{1}{4}gu^4\right]\Phi_u=Z_1\Phi_u, \tag{7.35}$$

$$\left[-\frac{1}{2}\left(\frac{1}{v}\partial_v(v\partial_v)-\frac{m^2}{v^2}\right)+\frac{1}{2}\Omega^2v^2+\frac{1}{4}gv^4\right]\Phi_v=Z_2\Phi_v, \tag{7.36}$$

where, again, $Z=Z_1+Z_2$ is used, and Ω and g are defined as

$$\frac{1}{2}\Omega^2=-\frac{\mathcal{E}}{4},\quad \mathcal{E}\le 0,\qquad g=-\frac{E}{4}. \tag{7.37}$$

The Schrödinger equations (7.35) and (7.36) have the shape of two-dimensional oscillators (with radial coordinates u and v, respectively) of frequency Ω and with a quartic perturbation that is proportional to the electric field. In the field-free case, the Coulomb problem is mapped to two two-dimensional oscillators where, however, the energy assumes the role of the oscillator frequency, and the nuclear charge (splitted into Z_1 and Z_2) assumes the role of the energy. The transformation to the coordinates (u,v,φ) corresponds to the Kustaanheimo–Stiefel transformation [31].

Let us now evaluate an improved critical field for the case of hydrogen-like ions [32]. As mentioned above, formula (7.23) underestimates the critical field by more than a factor of two.

In the unperturbed case ($g=0$) and for $m=0$ (groundstate) the solutions to (7.35) and (7.36) are Gaussians. We therefore use

$$\Phi_u(u)=\sqrt{\frac{a_u}{\pi}}\,\mathrm{e}^{-a_uu^2/2} \tag{7.38}$$

(and analogous for v) as trial functions with parameters a_u and a_v. Denoting the square bracket in (7.35) as $\hat{H}_u$ the "energy" reads

$$Z_1(g)=2\pi\int_0^\infty du\,u\Phi_u^*\hat{H}_u\Phi_u=\frac{1}{a_u}\left(\frac{\Omega^2}{2}-\frac{a_u^2}{2}\right)+a_u-\frac{g}{2a_u^2}. \tag{7.39}$$

Minimizing this energy yields up to first order in g

$$a_u=\Omega\left(1-\frac{g}{\Omega^3}\right),\qquad a_v=\Omega\left(1+\frac{g}{\Omega^3}\right). \tag{7.40}$$

The oscillator "energies" are

$$Z_1(g)=\Omega\left(1-\frac{g}{2\Omega^3}\right),\qquad Z_2(g)=\Omega\left(1+\frac{g}{2\Omega^3}\right). \tag{7.41}$$

Note that this is consistent with the fact that the linear Stark effect vanishes for the ground state since

$$Z_1(g)+Z_2(g)=2\Omega \tag{7.42}$$

is independent of the field g. Since $Z_1+Z_2=Z$ we have $Z=2\Omega$ which is [see (7.37)] equivalent to $\mathcal{E}=-Z^2/2$, as it should for the ground states of hydrogen-like ions.

In physical coordinates the variationally determined wave function for, e.g., hydrogen ($Z=1$) reads

$$\Psi_{\mathrm{H}}(\boldsymbol{r})=\frac{1-4E^2}{\sqrt{\pi}}\,\mathrm{e}^{-r}\,\mathrm{e}^{-2\boldsymbol{E}\cdot\boldsymbol{r}}, \tag{7.43}$$

i.e., the unperturbed wave function is multiplied by a "deformation factor".

If $E>0$ we have $g<0$ and vice versa. Let us assume $g>0$ so that the u-oscillator displays a barrier while the v-oscillator does not. The barrier is located at $u_{\mathrm{barr}}=\Omega/\sqrt{g}$ and the energy at the barrier maximum is $\Omega^2u_{\mathrm{barr}}^2/2-gu_{\mathrm{barr}}^4/4=\Omega^4/(4g)$. At the critical field strength the energy of the u-state coincides with the barrier-energy, giving us

$$Z_1(g)=\Omega-\frac{g}{2\Omega^2}=\frac{\Omega^4}{4g}\qquad\Rightarrow\qquad g_{\mathrm{crit}}=\Omega^3(1-2^{-1/2})\simeq 0.3\,\Omega^3 \tag{7.44}$$

which translates [using (7.37)] to [32]

$$E_{\mathrm{crit}}^{\mathrm{H-like}}=(\sqrt{2}-1)\,\mathcal{E}^{3/2}. \tag{7.45}$$

In the case of atomic hydrogen one obtains $E_{\mathrm{crit}}^{\mathrm{H-like}}=0.147$ instead of the 0.0625 predicted by (7.23). The new value is in agreement with [33]. The wrong prediction of (7.23) is due to the erroneous assumption that the electron motion in z-direction and in lateral direction are independent. Instead, the problem separates in parabolic coordinates. However, since the "exceptional" symmetry of hydrogen-like ions is broken in many-electron atoms, simple over-barrier estimates [such as those above leading to (7.23)] are useful and sufficiently accurate for many practical applications. Of particular interest is the "appearance intensity" $I_{\mathrm{app},Z}$ for a charge state Z of an atom with ionization potential $\mathcal{E}_{\mathrm{ip},Z}$. Here, "appearance intensity" should be understood as the intensity where a certain charge state Z is becoming abundant. This is the case once the electron may escape classically from the binding potential. The derivation is thus analogous to (7.20), (7.21), (7.22), and (7.23), leading to

$$I_{\mathrm{app},Z}=\frac{\mathcal{E}_{\mathrm{ip},Z}^4}{16Z^2}. \tag{7.46}$$

Comparison of the appearance intensities predicted by (7.46) for the experiments reported in, e.g., [34, 35] yields good agreement, and the scaling is confirmed by a Thomas–Fermi treatment [36].

7.2.2 Tunneling Ionization

Going one step beyond a classical over-barrier analysis amounts to take tunneling into account. This can be done in a semi-classical way. Let us consider the tunneling of the electron in atomic hydrogen through the barrier of the "downhill potential" in Fig. 7.3 [28]. We assume that the electron is initially in the 1s ground state. The Schrödinger equation (7.31) for $m = 0$, $Z_2 = 1/2$, $\mathcal{E} = -1/2$ reads

$$\left[-\frac{1}{2}\left(\frac{d^2}{d\eta^2} + \frac{1}{\eta}\frac{d}{d\eta}\right) - \frac{1}{4\eta} - \frac{E}{8}\eta\right] f_2(\eta) = -\frac{1}{8} f_2(\eta). \tag{7.47}$$

Substituting $\chi(\eta) = \sqrt{\eta} f_2(\eta)$ yields

$$\frac{d^2\chi}{d\eta^2} + \left(-\frac{1}{4} + \frac{1}{2\eta} + \frac{1}{4\eta^2} + \frac{1}{4}E\eta\right)\chi = 0. \tag{7.48}$$

Comparison with

$$-\frac{1}{2}\frac{d^2\chi}{d\eta^2} + V(\eta)\chi = \epsilon\chi \tag{7.49}$$

shows that we effectively deal with one-dimensional motion of an electron in the potential

$$V(\eta) = -\frac{1}{2}\left(\frac{1}{2\eta} + \frac{1}{4\eta^2} + \frac{1}{4}E\eta\right) \tag{7.50}$$

with total energy $\epsilon = -1/8$. The potential $V(\eta)$ is of the form depicted in Fig. 7.4. We now match at a position η_0 inside the barrier,

$$1 \ll \eta_0 \ll 1/E \tag{7.51}$$

the "left" quasi-classical wave function

$$\chi_{\text{left}}(\eta) = -\frac{\mathrm{i}C}{\sqrt{|p|}} \exp\left(\left|\int_{\eta_0}^{\eta} p(\eta')\,d\eta'\right|\right) \tag{7.52}$$

with the "right" quasi-classical outgoing wave function

$$\chi_{\text{right}}(\eta) = \frac{C}{\sqrt{p}} \exp\left(\mathrm{i}\int_{\eta_0}^{\eta} p(\eta')\,d\eta' + \mathrm{i}\pi/4\right) \tag{7.53}$$

where

$$p(\eta) = \sqrt{2[\epsilon - V(\eta)]} = \sqrt{-\frac{1}{4} + \frac{1}{2\eta} + \frac{1}{4\eta^2} + \frac{1}{4}E\eta}. \tag{7.54}$$

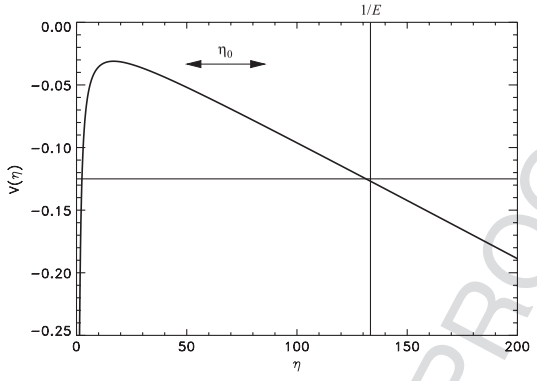

Fig. 7.4 Plot of the potential $V(\eta)$ (7.50) for $E = 0.0075$. The tunnel "exit" η_1 for sufficiently low fields E is in good approximation given by $\eta_1 \simeq 1/E$. The matching point η_0 is located inside the barrier where $1 \ll \eta_0 \ll 1/E$ holds

The semi-classical approximation breaks down at the classical turning point $\eta_1 \simeq 1/E$ since $p(\eta_1) = 0$. In general, semi-classical wave functions are accurate as long as the de Broglie wave length $2\pi\hbar/p$ is small compared to the length scale characterizing changes in the potential (i.e., the potential should be sufficiently "flat"). For vanishing momentum p the de Broglie wave length is infinite so that the semi-classical approximation necessarily breaks down. However, for the calculation of the probability flux out of the potential the disagreement between the semi-classical wave function and the exact wave function in a narrow region around the classical turning point η_1 plays no role.

For the determination of the normalization constant C we set the left wave function at position η_0 equal to the unperturbed wave function so that

$$-\frac{\mathrm{i}C}{\sqrt{|p_0|}} = \sqrt{\eta_0}\frac{1}{\sqrt{\pi}}\mathrm{e}^{-(\xi+\eta_0)/2} \tag{7.55}$$

with $p_0 = p(\eta_0)$. The "uphill" coordinate ξ appears as a parameter here which will be integrated out later on; in other words: the wave function is assumed to retain its ground state shape with respect to ξ (i.e., the Stark effect is neglected). We obtain for the right wave function

$$\chi_{\text{right}}(\eta, \xi) = \mathrm{i}\sqrt{\frac{\eta_0|p_0|}{\pi p(\eta)}}\mathrm{e}^{-(\xi+\eta_0)/2} \exp\left(\mathrm{i}\int_{\eta_0}^{\eta} p(\eta')\,d\eta' + \mathrm{i}\pi/4\right) \tag{7.56}$$

so that

$$|\chi_{\text{right}}(\eta, \xi)|^2 = \frac{\eta_0|p_0|}{\pi p(\eta)} \exp\left(-\xi - \eta_0 + 2\Re\left[\mathrm{i}\int_{\eta_0}^{\eta} p(\eta')\,d\eta'\right]\right) \tag{7.57}$$

where $\Re$ denotes the real part. Because of (7.51) we can expand $p(\eta)$ in $\varepsilon = 1/\eta$,

$$p(\eta) = \begin{cases} \frac{1}{2}\left(\sqrt{E\eta - 1} + \frac{1}{\eta\sqrt{E\eta - 1}} + \cdots\right) & \text{outside barrier, } \eta > \eta_1 \\ \frac{1}{2}\left(\mathrm{i}\sqrt{1 - E\eta} + \frac{1}{\mathrm{i}\eta\sqrt{1 - E\eta}} + \cdots\right) & \text{inside barrier, } \eta < \eta_1 \end{cases} . \quad (7.58)$$

Since $E\eta_0 \ll 1$, it is sufficient to take $|p_0| = 1/2$. In order to keep the leading terms dependent on E in the prefactor as well as in the exponent, we set in the denominator of the prefactor in (7.57) $p(\eta) = (\sqrt{E\eta - 1})/2$. In the exponent we integrate inside the barrier and have to keep both terms in the expansion (7.58). We thus obtain

$$|\chi_{\text{right}}(\eta, \xi)|^2 = \frac{\eta_0}{\pi\sqrt{E\eta - 1}} \mathrm{e}^{-(\xi + \eta_0)} \times \exp\left(-\int_{\eta_0}^{\eta_1} \left[\sqrt{E\eta - 1} - \frac{1}{\eta\sqrt{E\eta - 1}}\right] d\eta\right). \quad (7.59)$$

The integral can be solved. Using $\eta_1 \simeq 1/E$ and $\eta_0 E \ll 1$ we obtain for the probability density outside the barrier

$$|\chi_{\text{right}}(\eta, \xi)|^2 = \frac{4\,\mathrm{e}^{-\xi}}{\pi E\sqrt{E\eta - 1}} \mathrm{e}^{-2/(3E)}. \quad (7.60)$$

The total probability current through a plane perpendicular to the z-axis is

$$\Gamma = \int_0^\infty |f_1(\xi) f_2(\eta)|^2 v_z 2\pi\rho\, d\rho \quad (7.61)$$

where $f_1(\xi)$, $f_2(\eta)$ are the wave functions introduced in (7.26), v_z is the velocity in z-direction and ρ is the radial cylindrical coordinate. The ξ-dependent part $|f_1|^2$ is included in $|\chi_{\text{right}}(\eta, \xi)|^2$ so that

$$\Gamma = \int_0^\infty \frac{|\chi_{\text{right}}(\eta, \xi)|^2}{\eta} v_z 2\pi\rho\, d\rho. \quad (7.62)$$

With $z = (\xi - \eta)/2 \simeq -\eta/2$ for small ξ and large η, we estimate for v_z

$$-\frac{1}{2} = \frac{1}{2}v_z^2 + Ez \simeq \frac{1}{2}v_z^2 - \frac{1}{2}E\eta \qquad \Rightarrow \qquad v_z \simeq \sqrt{E\eta - 1} \quad (7.63)$$

so that

$$\Gamma = \int_0^\infty \frac{|\chi_{\text{right}}(\eta, \xi)|^2}{\eta} \sqrt{E\eta - 1}\, 2\pi\rho\, d\rho. \quad (7.64)$$

Finally, with

$$\rho = \sqrt{\xi\eta} \qquad \Rightarrow \qquad d\rho = d\sqrt{\xi\eta} = \frac{1}{2}\frac{\eta}{\sqrt{\xi\eta}}d\xi + \frac{1}{2}\frac{\xi}{\sqrt{\xi\eta}}d\eta \simeq \frac{1}{2}\sqrt{\frac{\eta}{\xi}}\,d\xi \quad (7.65)$$

(where the last step again follows from $\eta \gg \xi$) we arrive at

$$\Gamma = \int_0^\infty \frac{|\chi_{\text{right}}(\eta, \xi)|^2}{\eta} \sqrt{E\eta - 1}\, 2\pi\sqrt{\xi\eta}\frac{1}{2}\sqrt{\frac{\eta}{\xi}}\,d\xi = \int_0^\infty \frac{4}{E}\,\mathrm{e}^{-2/(3E)}\,\mathrm{e}^{-\xi}\,d\xi$$

so that

$$\Gamma = \frac{4}{E}\,\mathrm{e}^{-2/(3E)}. \quad (7.66)$$

This is the Landau-rate for tunneling ionization of atomic hydrogen from the ground state [28]. The Landau-rate is exact in the limit of low field strengths E while it overestimates ionization as the over-barrier field strength is approached. Figure 7.5 shows the rate Γ vs the field strength E.

It is desirable to extend the above calculation to laser fields, to more complex atoms, and to higher field strengths. All directions have been pursued, and there exists a vast amount of literature on tunneling ionization (see [5] for a review). Undeservedly, the most commonly cited tunneling formula is the so-called "ADK-rate" [37] while full credit should go to the authors of [38–41] instead (see also Sect. 13.13 in [5]). Introducing the characteristic momentum κ, the reduced field strength F, the effective principal quantum number n^*, and the Keldysh parameter γ [42] (derived below in Sect. 7.3),

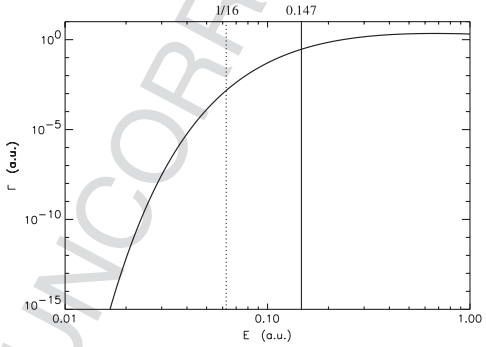

Fig. 7.5 The Landau-rate (7.66) vs field strength E. The vertical lines indicate the (here wrong) over-barrier field strength (7.23) (1/16, dashed) and the correct (7.45) 0.147 (*solid*), respectively

$$\kappa = \sqrt{2\mathcal{E}_{\rm ip}}, \qquad F = E/\kappa^3, \qquad n^* = Z/\kappa, \qquad \gamma = \frac{\kappa\omega}{E}, \tag{7.67}$$

with ω the laser frequency, the so-called "PPT-rate" [39] for initial states of vanishing angular momentum ℓ and for a linearly polarized laser field reads

$$\Gamma = \kappa^2 C_\kappa^2 \sqrt{\frac{3F}{\pi}} 2^{2n^*} F^{1-2n^*} \exp\left[-\frac{2}{3F}\left(1-\frac{\gamma^2}{10}\right)\right], \tag{7.68}$$

where

$$C_\kappa^2 = \frac{2^{2n^*-2}}{n^*(n^*)!(n^*-1)!}. \tag{7.69}$$

The factor $\sqrt{3F/\pi}$ arises from the averaging over one laser cycle. This factor is absent for circular polarization, for which also the correction term $\gamma^2/10$ should be replaced by $\gamma^2/15$. A rate formula for $\ell > 0$ has also been derived (see the review [5] or the original articles [38–41]). However, since ℓ and m are no "good quantum numbers" for many-electron atoms or ions, the question arises which values to take in actual calculations and whether in multiple ionization the electrons have time to configure in the "new" ionic ground state before the next ionization event occurs [35, 43].

7.3 Atoms in Strong Laser Fields

There are at least three different energy scales (and the related time scales) in the physics of atoms in strong laser fields: (i) the ionization potential $\mathcal{E}_{\rm ip} = |\mathcal{E}|$, (ii) the photon energy ω, and (iii) the ponderomotive energy $U_{\rm p}$. The pulse duration may introduce an additional laser-related time-scale while the energy spectrum of the atom, through typical transitions, could introduce an additional species-related time-scale. If one ignores the two latter parameters, the atomic species enter through $\mathcal{E}_{\rm ip}$ only.

In case $\omega > \mathcal{E}_{\rm ip} \gg U_{\rm p}$ or $\mathcal{E}_{\rm ip} > \omega \gg U_{\rm p}$ perturbation theory in lowest non-vanishing order (LOPT) can be applied. In contrast, when with the increasing laser intensity the regime $\mathcal{E}_{\rm ip} > U_{\rm p} > \omega$ is reached, non-perturbative effects such as above-threshold ionization (ATI) and channel-closings take place. This regime is commonly referred to as (nonperturbative) multiphoton ionization (MPI). Finally, increasing the intensity further (or decreasing the photon energy) one arrives at $U_{\rm p} > \mathcal{E}_{\rm ip} > \omega$. Translated into the time-domain this implies that both the inner-atomic time-scale and the ionization dynamics are fast with respect to a laser period. If this is the case, a quasi static field ionization picture may be applied where, at the instant of ionization t', the electron moves in an effective potential which is the sum of the Coulomb (or effective core) potential and the instantaneous potential of the laser, as depicted in Fig. 7.1. If the field reaches the critical field estimated above, the

electron may escape classically over the barrier [over-barrier or barrier suppression ionization (OBI) and (BSI), respectively], as already discussed in Sect. 7.2.1. Below the critical field strength the electron can escape via tunneling through the barrier (tunneling ionization, cf. Sect. 7.2.2).

The Keldysh parameter γ [42] introduced in (7.67) above can be interpreted as the ratio of the "tunneling time" and the laser period. In semi-classical WKB theory the time to tunnel through a static Coulomb barrier is

$$T_{\rm tunnel} \simeq \int_0^{z_{\rm exit}} \frac{dz}{|p(z)|} = \int_0^{\kappa^2/2E} \frac{dz}{\sqrt{\kappa^2 - 2Ez}} = \frac{\kappa}{E} \tag{7.70}$$

so that

$$\gamma = \omega T_{\rm tunnel} = \frac{\omega\kappa}{E} = \sqrt{\frac{\mathcal{E}_{\rm ip}}{2U_{\rm p}}}. \tag{7.71}$$

Hence, the Keldysh parameter indicates whether the tunneling process is fast on the inneratomic time scale ($\gamma < 1$, tunneling ionization) or the laser field reverses sign before the tunneling is completed ($\gamma > 1$, MPI). Besides $\gamma < 1$ also $\mathcal{E}_{\rm ip}/\omega \gg 1$ must be satisfied (i.e., very many photons are involved in the tunneling process) to render the semi-classical tunneling approach applicable. Moreover, for higher and higher field amplitude (and thus decreasing γ) one sooner or later enters the BSI regime. Extrapolating tunneling rate formulas to the BSI usually overestimates the ionization rate. By increasing the field strength or decreasing the laser frequency one also approaches the relativistic regime where $U_{\rm p} \simeq mc^2$ or greater. However, just because the laser driven *free* electron dynamics is relativistic does not mean that relativistic corrections are already important for the *tunneling* dynamics. Relativistic and QED corrections to the binding energy $\mathcal{E}$ because of a high nuclear charge Z have to be taken into account, of course.

Numerous strong laser-atom experiments operate around $\gamma \simeq 1$ or at $\gamma > 1$ and are thus not in the tunneling domain. Taking, for instance, the case of atomic hydrogen in an 800 nm and 10^{14} W/cm^2 laser pulse one finds $\gamma \simeq 1.1$. This is a typical value for ATI measurements.

What are the differences between the ionization dynamics in the MPI and in the tunneling domain? Since in the tunneling regime the process is fast compared to a laser period, significant ionization occurs during a single half laser cycle, predominantly around the electric field maximum because the barrier is lowest then. Furthermore, in tunneling ionization the quiver amplitude E/ω^2 of the freed electron in the laser field is large compared to the atomic dimension, unlike in MPI. This has consequences for the rescattering dynamics that is responsible for various effects, such as the ATI plateau, high-harmonic generation, and nonsequential ionization, as will be discussed below.

7.3.1 Floquet Theory and Dressed States

If the laser pulse duration is long, i.e., if the pulse contains many laser cycles, we may in good approximation consider it infinitely long. As a consequence the Hamiltonian is periodic,

$$\hat{H}(t+T) = \hat{H}(t), \qquad T = \frac{2\pi}{\omega}, \tag{7.72}$$

and the time-dependent Schrödinger equation (TDSE) is a partial differential equation with periodic coefficients. This type of problem has been studied by Floquet more than 120 years ago [44]. The Floquet theorem ensures that the TDSE

$$\hat{\mathcal{H}}(t)|\Psi(t)\rangle = 0, \qquad \hat{\mathcal{H}}(t) = \hat{H}(t) - \mathrm{i}\frac{d}{dt} \tag{7.73}$$

has solutions of the form

$$|\Psi(t)\rangle = \mathrm{e}^{-\mathrm{i}\epsilon t}|\Phi(t)\rangle, \qquad |\Phi(t+T)\rangle = |\Phi(t)\rangle, \tag{7.74}$$

i.e., the wave function $|\Phi(t)\rangle$ is periodic (while $|\Psi(t)\rangle$ itself is not). The Bloch theorem used in solid state physics to treat particle motion in periodic potentials is the Floquet theorem applied to spatially periodic systems. Inserting (7.74) into (7.73) leads to the eigenvalue equation

$$\hat{\mathcal{H}}(t)|\Phi(t)\rangle = \epsilon|\Phi(t)\rangle. \tag{7.75}$$

ϵ is called quasi-energy or Floquet-energy. Note that if ϵ and $|\Phi(t)\rangle$ solve (7.75), then also

$$\epsilon' = \epsilon + m\omega, \qquad |\Phi(t)\rangle' = \mathrm{e}^{\mathrm{i}m\omega t}|\Phi(t)\rangle, \quad m \in \mathbb{Z} \tag{7.76}$$

do. Let $|\alpha\rangle$ be the solution of the unperturbed problem, i.e., $\hat{H}(t) = \hat{H}_0 + \hat{W}(t)$ and

$$\hat{H}_0|\alpha\rangle = \mathcal{E}^0_\alpha|\alpha\rangle. \tag{7.77}$$

Because of the periodicity of $|\Phi(t)\rangle$ we can Fourier-expand

$$|\Psi(t)\rangle = \mathrm{e}^{-\mathrm{i}\epsilon t}|\Phi(t)\rangle = \mathrm{e}^{-\mathrm{i}\epsilon t}\sum_{n=-\infty}^{\infty}\sum_{\alpha}\Phi^{(n)}_\alpha|\alpha\rangle\mathrm{e}^{-\mathrm{i}n\omega t} \tag{7.78}$$

where the expansion coefficients $\Phi^{(n)}_\alpha$ are time-independent. Inserting (7.78) into (7.73) gives

$$\sum_{n\alpha}[\hat{H}(t) - \epsilon - n\omega]\Phi^{(n)}_\alpha|\alpha\rangle\mathrm{e}^{-\mathrm{i}n\omega t} = 0. \tag{7.79}$$

Multiplying from the left with $\langle\beta|$, $\mathrm{e}^{\mathrm{i}m\omega t}$, and integrating $T^{-1}\int_0^T dt$ yields

$$\sum_{n\alpha}[\langle\beta|\hat{H}^{(m-n)}|\alpha\rangle - (\epsilon + m\omega)\delta_{nm}\delta_{\alpha\beta}]\Phi^{(n)}_\alpha = 0 \tag{7.80}$$

with the time-independent Hamiltonian

$$\hat{H}^{(m-n)} = \frac{1}{T}\int_0^T \hat{H}(t)\,\mathrm{e}^{\mathrm{i}(m-n)\omega t}\,dt. \tag{7.81}$$

Introducing the Floquet state

$$|\alpha n\rangle = |\alpha\rangle\otimes|n\rangle, \qquad \langle t|n\rangle = \mathrm{e}^{\mathrm{i}n\omega t} \tag{7.82}$$

we can recast (7.80) into

$$\sum_{n\alpha}[\langle\beta m|\hat{H}_\mathrm{F}|\alpha n\rangle - \epsilon\langle\beta m|\alpha n\rangle]\Phi^{(n)}_\alpha = 0 \tag{7.83}$$

where $\hat{H}_\mathrm{F}$ is the Floquet-Hamiltonian whose matrix elements read

$$\langle\beta m|\hat{H}_\mathrm{F}|\alpha n\rangle = \langle\beta|\hat{H}^{(m-n)}|\alpha\rangle - m\omega\delta_{mn}\delta_{\alpha\beta}. \tag{7.84}$$

Hence, we obtain the eigenvalue equation

$$\sum_{n\alpha}\langle\beta m|\hat{H}_\mathrm{F}|\alpha n\rangle\Phi^{(n)}_\alpha = \epsilon\Phi^{(m)}_\beta \tag{7.85}$$

or, in matrix notation,

$$\mathsf{H}_\mathrm{F}\boldsymbol{\Phi} = \epsilon\boldsymbol{\Phi}. \tag{7.86}$$

Here, H_F and $\boldsymbol{\Phi}$ are an infinite matrix and an infinite vector, respectively. In practice, the size of the system has to be truncated, of course. Numerical solutions of the time-dependent Schrödinger equation following the Floquet approach have been pursued by several groups (see, e.g., [3, 18] for reviews and [45] for a Floquet-solver). The Floquet method is not applicable to atoms interacting with few-cycle laser pulses because the assumption $\hat{W}(t+T) \simeq \hat{W}(t)$ is not valid in this case.

We illustrate the Floquet approach by applying it to a laser-driven two-level system where the Hamiltonian in dipole approximation reads

$$\hat{H}(t) = \underbrace{\omega_a|a\rangle\langle a| + \omega_b|b\rangle\langle b|}_{\hat{H}_0} - \underbrace{q\hat{E}z\cos\omega t}_{-\hat{W}(t)}, \qquad \omega_a > \omega_b. \tag{7.87}$$

We thus have

$$\hat{H}^{(n)} = \frac{1}{T}\int_0^T dt\, \hat{H}(t)\, \mathrm{e}^{\mathrm{i}n\omega t} = \hat{H}_0\delta_{n0} - \frac{q\hat{E}z}{2}(\delta_{n,-1} + \delta_{n1}), \tag{7.88}$$

i.e., a tridiagonal Hamiltonian in the "photon subspace". For (7.84) we obtain

$$\langle\beta m|\hat{H}_\mathrm{F}|\alpha n\rangle = \left(\langle\beta|\hat{H}_0|\alpha\rangle - m\omega\delta_{\alpha\beta}\right)\delta_{nm} - \frac{1}{2}q\hat{E}\langle\beta|z|\alpha\rangle(\delta_{m,n-1} + \delta_{m,n+1}) \tag{7.89}$$

so that (using $\langle\beta|\hat{H}_0|\alpha\rangle = \omega_\alpha\delta_{\alpha\beta}$) (7.85) reads

$$\sum_{n,\alpha}\left[(\omega_\alpha - m\omega)\delta_{\alpha\beta}\delta_{mn} - \frac{q\hat{E}}{2}\langle\beta|z|\alpha\rangle(\delta_{m,n-1} + \delta_{m,n+1})\right]\Phi_\alpha^{(n)} = \epsilon\Phi_\beta^{(m)}.$$

Defining

$$A = -\frac{1}{2}q\hat{E}\langle a|z|b\rangle = -\frac{1}{2}\Omega_\mathrm{R}\mathrm{e}^{-\mathrm{i}\varphi}, \qquad \mathcal{E}_\alpha^{(m)} = \omega_\alpha - m\omega, \tag{7.90}$$

where Ω_R is the Rabi-frequency, the corresponding matrix equation has the structure

$$\left(\begin{array}{cc|cc|cc} \mathcal{E}_a^{(-1)} & & & A & & \\ & \mathcal{E}_b^{(-1)} & A^* & & & \\ \hline & A & \mathcal{E}_a^{(0)} & & & A \\ A^* & & & \mathcal{E}_b^{(0)} & A^* & \\ \hline & & & A & \mathcal{E}_a^{(1)} & \\ & & A^* & & & \mathcal{E}_b^{(1)} \end{array}\right)\left(\begin{array}{c} \Phi_a^{(-1)} \\ \Phi_b^{(-1)} \\ \hline \Phi_a^{(0)} \\ \Phi_b^{(0)} \\ \hline \Phi_a^{(1)} \\ \Phi_b^{(1)} \end{array}\right) = \epsilon\left(\begin{array}{c} \Phi_a^{(-1)} \\ \Phi_b^{(-1)} \\ \hline \Phi_a^{(0)} \\ \Phi_b^{(0)} \\ \hline \Phi_a^{(1)} \\ \Phi_b^{(1)} \end{array}\right) \tag{7.91}$$

around $m = 0$. We now restrict ourselves to "energy-conserving" transitions between Floquet states $|\alpha n\rangle$ and $|\beta m\rangle$ where $\mathcal{E}_\alpha^{(n)} = \mathcal{E}_\beta^{(m)}$ holds. This is equivalent to the application of the rotating wave approximation (RWA) (see any volume on quantum optics, e.g., [46]). Hence, $\mathcal{E}_a^{(n)} = \omega_a - n\omega \stackrel{!}{=} \omega_b - m\omega = \mathcal{E}_b^{(m)}$ so that

$$\mathcal{E}_a^{(n)} - \mathcal{E}_b^{(m)} = \Delta = \underbrace{\omega_a - \omega_b}_{\omega_{ab}} - \underbrace{(n-m)}_{\stackrel{!}{=}1}\omega$$

where Δ is the detuning, and we are only interested in one-photon transitions between $|a\rangle$ and $|b\rangle$ (so that $n - m = 1$). Equation (7.91) now reduces to the 2×2 equation

$$\begin{pmatrix} \mathcal{E}_b^{(n-1)} & A^* \\ A & \mathcal{E}_a^{(n)} \end{pmatrix}\begin{pmatrix} \Phi_b^{(n-1)} \\ \Phi_a^{(n)} \end{pmatrix} = \epsilon\begin{pmatrix} \Phi_b^{(n-1)} \\ \Phi_a^{(n)} \end{pmatrix}. \tag{7.92}$$

The eigenvalues are

$$\epsilon_{1,2}^{(n)} = \frac{1}{2}(\omega_a + \omega_b) + \omega\left(\frac{1}{2} - n\right) \pm \frac{1}{2}\sqrt{\Omega_\mathrm{R}^2 + \Delta^2}. \tag{7.93}$$

The first term is the energy half way between $|b\rangle$ and $|a\rangle$, the second term is the energy of the "photon field", and the third term gives rise to two levels, separated by the frequency $\Omega = \sqrt{\Omega_\mathrm{R}^2 + \Delta^2}$. Figure 7.6 illustrates the situation for vanishing detuning $\Delta = 0$. The energy levels (7.93) are called field-dressed states.

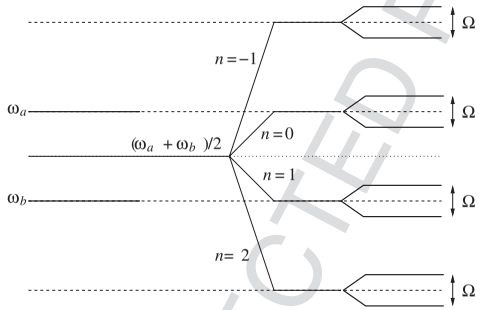

Fig. 7.6 Illustration of (7.93) for $\Delta = 0$. The coupling of the two unperturbed levels b and a to the laser field gives rise to an infinite manifold of pairs of field-dressed levels (labelled by n). Because of (7.76) all the different ns are equivalent. The field-dressed levels are separated by the energy $\Omega = \sqrt{\Omega_\mathrm{R}^2 + \Delta^2}$ (which equals Ω_R for the vanishing detuning considered here)

Let us finally calculate the field-dressed states for our two-state problem in RWA and vanishing detuning. Because of (7.76) we are free to choose, say, $n = 1$. We also can, without loss of generality, set $\omega_b = 0$. Vanishing detuning $\Delta = 0$ then implies $\omega_a = \omega$. Moreover we assume A to be real. Then

$$\epsilon_{1,2} = \pm\frac{1}{2}\Omega_\mathrm{R}, \tag{7.94}$$

and the eigenvalue problem reduces to

$$\begin{pmatrix} 0 & A \\ A & 0 \end{pmatrix}\begin{pmatrix} \Phi_b^{(0)} \\ \Phi_a^{(1)} \end{pmatrix} = \epsilon_{1,2}\begin{pmatrix} \Phi_b^{(0)} \\ \Phi_a^{(1)} \end{pmatrix}. \tag{7.95}$$

The matrix

$$\mathsf{M} = \frac{1}{\sqrt{2}} \begin{pmatrix} -1 & 1 \\ 1 & 1 \end{pmatrix} = \mathsf{M}^{-1} \tag{7.96}$$

diagonalizes (7.95). The two eigenvectors correspond to the field-dressed or Floquet states

$$|\Psi^+\rangle = \frac{1}{\sqrt{2}} \left(|a\rangle + |b\rangle\right), \qquad |\Psi^-\rangle = \frac{1}{\sqrt{2}} \left(|a\rangle - |b\rangle\right). \tag{7.97}$$

If the system is, e.g., at time $t = 0$ in state $|a\rangle$, we have to choose a *superposition* of field-dressed states to fulfill the initial conditions:

$$|\Psi(t)\rangle = \frac{1}{\sqrt{2}}(|\Psi^+(t)\rangle + |\Psi^-(t)\rangle). \tag{7.98}$$

Here, according (7.78)

$$|\Psi^+(t)\rangle = \mathrm{e}^{-\mathrm{i}\epsilon_1 t} \left[\mathrm{e}^{-\mathrm{i}\omega t}|a\rangle + |b\rangle\right], \tag{7.99}$$

$$|\Psi^-(t)\rangle = \mathrm{e}^{-\mathrm{i}\epsilon_2 t} \left[\mathrm{e}^{-\mathrm{i}\omega t}|a\rangle - |b\rangle\right]. \tag{7.100}$$

Calculating the populations $|a(t)|^2 = |\langle a|\Psi(t)\rangle|^2$ or $|b(t)|^2 = |\langle b|\Psi(t)\rangle|^2$, one obtains the well-known Rabi-oscillations of frequency Ω.

7.3.2 Non-Hermitian Floquet Theory

As long as we are dealing only with discrete states the quasi-energies ϵ are real. If, on the other hand, we allow for transitions into the continuum, e.g., via (multiphoton) ionization, the quasi-energies become complex,

$$\epsilon = \epsilon_0 + \Delta\epsilon - \mathrm{i}\frac{\Gamma}{2}. \tag{7.101}$$

Here, ϵ_0 is the unperturbed energy, $\Delta\epsilon$ is the AC Stark shift, and Γ is the ionization rate. One may wonder why a Hermitian Floquet Hamiltonian should yield complex eigenvalues. The reason for complex quasi-energies lies in the boundary conditions. Decaying dressed bound states or dressed resonances must fulfill the so-called Siegert boundary conditions [47]. Instead of explicitly taking these boundary conditions into account one may apply the complex dilation (also called complex scaling) method (see, e.g., [18, 48–50]).

Figure 7.7 shows the ionization rate of atomic hydrogen H(1s) for $\lambda = 1064\,\mathrm{nm}$ laser light as a function of the laser intensity, calculated by Potvliege and Shakeshaft [51] using the non-Hermitian Floquet method. At this wavelength at least 12 photons

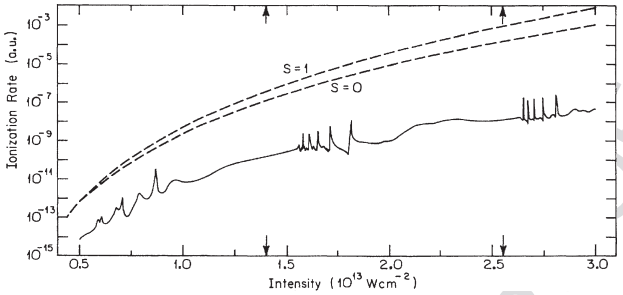

Fig. 7.7 Ionization rate vs laser intensity for H(1s) irradiated by linearly polarized light of wavelength $\lambda = 1064\,\mathrm{nm}$. *Dashed curves* are partial rates for $(12+S)$-photon ionization obtained within LOPT. The *arrows* indicate the intensities at which the real part of the 1s Floquet eigenvalue crosses the 13- and 14-photon ionization thresholds (from [51])

must be absorbed by the electron in order to escape. The LOPT results for S excess photon-ionization (i.e., $(12 + S)$-photon ionization) are included in Fig. 7.7. They by far overestimate the ionization rate. The exact Floquet-result displays interesting structures. As the AC Stark up-shift of the continuum (which is given by the ponderomotive potential U_p) increases, the minimum number of photons required for ionization increases from 12 to 13 (first arrow) and to 14 (second arrow). After these thresholds are passed because of the increasing laser intensity, structures appear, indicating a strong enhancement of the ionization rate at certain laser intensities. This is due to Rydberg states that are brought into $(12 + S)$-photon resonance with the ground state via the AC Stark effect (Freeman resonances) [52].

7.3.3 Stabilization

The coupling $\hat{W}(t)$ to the laser field in (7.72) reads in dipole approximation and velocity gauge

$$\hat{W}(t) = \hat{\boldsymbol{p}} \cdot \boldsymbol{A}(t) + \frac{1}{2}\boldsymbol{A}^2(t) \tag{7.102}$$

with $\boldsymbol{A}(t)$ the vector potential. The transformation of the wave function

$$|\Psi(t)\rangle = \mathrm{e}^{-\frac{\mathrm{i}}{2}\int_{-\infty}^{t} \boldsymbol{A}^2(t')\,dt'} \mathrm{e}^{-\mathrm{i}\boldsymbol{\alpha}(t)\cdot\hat{\boldsymbol{p}}} |\Psi_\mathrm{PF}(t)\rangle \tag{7.103}$$

removes the $\boldsymbol{A}^2$-term and transforms to the system of an electron oscillating with an excursion

$$\boldsymbol{\alpha}(t) = \int_{-\infty}^{t} \boldsymbol{A}(t')\,dt' \tag{7.104}$$

in the laser field [Pauli–Fierz (PF) or Kramers–Henneberger transformation] [53–55]. In this system the nuclear potential appears to oscillate. The TDSE then reads

$$\mathrm{i}\frac{d}{dt}|\Psi_{\mathrm{PF}}(t)\rangle = \left(\frac{\hat{\boldsymbol{p}}^2}{2} + V[\boldsymbol{r}+\boldsymbol{\alpha}(t)]\right)|\Psi_{\mathrm{PF}}(t)\rangle. \tag{7.105}$$

The PF Hamiltonian

$$\hat{H}_{\mathrm{PF}}(t) = \frac{\hat{\boldsymbol{p}}^2}{2} + V[\boldsymbol{r}+\boldsymbol{\alpha}(t)] \tag{7.106}$$

is for an infinitely long laser pulse periodic as well so that we may apply the Floquet theorem. Introducing the time-averaged potential

$$V_{\mathrm{PF}}(\hat{\boldsymbol{\alpha}},\boldsymbol{r}) = \frac{1}{T}\int_0^T V[\boldsymbol{r}+\boldsymbol{\alpha}(t)]\,dt, \qquad \hat{\boldsymbol{\alpha}} = \max|\boldsymbol{\alpha}(t)|, \tag{7.107}$$

which is the zero-frequency contribution in the Fourier-expansion of the potential [see (7.81)], (7.80) can be written as

$$-(\epsilon+m\omega)\Phi_\beta^{(m)} + \sum_\alpha \langle\beta|\frac{\hat{\boldsymbol{p}}^2}{2} + V_{\mathrm{PF}}(\hat{\boldsymbol{\alpha}},\boldsymbol{r})|\alpha\rangle\Phi_\alpha^{(m)} + \sum_{\substack{\alpha n\\ n\neq m}}\langle\beta|V^{(m-n)}|\alpha\rangle\Phi_\alpha^{(n)} = 0. \tag{7.108}$$

If the laser frequency is large compared to the relevant inner-atomic transitions, we may neglect the third term so that we are left with an equation diagonal in the photon index, which corresponds to the solution of the time-independent Schrödinger equation

$$\epsilon|\Psi_{\mathrm{PF}}\rangle = \left(\frac{\hat{\boldsymbol{p}}^2}{2} + V_{\mathrm{PF}}(\hat{\boldsymbol{\alpha}},\boldsymbol{r})\right)|\Psi_{\mathrm{PF}}\rangle. \tag{7.109}$$

If it is possible to transfer the entire electron population to the bound states of $V_{\mathrm{PF}}(\hat{\boldsymbol{\alpha}},\boldsymbol{r})$ there will be no ionization whatsoever. For intense fields where $\hat{\boldsymbol{\alpha}} \gg 1$ the potential $V_{\mathrm{PF}}(\hat{\boldsymbol{\alpha}},\boldsymbol{r})$ looks very different from the unperturbed nuclear potential since it has a double-well structure with the minima close to the classical turning points $\pm\hat{\boldsymbol{\alpha}}$. If electronic probability density is trapped in this potential the ionization rate decreases despite increasing laser field strength. This has indeed been observed in numerical simulations and is called adiabatic stabilization (see [11] for a review). The stabilization effect survives also for a "real" laser pulse with an up- and a down-ramp (dynamic stabilization).

Figure 7.8 illustrates stabilization of a one-dimensional model atom employing a soft-core binding potential $V(x) = -(x^2+\varepsilon)^{-1/2}$ with $\varepsilon = 1.9$ (leading to a binding energy of -0.5). The full TDSE was solved. The laser pulse of frequency

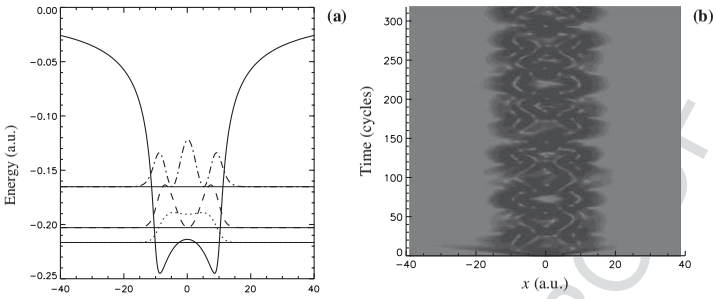

Fig. 7.8 Dynamic stabilization in a one-dimensional model atom. The cycle-averaged ionic potential in a reference frame where a freely oscillating electron is at rest is depicted in (**a**) (*solid line*). The three lowest energy levels in this "dressed" potential and the corresponding probability densities are also plotted. In (**b**) a shadowgraph of the probability density, obtained from the full solution of the time-dependent Schrödinger equation, is shown. The probability density remains trapped in the effective potential. Low-frequency Rabi-floppings are responsible for the oscillatory pattern. Note that the time scale of these oscillations is small compared to the laser period

$\omega = 2.5$ was ramped over 10 cycles up to $\hat{E} = 62.5$ and thereafter held constant. The excursion of a free electron in this field is $\alpha(t) = 10\sin\omega t$. The cycle-averaged potential, its three lowest levels and the corresponding probability densities are indicated in Fig. 7.8a. The potential has the above mentioned double-well shape with the minima close to the classical turning points $\pm\hat{\alpha}$. In Fig. 7.8b a shadowgraph of the probability density obtained from the TDSE solution in the PF frame is shown. The probability density remains confined between the two turning points. Only during the up-ramping of the pulse some density escapes. Obviously, not only a single dressed state is occupied since the probability density distribution oscillates in time. Note that the time-scale of this dynamics is slow compared to the laser period. The splitting of the probability density due to the double-well character of the PF potential is called "dichotomy" [56]. In circularly polarized multi-color laser field configurations more complex structures were observed [57].

Figure 7.9 shows the lifetime (i.e., the inverse ionization rate) of atomic H in circularly laser pulses of various frequencies and intensities as predicted by the high-frequency Floquet theory [58]. With increasing laser intensity the lifetime first decreases (i.e., ionization increases). This is the expected behavior from LOPT. Then, however, the lifetime passes through a minimum (the "death valley" [11, 59]) before it increases again (i.e., ionization is reduced).

So far, adiabatic stabilization with the electron starting from the ground state was observed in numerical simulations only. This is because there are no sufficiently strong lasers available yet at short wavelengths. The photon energy ω has to exceed the ionization potential, and the laser intensity must be strong enough in order to lead to the two minima in the time-averaged potential. Since the elongation α is inversely proportional to ω^2, the laser intensity necessary for adiabatic stabilization

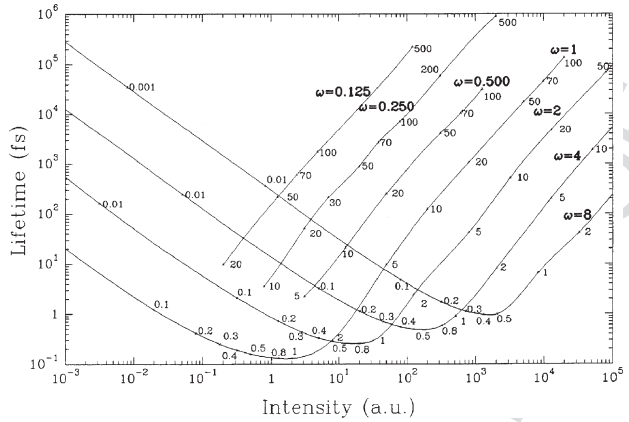

Fig. 7.9 Lifetime of the H atom in the ground state according to the high-frequency Floquet theory, vs intensity, at various laser frequencies ω; circular polarization. Numbers adjacent to points on the curves are the corresponding values of $\hat{\alpha}$. The descending branches of the curves correspond to LOPT, the ascending ones to adiabatic stabilization (the latter can be "trusted" as the laser frequency increases beyond the ionization potential 0.5). From [59]

increases with ω. Because $\omega > \mathcal{E}_{\rm ip}$ it is thus desirable to reduce $\mathcal{E}_{\rm ip}$ so that already available laser sources can be used. In fact, the stabilization of Rydberg atoms was already demonstrated [60].

There are (at least) three effects which counteract against adiabatic stabilization. Firstly, there is the so-called "death-valley" effect [59]: an atom experiences during the rising edge of a strong laser pulse field intensities in which violent ionization occurs and hence no more electrons are left to be stabilized once the optimal stabilization condition is reached. Secondly, in more complex atoms or ions inner electrons might be excited or removed by few photon processes induced by the incident high frequency radiation. Then the question arises whether an outer electron can stabilize although there are electron holes in the lower lying shells [61]. Thirdly, at high frequencies and high intensities the dipole approximation breaks down, and the magnetic $\boldsymbol{v} \times \boldsymbol{B}$-force pushes the electron into the propagation direction, thus enhancing ionization [62, 63]. These three effects will probably make the experimental verification of stabilization of atoms starting from the ground state a formidable task. Even the new short-wavelength free electron laser sources under construction worldwide are of too low intensity, let alone that they do not deliver long flat-top pulses, which would be ideal to observe dynamic stabilization. However, there is no doubt that sooner or later such light sources will be available so that a new and interesting kind of "meta-matter" will be produced: pseudo atoms with charge clouds extending over tens or more atomic units and artificial molecules of tunable internuclear separations.

7.3.4 Strong Field Approximation

The strong field approximation (SFA), also known as "Keldysh–Faisal–Reiss" (KFR)-theory [42, 64, 65], and its extensions are the theoretical workhorse in strong field laser–atom and laser–molecule interaction and often gives insight into the mechanisms behind strong field effects. As the laser field is far from being a small perturbation, "conventional" perturbation theory in the number of photons involved is not applicable [66]. The SFA does neither consider the laser field being small compared to the binding forces nor does it assume the contrary at all times during the interaction. Instead, in the SFA the binding potential is considered dominant until ionization whereas the laser field takes over after ionization. The SFA has been applied to ionization, harmonic generation, and nonsequential ionization. The beauty of the SFA lies, besides in its predictive power, in the possibility to interpret its equations in intuitively accessible terms, as will be shown below in Sect. 7.3.5. However, there are limits as well, to be discussed in the last part of this section.

Let the initial state be an electronic eigenstate of the field-free Hamiltonian. The electron may at time $t_{\rm i}$ be in the ground state $|\Psi_0\rangle = |\Psi_0(t_{\rm i})\rangle$ of energy $\mathcal{E}_0 < 0$, for instance, and the laser field is not yet switched on. Now let us consider the picture-independent bound-free transition matrix element

$$M_{\boldsymbol{p}}(t) = \langle \Psi_{\boldsymbol{p}} | \hat{U}(t, t_{\rm i}) | \Psi_0 \rangle \tag{7.110}$$

for a transition from the initial state $|\Psi_0\rangle$ to the target state $|\Psi_{\boldsymbol{p}}\rangle = |\Psi_{\boldsymbol{p}}(t_{\rm i})\rangle$, which is a continuum state of asymptotic momentum $\boldsymbol{p}$. $\hat{U}(t, t_{\rm i})$ is the (picture-independent) time evolution operator. The probability to find the electron at time t in the scattering state $|\Psi_{\boldsymbol{p}}\rangle$ is $w(t) = |M_{\boldsymbol{p}}(t)|^2$. The time-evolution operator $\hat{U}(t, t') = \hat{U}^{\dagger}(t', t)$ fulfills

$$\mathrm{i}\frac{d}{dt}\hat{U}(t, t') = \hat{H}(t)\hat{U}(t, t') \tag{7.111}$$

in any picture [67]. The TDSE in the Schrödinger picture reads

$$\mathrm{i}\frac{d}{dt}|\Psi(t)\rangle = \hat{H}(t)|\Psi(t)\rangle, \qquad \hat{H}(t) = \frac{1}{2}\left[\hat{\boldsymbol{p}} + \boldsymbol{A}(t)\right]^2 + \hat{V}(\boldsymbol{r}) \tag{7.112}$$

where $\boldsymbol{A}(t)$ is the vector potential describing the laser field (in dipole approximation). The minimum coupling Hamiltonian $\hat{H}(t)$ can be splitted in various ways:

$$\mathrm{i}\frac{d}{dt}|\Psi(t)\rangle = [\hat{H}_0 + \hat{W}(t)]|\Psi(t)\rangle = [\hat{H}^{(\mathrm{V})}(t) + \hat{V}(\boldsymbol{r})]|\Psi(t)\rangle, \tag{7.113}$$

with

$$\hat{H}_0 = \frac{\hat{\boldsymbol{p}}^2}{2} + \hat{V}(\boldsymbol{r}), \qquad \hat{H}^{(\mathrm{V})}(t) = \frac{\hat{\boldsymbol{p}}^2}{2} + \hat{W}(t), \tag{7.114}$$

and $\hat{W}(t)$ the interaction with the laser field,

$$\hat{W}(t) = \hat{\boldsymbol{p}} \cdot \boldsymbol{A}(t) + \frac{1}{2}\boldsymbol{A}^2(t) \qquad \text{(velocity gauge)}. \tag{7.115}$$

The gauge transformation of the potentials (both scalar potential ϕ and vector potential $\boldsymbol{A}$) and the wave function $|\Psi(t)\rangle$,

$$\boldsymbol{A}' = \boldsymbol{A} + \boldsymbol{\nabla}\chi(\boldsymbol{r}, t), \qquad \phi' = \phi - \frac{\partial\chi(\boldsymbol{r}, t)}{\partial t}, \qquad |\Psi'(t)\rangle = \mathrm{e}^{-\mathrm{i}\chi(\boldsymbol{r},t)}|\Psi(t)\rangle$$

where $\chi(\boldsymbol{r}, t)$ is an arbitrary differential scalar function, leaves the electric and the magnetic field unchanged:

$$\boldsymbol{E} = -\partial_t \boldsymbol{A} - \boldsymbol{\nabla}\phi = \boldsymbol{E}', \qquad \boldsymbol{B} = \boldsymbol{\nabla} \times \boldsymbol{A} = \boldsymbol{B}'. \tag{7.116}$$

This gauge invariance offers the possibility to choose a gauge that suits best, e.g., as far as computational simplicity is concerned. Observables are not affected by gauge transformations while the interpretation of the underlying physics may change (e.g., there is no potential barrier in velocity gauge to tunnel through). Moreover, approximations may destroy the gauge invariance (see below).

The transformation to the so-called length gauge (also known as the Göppert–Mayer gauge [68]) is achieved by choosing

$$\chi(\boldsymbol{r}, t) = -\boldsymbol{A}(t) \cdot \boldsymbol{r}. \tag{7.117}$$

Because of $\boldsymbol{\nabla}\chi = -\boldsymbol{A}$ the vector potential is "transformed away" while $\phi' = -\partial_t\chi = -\boldsymbol{E} \cdot \boldsymbol{r}$. The Hamiltonian in length gauge reads

$$\hat{H}'(t) = \frac{\hat{p}^2}{2} + \hat{V}(\boldsymbol{r}) - \phi'(\boldsymbol{r}, t) = \frac{\hat{p}^2}{2} + \hat{V}(\boldsymbol{r}) + \boldsymbol{E}(t) \cdot \hat{\boldsymbol{r}} \tag{7.118}$$

(one could also absorb $\hat{V}(\boldsymbol{r})$ in ϕ and ϕ'). Note that the transformation of the wave function

$$|\Psi'(t)\rangle = \mathrm{e}^{\mathrm{i}\hat{\boldsymbol{r}}\cdot\boldsymbol{A}(t)}|\Psi(t)\rangle \tag{7.119}$$

can be interpreted as a translation in momentum space. In fact, while in velocity gauge the quiver momentum is effectively subtracted from the kinetic momentum, leading to a canonical momentum different from the kinetic momentum, in length gauge kinetic and canonical momentum are equal.

From (7.118) we infer

$$\hat{W}'(t) = \boldsymbol{E}(t) \cdot \hat{\boldsymbol{r}} \qquad \text{(length gauge)} \tag{7.120}$$

with $\boldsymbol{E}(t) = -\partial_t \boldsymbol{A}(t)$.

$\hat{H}_0$ describes the unperturbed atom and seemingly does not depend on the gauge chosen, i.e., $\hat{H}_0 = \hat{H}_0'$. However, one should bear in mind that the momentum $\hat{\boldsymbol{p}}$ in $\hat{H}_0$ is not the kinetic momentum (which, in atomic units, equals the velocity) while in $\hat{H}_0'$ (length gauge) it is.

The Gordon–Volkov–Hamiltonian $\hat{H}^{(\mathrm{V})}(t)$ governs the free motion of the electron in the laser field [69, 70]. The Gordon–Volkov state $|\Psi_{\boldsymbol{p}}^{(\mathrm{V})}\rangle$ fulfills in the Schrödinger picture and velocity gauge

$$\mathrm{i}\frac{d}{dt}|\Psi_{\boldsymbol{p}}^{(\mathrm{V})}(t)\rangle = \hat{H}^{(\mathrm{V})}(t)|\Psi_{\boldsymbol{p}}^{(\mathrm{V})}(t)\rangle = \frac{1}{2}[\hat{\boldsymbol{p}} + \boldsymbol{A}(t)]^2|\Psi_{\boldsymbol{p}}^{(\mathrm{V})}(t)\rangle. \tag{7.121}$$

Thanks to the dipole approximation the Gordon–Volkov–Hamiltonian is diagonal in momentum space. The solution of (7.121), i.e., the Gordon–Volkov-state, is thus readily written down:

$$|\Psi_{\boldsymbol{p}}^{(\mathrm{V})}(t, t_\mathrm{i})\rangle = \mathrm{e}^{-\mathrm{i}S_{\boldsymbol{p}}(t,t_\mathrm{i})}|\boldsymbol{p}\rangle, \qquad S_{\boldsymbol{p}}(t, t_\mathrm{i}) = \frac{1}{2}\int_{t_\mathrm{i}}^{t} dt'\,[\boldsymbol{p} + \boldsymbol{A}(t')]^2 \tag{7.122}$$

where $|\boldsymbol{p}\rangle$ are momentum eigenstates, $\langle\boldsymbol{r}|\boldsymbol{p}\rangle = \mathrm{e}^{\mathrm{i}\boldsymbol{p}\cdot\boldsymbol{r}}/(2\pi)^{3/2}$. Note that the lower integration limit t_i affects the overall phase of the Gordon–Volkov solution only. As mentioned above, the transition to the length gauge corresponds to a translation in momentum space. It is thus easy to check that in length gauge one has

$$|\Psi_{\boldsymbol{p}}^{(\mathrm{V})'}(t, t_\mathrm{i})\rangle = \mathrm{e}^{-\mathrm{i}S_{\boldsymbol{p}}(t,t_\mathrm{i})}|\boldsymbol{p} + \boldsymbol{A}(t)\rangle \qquad \text{(length gauge)} \tag{7.123}$$

with the same action $S_{\boldsymbol{p}}(t, t_\mathrm{i})$ as in (7.122).

Let us now continue to derive the SFA transition matrix element. As the time evolution operator $\hat{U}(t, t')$ satisfies (7.111),

$$\mathrm{i}\frac{d}{dt}\hat{U}(t, t') = [\hat{H}_0 + \hat{W}(t)]\hat{U}(t, t'), \tag{7.124}$$

the integral equations

$$\begin{aligned}\hat{U}(t, t') &= \hat{U}_0(t, t') - \mathrm{i}\int_{t'}^{t} dt''\,\hat{U}(t, t'')\hat{W}(t'')\hat{U}_0(t'', t'), \\ &= \hat{U}_0(t, t') - \mathrm{i}\int_{t'}^{t} dt''\,\hat{U}_0(t, t'')\hat{W}(t'')\hat{U}(t'', t'),\end{aligned} \tag{7.125}$$

are fulfilled [71]. Here, $\hat{U}_0(t, t')$ is the evolution operator corresponding to the TDSE with $\hat{H}_0$ only. Inserting (7.125) in the matrix element (7.110) leads to

$$M_{\boldsymbol{p}}(t) = -\mathrm{i}\int_{t_\mathrm{i}}^{t} dt'\,\langle\Psi_{\boldsymbol{p}}|\hat{U}(t,t')\hat{W}(t')|\Psi_0(t')\rangle \tag{7.126}$$

where use of $\langle\Psi_{\boldsymbol{p}}|\hat{U}_0(t,t_\mathrm{i})|\Psi_0\rangle = \langle\Psi_{\boldsymbol{p}}|\Psi_0(t)\rangle = 0$ was made because $|\Psi_{\boldsymbol{p}}\rangle$ is a scattering state orthogonal to $|\Psi_0(t)\rangle = \mathrm{e}^{-\mathrm{i}\mathcal{E}_0(t-t_\mathrm{i})}|\Psi_0\rangle$, and $\hat{U}_0(t',t_\mathrm{i})|\Psi_0\rangle = |\Psi_0(t')\rangle$. Since the propagator $\hat{U}(t,t')$ also satisfies the integral equations

$$\begin{aligned}\hat{U}(t,t') &= \hat{U}^{(\mathrm{V})}(t,t') - \mathrm{i}\int_{t'}^{t} dt''\,\hat{U}^{(\mathrm{V})}(t,t'')\hat{V}\hat{U}(t'',t'), \\ &= \hat{U}^{(\mathrm{V})}(t,t') - \mathrm{i}\int_{t'}^{t} dt''\,\hat{U}(t,t'')\hat{V}\hat{U}^{(\mathrm{V})}(t'',t'),\end{aligned} \tag{7.127}$$

where $\hat{U}^{(\mathrm{V})}(t,t')$ is the evolution operator corresponding to the TDSE (7.121), one obtains, upon inserting (7.127) in (7.126),

$$\begin{aligned}M_{\boldsymbol{p}}(t) = -\mathrm{i}\Bigg[&\int_{t_\mathrm{i}}^{t} dt'\,\langle\Psi_{\boldsymbol{p}}|\hat{U}^{(\mathrm{V})}(t,t')\hat{W}(t')|\Psi_0(t')\rangle \\ &-\mathrm{i}\int_{t_\mathrm{i}}^{t} dt''\int_{t''}^{t} dt'\,\langle\Psi_{\boldsymbol{p}}|\hat{U}^{(\mathrm{V})}(t,t')\hat{V}\hat{U}(t',t'')\hat{W}(t'')|\Psi_0(t'')\rangle\Bigg].\end{aligned} \tag{7.128}$$

Using $\int_{t_\mathrm{i}}^{t} dt'' \int_{t''}^{t} dt' = \int_{t_\mathrm{i}}^{t} dt' \int_{t_\mathrm{i}}^{t} dt''\,\Theta(t'-t'') = \int_{t_\mathrm{i}}^{t} dt' \int_{t_\mathrm{i}}^{t'} dt''$ expression (7.128) may be recast in the form

$$\begin{aligned}M_{\boldsymbol{p}}(t) = -\mathrm{i}\int_{t_\mathrm{i}}^{t} dt'\,\langle\Psi_{\boldsymbol{p}}|\hat{U}^{(\mathrm{V})}(t,t')\Bigg[&\hat{W}(t')|\Psi_0(t')\rangle \\ &-\mathrm{i}\int_{t_\mathrm{i}}^{t'} dt''\,\hat{V}\hat{U}(t',t'')\hat{W}(t'')|\Psi_0(t'')\rangle\Bigg].\end{aligned} \tag{7.129}$$

Equation (7.129) is still exact and gauge invariant. Whatever is missed in the first term of (7.129) is included in the second term where the full but unknown time evolution operator $\hat{U}(t',t'')$ appears. Neglecting the second term, replacing the final state $|\Psi_{\boldsymbol{p}}\rangle$ by a plane wave $|\boldsymbol{p}\rangle$, and making use of the expansion of the Gordon–Volkov-propagator into Gordon–Volkov waves

$$\hat{U}^{(\mathrm{V})}(t,t') = \int d^3k\,|\Psi_{\boldsymbol{k}}^{(\mathrm{V})}(t,t_\mathrm{i})\rangle\langle\Psi_{\boldsymbol{k}}^{(\mathrm{V})}(t',t_\mathrm{i})|, \tag{7.130}$$

(t_i is arbitrary since it cancels) we obtain the SFA or so-called Keldysh-amplitude

$$M_{\boldsymbol{p}}^{(\mathrm{SFA})}(t) = -\mathrm{i}\int_{t_\mathrm{i}}^{t} dt'\,\langle\Psi_{\boldsymbol{p}}^{(\mathrm{V})}(t',t))|\hat{W}(t')|\Psi_0(t')\rangle. \tag{7.131}$$

The SFA transition amplitude integrates over all ionization times t' where the transition from the bound state $|\Psi_0(t')\rangle$ to the Gordon-Volkov state $|\Psi_{\boldsymbol{p}}^{(\mathrm{V})}(t',t))\rangle$, mediated by the interaction with the laser field $\hat{W}(t')$, may take place. Unfortunately, the replacement of the final state by a plane wave destroys the gauge invariance, and under certain circumstances SFA results can be very different in different gauges [72–74].

In velocity gauge, where $\hat{W}(t) = \hat{\boldsymbol{p}}\cdot\boldsymbol{A}(t) + \boldsymbol{A}^2(t)/2$ is diagonal in momentum representation, the Keldysh amplitude (7.131) becomes

$$M_{\boldsymbol{p}}^{(\mathrm{SFA})}(t) = -\mathrm{i}\int_{t_\mathrm{i}}^{t} dt'\,\mathrm{e}^{\mathrm{i}S_{\boldsymbol{p}}(t',t)}\left[\boldsymbol{p}\cdot\boldsymbol{A}(t') + \frac{1}{2}A^2(t')\right]\langle\boldsymbol{p}|\Psi_0\rangle\mathrm{e}^{-\mathrm{i}\mathcal{E}_0(t'-t_\mathrm{i})} \tag{7.132}$$

with $\mathcal{E}_0$ the initial energy. Multiplying this matrix element by the overall phase factor $\exp[\mathrm{i}S_{\boldsymbol{p}}(t,t_\mathrm{i})]$ and splitting $\boldsymbol{p}\cdot\boldsymbol{A}(t') + A^2(t')/2$ in the form $[\boldsymbol{p}+\boldsymbol{A}(t')]^2/2 - \mathcal{E}_0 - p^2/2 + \mathcal{E}_0$ leads – upon integration by parts—to

$$\begin{aligned}M_{\boldsymbol{p}}^{(\mathrm{SFA})\prime}(t) = &-\Psi_0(\boldsymbol{p})\,\mathrm{e}^{\mathrm{i}S_{\boldsymbol{p},\mathcal{E}_0}(t',t_\mathrm{i})}\Big|_{t_\mathrm{i}}^{t} \\ &+\mathrm{i}\Psi_0(\boldsymbol{p})\left(\frac{\boldsymbol{p}^2}{2} - \mathcal{E}_0\right)\int_{t_\mathrm{i}}^{t}\mathrm{e}^{\mathrm{i}S_{\boldsymbol{p},\mathcal{E}_0}(t',t_\mathrm{i})}\,dt'\end{aligned} \tag{7.133}$$

with the classical action

$$S_{\boldsymbol{p},\mathcal{E}_0}(t,t_\mathrm{i}) = \int_{t_\mathrm{i}}^{t}\left[\frac{\boldsymbol{p}^2}{2} - \mathcal{E}_0 + \hat{W}(t')\right]dt' \tag{7.134}$$

and $\Psi_0(\boldsymbol{p}) = \langle\boldsymbol{p}|\Psi_0\rangle$ the Fourier-transformed initial state wave function

$$\Psi_0(\boldsymbol{p}) = \frac{1}{(2\pi)^{3/2}}\int d^3r\,\mathrm{e}^{-\mathrm{i}\boldsymbol{p}\cdot\boldsymbol{r}}\Psi_0(\boldsymbol{r}). \tag{7.135}$$

The first term in (7.133) vanishes when the asymptotic rate

$$\Gamma_{\boldsymbol{p}} = \lim_{T\to\infty}\frac{|M_{\boldsymbol{p}}|^2}{T}, \qquad M_{\boldsymbol{p}} = \lim_{\substack{t_\mathrm{i}\to-\infty\\ t\to\infty}} M_{\boldsymbol{p}}(t) \tag{7.136}$$

is calculated. In this way we recover Reiss' result [65]

$$M_{\boldsymbol{p}}^{(\mathrm{SFA})\prime} = \mathrm{i}\Psi_0(\boldsymbol{p})\left(\frac{\boldsymbol{p}^2}{2} - \mathcal{E}_0\right)\int_{-\infty}^{\infty}\mathrm{e}^{\mathrm{i}S_{\boldsymbol{p},\mathcal{E}_0}(t,-\infty)}\,dt. \tag{7.137}$$

7.3.4.1 Circular Polarization and Long Pulses

In this case one may write the vector potential in dipole approximation as

$$\boldsymbol{A}(t) = \frac{1}{2}\hat{A}[\boldsymbol{\varepsilon}\exp(\mathrm{i}\omega t) + \boldsymbol{\varepsilon}^*\exp(-\mathrm{i}\omega t)] \tag{7.138}$$

where the polarization vectors $\boldsymbol{\varepsilon}, \boldsymbol{\varepsilon}^*$ fulfill $\boldsymbol{\varepsilon}^2 = \boldsymbol{\varepsilon}^{*2} = 0$ and $\boldsymbol{\varepsilon}\cdot\boldsymbol{\varepsilon}^* = 1$, e.g., $\boldsymbol{\varepsilon} = (\boldsymbol{e}_x + \mathrm{i}\boldsymbol{e}_y)/\sqrt{2}$. The factor $1/2$ is introduced in order to obtain $U_\mathrm{p} = \hat{A}^2/4$, as in the linearly polarized case. With

$$[\boldsymbol{p} + \boldsymbol{A}(t)]^2 = \boldsymbol{p}^2 + \frac{1}{2}\hat{A}^2 + 2\hat{A}|\boldsymbol{p}\cdot\boldsymbol{\varepsilon}|\cos(\omega t - \varphi), \tag{7.139}$$

where $\boldsymbol{p}\cdot\boldsymbol{\varepsilon} = |\boldsymbol{p}\cdot\boldsymbol{\varepsilon}|\exp(-\mathrm{i}\varphi)$, the action (7.134) reads

$$S_{\boldsymbol{p},\mathcal{E}_0}(t,-\infty) = \left(\frac{\boldsymbol{p}^2}{2} - \mathcal{E}_0 + U_\mathrm{p}\right)t + \frac{\hat{A}}{\omega}|\boldsymbol{p}\cdot\boldsymbol{\varepsilon}|\sin(\omega t - \varphi) \tag{7.140}$$

where we neglected contributions from $t_\mathrm{i} = -\infty$ since they just affect the irrelevant, overall phase of the SFA transition matrix element

$$M^{(\mathrm{SFA})\ \prime}_{\boldsymbol{p},\ \mathrm{circ.}} = 2\pi\mathrm{i}\Psi_0(\boldsymbol{p})\sum_{n=-\infty}^{\infty}(n\omega - U_p)\exp(\mathrm{i}n\varphi) \times J_n\!\left(\frac{-\hat{A}|\boldsymbol{p}\cdot\boldsymbol{\varepsilon}|}{\omega}\right)\delta(p^2/2 - \mathcal{E}_0 + U_\mathrm{p} - n\omega). \tag{7.141}$$

$J_n(\zeta)$ are Bessel functions obeying

$$\exp[-\mathrm{i}\zeta\,\sin(\omega t - \varphi)] = \sum_{n=-\infty}^{\infty} J_n(\zeta)\exp[-\mathrm{i}n(\omega t - \varphi)], \tag{7.142}$$

was made. The time integration in (7.137) leads to the energy-conserving δ-function. Employing (7.136) and using

$$\delta(\Omega) = \frac{1}{2\pi}\lim_{T\to\infty}\int_{-T/2}^{T/2}\exp(\mathrm{i}\Omega t)\,dt = \lim_{T\to\infty}\frac{T}{2\pi} \quad \text{for } \Omega = 0 \tag{7.143}$$

(and zero otherwise) to evaluate the square of the δ-function one obtains the ionization rate

$$\Gamma^{(\mathrm{SFA})}_{\boldsymbol{p},\ \mathrm{circ.}} = 2\pi|\Psi_0(\boldsymbol{p})|^2\sum_{n=-\infty}^{\infty}(n\omega - U_\mathrm{p})^2\,J_n^2\left(\frac{-\hat{A}|\boldsymbol{p}\cdot\boldsymbol{\varepsilon}|}{\omega}\right)\delta(p^2/2 - \mathcal{E}_0 + U_\mathrm{p} - n\omega). \tag{7.144}$$

$\Gamma^{(\mathrm{SFA})}_{\boldsymbol{p},\ \mathrm{circ.}}$ has the dimension of a density in momentum space per time. To evaluate the total rate Γ the partial rate $\Gamma_{\boldsymbol{p}}$ has to be integrated over all final momenta $\boldsymbol{p}$,

$$\Gamma = \int d^3p\,\Gamma_{\boldsymbol{p}} = \int dp\,d\Omega\,p^2\Gamma_{\boldsymbol{p}} = \int d\Omega\,\frac{d\Gamma}{d\Omega} \tag{7.145}$$

where $d\Omega = \sin\vartheta\,d\vartheta\,d\varphi$ is the solid angle element. The final rate for ionization with the electron ejected into the solid angle $d\Omega$ is given by

$$\frac{d\Gamma^{(\mathrm{SFA})}_{\mathrm{circ.}}}{d\Omega} = 2\pi\sqrt{8\omega^5}\sum_{n=n_{\min}}^{\infty}(n - U_\mathrm{p}/\omega)^2\frac{p_n}{\sqrt{2\omega}}\,|\Psi_0(p_n)|^2\,J_n^2\left(\frac{-\hat{A}\,p_n\sin\vartheta}{\sqrt{2}\omega}\right), \tag{7.146}$$

with

$$p_n = \sqrt{2(n\omega - U_\mathrm{p} + \mathcal{E}_0)}. \tag{7.147}$$

The sum in (7.146) runs over all n which yield real p_n and starts with the minimum number of absorbed photons $n_{\min}$, which depends not only on $\mathcal{E}_0$ but also on U_p – an utterly nonperturbative, nonlinear effect!

7.3.4.2 Channel-Closing in Above-Threshold Ionization

The increase of $n_{\min}$ with increasing U_p is the channel-closing phenomenon (see, e.g., [75, 76]). This is illustrated in Fig. 7.10. We expect peaks in the photoelectron spectra at the positions

$$\mathcal{E}_n = \frac{1}{2}p_n^2 = n\omega - (U_\mathrm{p} + \mathcal{E}_\mathrm{ip}), \qquad n \geq n_{\min} \tag{7.148}$$

where $\mathcal{E}_\mathrm{ip} = |\mathcal{E}_0|$ is the ionization potential and $U_\mathrm{p} + \mathcal{E}_\mathrm{ip}$ is the "effective" ionization potential due to the AC Stark shift of the continuum threshold with respect to the ground state level. Due to the fact that peaks $n > n_{\min}$ are present – even with higher probability than $n = n_{\min}$ – the name above-threshold ionization (ATI) has been coined for this strong field ionization phenomenon, which was first observed by Agostini et al. [77]. The peak positions in strong field photoelectron spectra according (7.148) are well confirmed by ab initio solutions of the TDSE in dipole approximation. However, in actual measurements the positions of the peaks depend on the laser pulse duration. In short-pulse experiments the released electrons have no time to leave the focus before the laser pulse is over. In long pulses, instead, the electron has time to leave the focus and, in so doing, gain back the energy U_p. As a consequence the U_p-term in (7.148) is canceled and the peak positions in the long-pulse regime are determined by

$$\mathcal{E}_n^{(\text{long pulse})} = \frac{1}{2}p_n^2 = n\omega - \mathcal{E}_\mathrm{ip}, \qquad n \geq n_{\min} \tag{7.149}$$

with $n_{\min}$, however, still to be calculated with U_p (since before leaving the laser focus, ionization has to occur in the first place).

In Fig. 7.10a the U_p-shift of the continuum threshold is small, and the channel $n = 5$ is responsible for the first peak in the photoelectron spectrum. At higher laser intensity, in Fig. 7.10b, the channels $n = 5$ and $n = 6$ are closed since 6 photons are not sufficient to overcome the effective ionization potential $\mathcal{E}_{ip} + U_p$. In the long pulse regime peaks corresponding to a certain channel are always at the same positions in the energy spectrum whereas in the short pulse regime the peaks move with U_p. As a consequence, focal averaging reduces the contrast in the short pulse regime whereas it has less of an effect in the long pulse regime because of the automatic cancellation of U_p at the position of electron-emission.

In Fig. 7.11 we show the example of an experimental long-pulse spectrum where lower order peaks are indeed suppressed due to channel-closings.

7.3.4.3 Linear Polarization and Long Pulses

We assume a laser field of the form

$$\boldsymbol{A}(t) = \hat{A}\boldsymbol{\varepsilon}\cos(\omega t), \qquad \boldsymbol{\varepsilon}^2 = 1. \tag{7.150}$$

The action (7.134) reads in this case

$$S_{\boldsymbol{p},\mathcal{E}_0}(t,-\infty) = \left(\frac{\boldsymbol{p}^2}{2} - \mathcal{E}_0 + U_p\right)t - \frac{\hat{A}}{\omega}\boldsymbol{p}\cdot\boldsymbol{\varepsilon}\sin(\omega t) + \frac{\hat{A}^2}{8\omega}\sin(2\omega t).$$

Proceeding as in the circular field-case one arrives at [65]

$$M^{(\mathrm{SFA})'}_{\boldsymbol{p},\mathrm{lin.}} = 2\pi \mathrm{i}\Psi_0(\boldsymbol{p})\sum_{n=-\infty}^{\infty}(n\omega - U_p)\tilde{J}_n\left(\frac{-\hat{A}\boldsymbol{p}\cdot\boldsymbol{\varepsilon}}{\omega}, -\frac{U_p}{2\omega}\right)\delta(p^2/2 - \mathcal{E}_0 + U_p - n\omega),$$

$$\Gamma^{(\mathrm{SFA})}_{\boldsymbol{p},\mathrm{lin.}} = 2\pi|\Psi_0(\boldsymbol{p})|^2\sum_{n=-\infty}^{\infty}(n\omega - U_p)^2\tilde{J}_n^2\left(\frac{-\hat{A}\boldsymbol{p}\cdot\boldsymbol{\varepsilon}}{\omega}, -\frac{U_p}{2\omega}\right)\delta(p^2/2 - \mathcal{E}_0 + U_p - n\omega),$$

$$\frac{d\Gamma^{(\mathrm{SFA})}_{\mathrm{lin.}}}{d\Omega} = 2\pi\sqrt{8\omega^5}\sum_{n=-\infty}^{\infty}(n - U_p/\omega)^2\frac{p_n}{\sqrt{2m\omega}}|\Psi_0(p_n)|^2\tilde{J}_n^2\left(\frac{-\hat{A}\boldsymbol{p}\cdot\boldsymbol{\varepsilon}}{\omega}, -\frac{U_p}{2\omega}\right).$$

$\tilde{J}_n$ is the generalized Bessel function of integer order n defined by

$$\tilde{J}_n(u,v) = \frac{1}{2\pi}\int_{-\pi}^{\pi} d\theta\, \exp[\mathrm{i}(u\sin\theta + v\sin(2\theta) - n\theta)].$$

The relation to the ordinary Bessel functions is

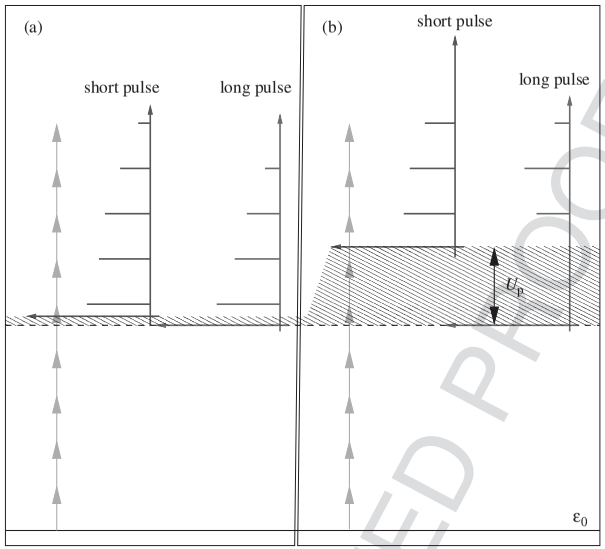

Fig. 7.10 Channel-closing in the short and long pulse regime. In (**a**) the laser intensity is small so that the U_p-shift of the continuum threshold is less than a photon energy. In (**b**) the channels $n = 5$ and $n = 6$ are closed due to the pronounced AC Stark shift of the continuum. The photoelectron spectra look different in the short and long pulse regime since the released electrons gain U_p in the latter case upon leaving the laser focus

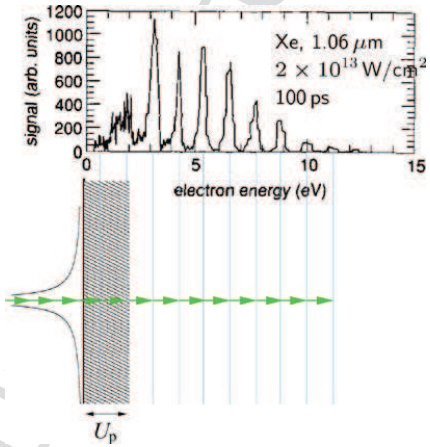

Fig. 7.11 Channel-closing in the long-pulse regime. The experimental spectrum was taken from [78]. The two channels in the shaded area are closed

$$\tilde{J}_n(u, v) = \sum_{k=-\infty}^{\infty} J_{n-2k}(u) J_k(v)$$

and

$$\sum_{n=-\infty}^{\infty} \exp(\mathrm{i}n\theta)\tilde{J}_n(u, v) = \exp[\mathrm{i}u \sin\theta + \mathrm{i}v \sin(2\theta)].$$

Further properties of the generalized Bessel functions may be found in the appendix B of the original SFA paper by Reiss [65]. In the same article it is also demonstrated how the typical exponential behavior $\sim \exp[-2(2\mathcal{E}_{\mathrm{ip}})^{3/2}/(3E)]$ arises in the case of tunneling ionization [see (7.66)] through the asymptotic behavior of the generalized Bessel functions $\tilde{J}_n$.

7.3.5 *Few-Cycle Above-Threshold Ionization*

In few-cycle pulses the pulse envelope $\hat{A}(t)$ varies on a time scale comparable to the period $T = 2\pi/\omega$ determined by the carrier frequency ω. Moreover, the carrier envelope phase ϕ, governing the shift of the carrier wave with respect to the envelope, affects many observables. Hence, instead of (7.150) we write

$$\boldsymbol{A}(t) = \hat{A}(t)\boldsymbol{\varepsilon} \sin(\omega t + \phi) \tag{7.151}$$

with $\hat{A}(t)$ a $\sin^2$ or a Gaussian envelope, for instance.

In the case of few-cycle pulses it would be very cumbersome to deal with Bessel functions, as we did above for constant (or slowly varying) $\hat{A}$. Instead, we start off with the still exact matrix element (7.129) and replace once again the final state by a plane wave and the full propagator $\hat{U}(t', t)$ by $\hat{U}^{(\mathrm{V})}(t', t)$. In that way we obtain the extended SFA transition matrix element

$$M_{\boldsymbol{p}}^{(\mathrm{SFA})}(t) = M_{\boldsymbol{p}}^{(\mathrm{SFA,dir})}(t) + M_{\boldsymbol{p}}^{(\mathrm{SFA,resc})}(t), \tag{7.152}$$

$$M_{\boldsymbol{p}}^{(\mathrm{SFA,dir})}(t) = M_{\boldsymbol{p}}^{(\mathrm{SFA})}(t) = -\mathrm{i}\int_{t_\mathrm{i}}^{t} dt' \, \langle \Psi_{\boldsymbol{p}}^{(\mathrm{V})}(t', t))|\hat{W}(t')|\Psi_0(t')\rangle, \tag{7.153}$$

$$M_{\boldsymbol{p}}^{(\mathrm{SFA,resc})}(t) \tag{7.154}$$
$$= -\int_{t_\mathrm{i}}^{t} dt' \int_{t_\mathrm{i}}^{t'} dt'' \, \langle \Psi_{\boldsymbol{p}}^{(\mathrm{V})}(t', t)|\hat{V}\hat{U}^{(\mathrm{V})}(t', t'')\hat{W}(t'')|\Psi_0(t'')\rangle.$$

In what follows we set $t_\mathrm{i} = 0$, and we assume that

$$\boldsymbol{A}(0) = \boldsymbol{A}(T_\mathrm{p}) = \boldsymbol{0} \tag{7.155}$$

where T_p is the laser pulse duration. Note that the integral over the electric field of a realistic laser pulse must vanish (see, e.g., appendix A in [9]), so that $\boldsymbol{A}(0) = \boldsymbol{A}(T_\mathrm{p})$ and (7.155) does not pose a loss of generality. It is left as an exercise to the reader that relabeling the integration variables, multiplication by an overall phase factor and making use of the fact that ionization can only happen while the laser is on, (7.153) and (7.154) can be recast in length gauge in the form

$$M_{\boldsymbol{p}}^{(\mathrm{SFA,dir})'} = -\mathrm{i}\int_0^{T_\mathrm{p}} dt_\mathrm{ion} \langle \boldsymbol{p} + \boldsymbol{A}(t_\mathrm{ion})|\boldsymbol{r} \cdot \boldsymbol{E}(t_\mathrm{ion})|\Psi_0\rangle \, \mathrm{e}^{\mathrm{i}S_{p,\mathcal{E}_0}(t_\mathrm{ion})}, \tag{7.156}$$

where

$$S_{\boldsymbol{p},\mathcal{E}_0}(t) = \int_0^t dt' \left(\frac{1}{2}[\boldsymbol{p} + \boldsymbol{A}(t')]^2 - \mathcal{E}_0\right), \qquad S_{\boldsymbol{p}}(t) = \frac{1}{2}\int_0^t dt' \, [\boldsymbol{p} + \boldsymbol{A}(t')]^2.$$

t_ion can be interpreted as the ionization time. Analogously, the rescattering matrix element can be written for $t \to \infty$ in the form

$$M_{\boldsymbol{p}}^{(\mathrm{SFA,resc})'} = -\int_0^{T_\mathrm{p}} dt_\mathrm{ion} \int_{t_\mathrm{ion}}^{\infty} dt_\mathrm{resc} \int d^3k \, \mathrm{e}^{\mathrm{i}S_{\boldsymbol{p}}(t_\mathrm{resc})} \langle \boldsymbol{p} + \boldsymbol{A}(t_\mathrm{resc})|\hat{V}|\boldsymbol{k} + \boldsymbol{A}(t_\mathrm{resc})\rangle$$
$$\times \mathrm{e}^{-\mathrm{i}S_{\boldsymbol{k}}(t_\mathrm{resc})} \langle \boldsymbol{k} + \boldsymbol{A}(t_\mathrm{ion})|\boldsymbol{r} \cdot \boldsymbol{E}(t_\mathrm{ion})|\Psi_0\rangle \mathrm{e}^{\mathrm{i}S_{k,\mathcal{E}_0}(t_\mathrm{ion})} \tag{7.157}$$

with t_resc the rescattering time or, introducing the new variables $t = t_\mathrm{resc}$, $\tau = t_\mathrm{resc} - t_\mathrm{ion}$,

$$M_{\boldsymbol{p}}^{(\mathrm{SFA,resc})'} = -\int_0^{\infty} dt \, \mathrm{e}^{\mathrm{i}S_{p,\mathcal{E}_0}(t)} \int_0^t d\tau \int d^3k \, V_{\boldsymbol{p}-\boldsymbol{k}} \mathrm{e}^{-\mathrm{i}S_{k,\mathcal{E}_0}(t,t-\tau)} \tag{7.158}$$
$$\times \langle \boldsymbol{k} + \boldsymbol{A}(t-\tau)|\boldsymbol{r} \cdot \boldsymbol{E}(t-\tau)|\Psi_0\rangle$$

where

$$S_{\boldsymbol{k},\mathcal{E}_0}(t, t-\tau) = \int_{t-\tau}^{t} dt' \left(\frac{1}{2}\left[\boldsymbol{k} + \boldsymbol{A}(t')\right]^2 - \mathcal{E}_0\right) \tag{7.159}$$

and $V_{\boldsymbol{p}-\boldsymbol{k}} = \langle \boldsymbol{p}|\hat{V}|\boldsymbol{k}\rangle$. The time τ is the time the electron spends in the continuum between ionization and rescattering. The infinite upper limit in the integration over the rescattering time in (7.157) can be restricted to T_p since rescattering after the laser is off will not lead to energy absorption. As a consequence, the final energy will be within a region strongly dominated by the more probable direct ionization process.

The integration over the intermediate momentum $\boldsymbol{k}$ can be approximated seeking the stationary momentum $\boldsymbol{k}_\mathrm{s}(t, \tau)$ contributing most to the $\boldsymbol{k}$-integration:

$$\nabla_{\boldsymbol{k}} S_{\boldsymbol{k},\mathcal{E}_0}(t, t-\tau) \stackrel{!}{=} \boldsymbol{0} \qquad \Rightarrow \qquad \boldsymbol{k}_{\rm s}(t,\tau) = -\frac{\boldsymbol{\alpha}(t) - \boldsymbol{\alpha}(t-\tau)}{\tau} \tag{7.160}$$

with $\boldsymbol{\alpha}(t)$ the excursion as in (7.104). Hence,

$$M_{\boldsymbol{p}}^{(\mathrm{SFA,resc})'} = -\int_0^{T_{\rm p}} dt\, \mathrm{e}^{\mathrm{i}S_{\boldsymbol{p},\mathcal{E}_0}(t)} \int_0^t d\tau \left(\frac{2\pi}{\mathrm{i}\tau}\right)^{3/2} V_{\boldsymbol{p}-\boldsymbol{k}_{\rm s}(t,\tau)} \mathrm{e}^{-\mathrm{i}S_{\rm s,\mathcal{E}_0}(t,t-\tau)} \times \langle \boldsymbol{k}_{\rm s}(t,\tau) + \boldsymbol{A}(t-\tau) | \boldsymbol{r}\cdot\boldsymbol{E}(t-\tau) | \Psi_0 \rangle \tag{7.161}$$

where the stationary action $S_{\rm s,\mathcal{E}_0}(t, t-\tau)$ is given by

$$S_{\rm s,\mathcal{E}_0}(t, t-\tau) = S_{\boldsymbol{k}_{\rm s}(t,\tau),\mathcal{E}_0}(t, t-\tau) \tag{7.162}$$

and the factor $[2\pi/(\mathrm{i}\tau)]^{3/2}$ arises from the saddle-point integration (see, e.g., [79]). In actual numerical evaluations the denominator $\mathrm{i}\tau$ is regularized by adding a real, positive ϵ. As long as ϵ is sufficiently small, the results are independent of it.

In the case of a hydrogen-like atom the matrix element needed in (7.161) reads

$$\langle \boldsymbol{k} | \boldsymbol{r}\cdot\boldsymbol{E}(t) | \Psi_0 \rangle = -\mathrm{i}2^{7/2}(2\mathcal{E}_{\rm ip})^{5/4} \frac{\boldsymbol{k}\cdot\boldsymbol{E}(t)}{\pi(k^2 + 2\mathcal{E}_{\rm ip})^3}. \tag{7.163}$$

For rescattering at potentials of the form

$$V(r) = -\left(b + \frac{a}{r}\right) \mathrm{e}^{-\lambda r} \tag{7.164}$$

the matrix element $V_{\boldsymbol{p}-\boldsymbol{k}}$ is given by

$$V_{\boldsymbol{p}-\boldsymbol{k}} = -\frac{2b\lambda + aC}{2\pi^2 C^2}, \qquad C = (\boldsymbol{p}-\boldsymbol{k})^2 + \lambda^2. \tag{7.165}$$

In few-cycle laser pulses the concept of an ionization rate is not useful since the latter would be time-dependent and sensitive to all details of the pulse (duration, shape, carrier-envelope phase, peak field strength). In experiments one measures the differential ionization probability $w_{\boldsymbol{p}}$, which is the probability to find an electron of final energy $\mathcal{E}_{\boldsymbol{p}} = p^2/2$ emitted in a certain direction corresponding to the solid angle element $d\Omega_{\boldsymbol{p}}$. The probability $w_{\boldsymbol{p}}$ is related to the transition matrix element $M_{\boldsymbol{p}}$ through

$$w_{\boldsymbol{p}} \underbrace{d\mathcal{E}_{\boldsymbol{p}}}_{p\,dp}\, d\Omega_{\boldsymbol{p}} = |M_{\boldsymbol{p}}|^2\, d^3p = |M_{\boldsymbol{p}}|^2\, p^2 dp\, d\Omega_{\boldsymbol{p}} \tag{7.166}$$

so that

$$w_{\boldsymbol{p}} = p\,|M_{\boldsymbol{p}}|^2. \tag{7.167}$$

7.3.6 Simple Man's Theory

The remaining time integral(s) in (7.156) and (7.161) can be either solved numerically or approximately by using (modifications of) the saddle-point method with respect to time (see [8] and Appendix B in [9]). We do not want to go into the details but only emphasize here that the SFA transition matrix element can be approximated by a sum over the stationary contributions,

$$M_{\boldsymbol{p}}^{(\mathrm{SFA})} = \sum_s a_{s,\boldsymbol{p}} \mathrm{e}^{\mathrm{i}S_{s,\boldsymbol{p}}}. \tag{7.168}$$

As it turns out the saddle-point equations define quantum orbits [80, 81] that are close to the classical orbits of the so-called simple man's theory. In the following we will use simple man's theory to derive the cut-off laws for the photoelectron spectra.

If an electron is set free at time $t_{\rm ion}$ and from thereon does not interact with the ionic potential anymore, its momentum and position at times $t > t_{\rm ion}$ are given by

$$\boldsymbol{p}(t) = -\int_{t_{\rm ion}}^t dt'\, \boldsymbol{E}(t') = \boldsymbol{A}(t) - \boldsymbol{A}(t_{\rm ion}), \tag{7.169}$$

$$\begin{aligned}\boldsymbol{r}(t) &= \int_{t_{\rm ion}}^t dt'\, \boldsymbol{A}(t') - \boldsymbol{A}(t_{\rm ion})(t - t_{\rm ion}) \\ &= \boldsymbol{\alpha}(t) - \boldsymbol{\alpha}(t_{\rm ion}) - \boldsymbol{A}(t_{\rm ion})(t - t_{\rm ion})\end{aligned} \tag{7.170}$$

with the excursion $\boldsymbol{\alpha}(t)$ as defined in (7.104). If the vector potential fulfills (7.155) the momentum at the end of the pulse is determined by the value of the vector potential at the time of ionization, $\boldsymbol{p}(T_{\rm p}) = -\boldsymbol{A}(t_{\rm ion})$, so that the final energy is

$$\mathcal{E}_{\mathrm{dir},\boldsymbol{p}}(t_{\rm ion}) = \frac{1}{2}\boldsymbol{A}^2(t_{\rm ion}) \le 2U_{\rm p} \tag{7.171}$$

because the ponderomotive potential is $U_{\rm p} = \hat{A}^2/4$. The fact that the direct electrons are classically restricted to energies up to $2U_{\rm p}$ is one of the celebrated cut-off laws in strong field physics.

Let us now allow for one rescattering event, i.e., at the time $t_{\rm resc}$ the electron returns to the origin (where the ion is located),

$$\epsilon \stackrel{!}{>} |\boldsymbol{r}(t_{\rm resc})| = |\boldsymbol{\alpha}(t_{\rm resc}) - \boldsymbol{\alpha}(t_{\rm ion}) - \boldsymbol{A}(t_{\rm ion})\tau| \tag{7.172}$$

where ϵ is a distance small compared to the Bohr radius. Let us assume the extreme case of 180° back-reflection where the electron changes the sign of its momentum so that immediately after the scattering event

$$\boldsymbol{p}(t_{\rm resc+}) = -[\boldsymbol{A}(t_{\rm resc}) - \boldsymbol{A}(t_{\rm ion})]. \tag{7.173}$$

At later times we have

$$\begin{aligned} \boldsymbol{p}(t > t_{\mathrm{resc}}) &= -\int_{t_{\mathrm{resc}}}^{t} dt'\, \boldsymbol{E}(t') - [\boldsymbol{A}(t_{\mathrm{resc}}) - \boldsymbol{A}(t_{\mathrm{ion}})] \\ &= \boldsymbol{A}(t) - 2\boldsymbol{A}(t_{\mathrm{resc}}) + \boldsymbol{A}(t_{\mathrm{ion}}) \end{aligned} \tag{7.174}$$

so that $\boldsymbol{p}_{\mathrm{resc}}(T_{\mathrm{p}}) = -2\boldsymbol{A}(t_{\mathrm{resc}}) + \boldsymbol{A}(t_{\mathrm{ion}})$ and

$$\mathcal{E}_{\mathrm{resc},\boldsymbol{p}}(t_{\mathrm{resc}}, t_{\mathrm{ion}}) = \frac{1}{2}[\boldsymbol{A}(t_{\mathrm{ion}}) - 2\boldsymbol{A}(t_{\mathrm{resc}})]^2 \leq 10U_{\mathrm{p}}. \tag{7.175}$$

Because of the condition (7.172) the $10U_{\mathrm{p}}$ cut-off law for the rescattered electrons is not so obvious. However, it can be readily checked numerically by plotting $\mathcal{E}_{\mathrm{resc},\boldsymbol{p}}(t_{\mathrm{resc}}, t_{\mathrm{ion}})$ vs all possible t_{resc}, t_{ion} (where $t_{\mathrm{resc}} > t_{\mathrm{ion}}$) and then indicating those pairs of t_{ion}, t_{resc} that fulfill (7.172). The result is shown in Fig. 7.12.

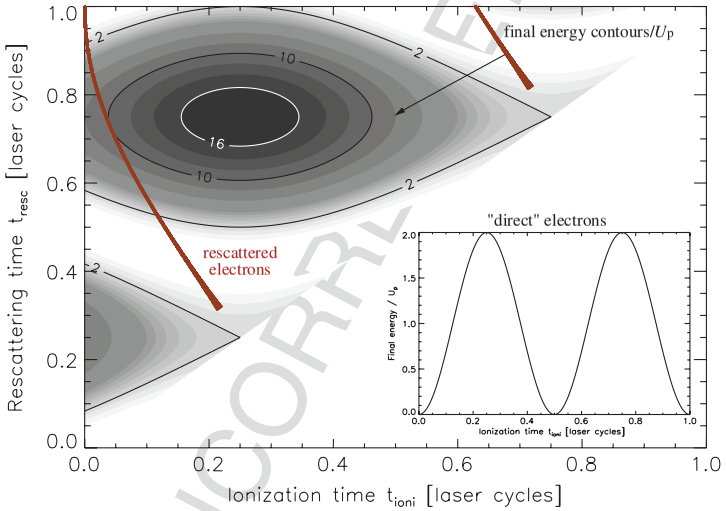

Fig. 7.12 Final photoelectron energy $\mathcal{E}_{\mathrm{resc},\boldsymbol{p}}$ vs ionization time t_{ion} and rescattering time $t_{\mathrm{resc}} > t_{\mathrm{ion}}$ (*black*: high value of $\mathcal{E}_{\mathrm{resc},\boldsymbol{p}}$, white: small value of $\mathcal{E}_{\mathrm{resc},\boldsymbol{p}}$, contours 2, 10 and $16U_{\mathrm{p}}$ labeled explicitly). The branch labeled "rescattered electrons" indicates times t_{ion} and t_{resc} where (7.172) is fulfilled (for an $\epsilon \ll 1$). The highest energy those rescattered electrons can have is $10U_{\mathrm{p}}$ (see branch touching the $10U_{\mathrm{p}}$-contour). The inlet shows the final energy (7.171) of the "direct" electrons vs the ionization time. The highest energy there is $2U_{\mathrm{p}}$

7.3.6.1 How Good Is the Strong Field Approximation?

In order to answer this question we compare the results of an ab initio TDSE solution with the corresponding SFA predictions. Apart from the dipole approximation (which is well applicable here) the TDSE result is exact. Comparisons with TDSE results serve as a much more demanding testing ground for approximate theories such as the SFA than comparison with experiments, because of focal averaging effects present in experiments, the uncertainties in laser intensity, pulse duration, and shape, the limited resolution in energy, and the limited dynamic range in the yields.

In Fig. 7.13 the results for an $n = 4$-cycle pulse of the form $\boldsymbol{E}(t) = \hat{E}\boldsymbol{e}_z \sin^2[\omega t/(2n)]\cos(\omega t + \phi)$ for $0 < t < n2\pi/\omega$, $\omega = 0.056$, $\hat{E} = 0.0834$, $\phi = 0$ are shown. The agreement between TDSE and SFA results improve with increasing photoelectron energy. A possible explanation for that might be that slow electrons spend more time in the vicinity of the atomic potential where Coulomb corrections are expected to be important. As can be seen in Fig. 7.13, the transition regime between the cut-off for the direct electrons at $\mathcal{E} = 2U_{\mathrm{p}} = 1.1$ up to energies where rescattered electrons start to take over at $\mathcal{E} \approx 2.5$ is quite smooth in the TDSE spectra whereas pronounced interference patterns are visible in the SFA results. Moreover, at very low energies the positions of the local maxima disagree. It has been shown that the agreement at lower energies improves if the binding potential is made short-range by cutting it at certain distances. This is expected since the crucial assumption in SFA is that the electron is not affected by the ionic potential anymore once ionization has occurred [9, 82]. This assumption is well justified for short-range potentials but less so for long range Coulombic ones as, e.g., in the H(1s) case.

A lot of effort has been devoted to the development of Coulomb-corrections, taking into account the effect of the Coulomb-potential on its way to the detector, e.g. in [83–86]. However, only a few of them are able to reproduce the striking features seen in experimental and numerical ab initio spectra, which are in strong disagreement with the plain SFA, such as rotated angular distributions [87], fan-like structures in momentum distributions at low energies [85], and the recently observed "low energy feature" at long wavelengths [88]. The pronounced interference pattern showing a spiky, downward-pointing structure in the rescattering plateau in Fig. 7.13 between energies $\approx$ 3 and 6 a.u. instead is remarkably well reproduced using the extended SFA taking into account (7.158) without further Coulomb-correction.

7.3.7 *Interference Effects*

The spiky structure in Fig. 7.13 is due to quantum interference. For a fixed final momentum $\boldsymbol{p}$ the sum (7.168) is a sum over all quantum orbits that end up with the same momentum at the detector. It turns out that, most of the time, there are two dominating contributions. Depending on their phase-difference those may interfere constructively (local maxima in Fig. 7.13) or destructively (downward-pointing

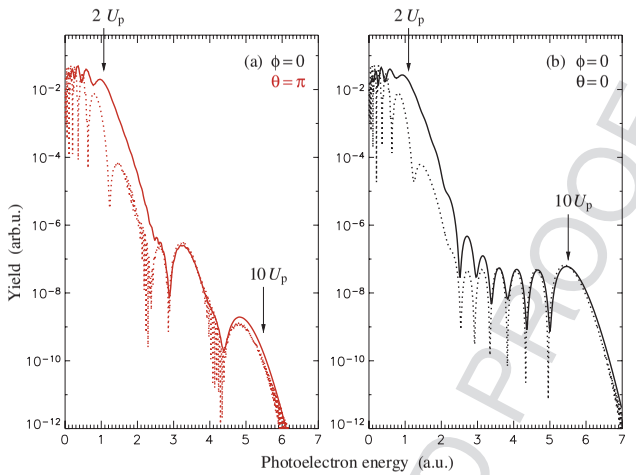

Fig. 7.13 Photoelectron spectra of the H(1s) electron after irradiation with a 4-cycle laser pulse ($\omega = 0.056$, $\phi = 0$, $\hat{E} = 0.0834$). The TDSE and SFA results are drawn solid and dashed, respectively. Panel (**a**) shows the "left-going" electrons (i.e., opposite to the laser polarization $\boldsymbol{e}_z$), panel (**b**) the "right-going" electrons (in $\boldsymbol{e}_z$)-direction. The spectra were adjusted vertically by multiplication with a single factor in such a way that agreement is best in the cut-off region for the right-going electrons. The spectra were not shifted in energy

spikes in Fig. 7.13). The corresponding two trajectories of simple man's theory can be readily calculated. As an example we show the final energy vs the ionization time for a "flat-top" pulse in Fig. 7.14. In the lower panel of Fig. 7.14 the course of the electric field is indicated. Let us focus on the time $t = 0.5$ cycles where the electric field has a maximum and ionization is therefore most likely. The upper panel shows that a "direct" electron emitted at that time will have vanishing final energy. In order for a direct, classical electron to have the maximum energy $2U_p$ it has to be emitted at times where the electric field is zero (which is unlikely in the tunneling and over-barrier regime). However, if an electron is emitted around the maximum of the electric field and rescatters once, its final energy may be close to $10U_p$. It is clearly seen that two emission times very close to each other lead to the same final energy (as indicated in the upper panel). These are the two trajectories that interfere. Exactly at the cut-off $10U_p$ those two solutions merge to a single one. The "travel times" $t_{resc} - t_{ion}$ between rescattering and ionization are color-coded from black ($t_{resc} - t_{ion} = 0$) to yellow ($t_{resc} - t_{ion} = 2$ cycles).

In very short pulses the situation is more complex than in the regular, flat-top pulse case. Since the ionization probability is strongly weighted with the modulus of the electric field, only a few "time-windows" may remain "open", thus affecting the number of interfering quantum orbits for a given $\boldsymbol{p}$. The interference pattern is

then very sensitive to the details of the few-cycle pulse, e.g., to the carrier-envelope phase. Because of the "time-windows" that are opened and closed depending on the parameters of the few-cycle pulse, one may view the setup as a "double slit experiment in time" [89], a detailed analysis of which is given in [16]. There are two dominating quantum trajectories contributing to a given final momentum in the case of linear polarization. One of them goes directly to the detector while the other one starts in the "wrong" direction but turns around within a fraction of a laser half period. It thus sweeps over the nucleus on the way towards the detector. The two quantum orbits correspond to the reference wave and the object wave in a holography experiment. Hence, the interference pattern in the momentum spectra may be viewed as a hologram of the binding potential [90, 91].

7.3.8 High-Order Harmonic Generation

When an intense laser pulse of frequency ω_1 impinges on any kind of target, in general harmonics of ω_1 are emitted. A typical signature of the emission spectrum in the case of strongly driven atoms, molecules or clusters is that the harmonic yield does not simply roll-off exponentially with increasing harmonic order. Instead, a plateau is observed. This is a prerequisite for high-order harmonic generation (HOHG)

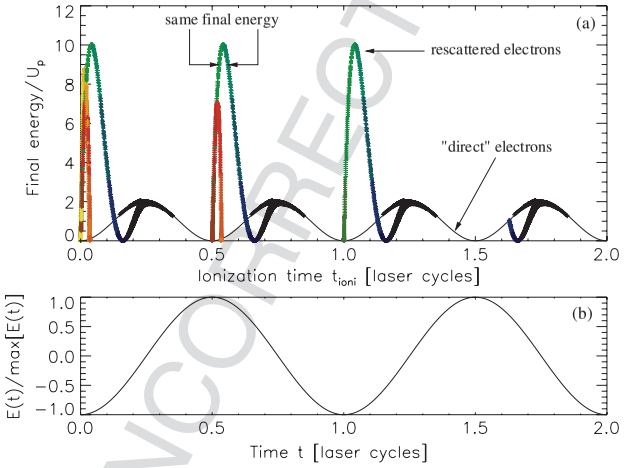

Fig. 7.14 (**a**) Final energy of direct electrons (*black line*) vs the ionization time. If rescattered is allowed, higher energies may occur. The color coding for the rescattered electrons indicates the time spent in the continuum between ionization and rescattering (the lighter the color the longer the time). The cut-off energies for the direct and the rescattered electrons are 2 and $10U_p$, respectively. Panel (**b**) shows the course of the laser field. Ionization is improbable for small $|E(t)|$

being of practical relevance as an efficient short wavelength source. As targets for HOHG one may think of single atoms, dilute gases of atoms, molecules, clusters, crystals, or the surface of a solid (which is rapidly transformed into a plasma by the laser). In fact, for all those targets HOHG has been observed experimentally. Even a strongly driven two-level system displays nonperturbative HOHG [92, 93]. The mechanism generating the harmonics and its efficiency, of course, vary with the target-type. In the case of atoms the so-called "three-step model" explains the basic mechanism in the spirit of simple man's theory: an electron is freed by the laser at a certain time t', subsequently it oscillates in the laser field, and eventually recombines with its parent ion upon emitting a photon of frequency

$$\omega = n\,\omega_1, \qquad n \geq 1. \tag{7.176}$$

This process is illustrated in Fig. 7.15. If the energy of the returning electron is $\mathcal{E}$, the energy of the emitted photon is $\omega = \mathcal{E} + |\mathcal{E}_\mathrm{f}|$ where $\mathcal{E}_\mathrm{f}$ is the energy of the level which is finally occupied by the electron, for example, the groundstate.

From this simple considerations we conclude that the maximum photon energy one can expect is $\omega_\mathrm{max} = \mathcal{E}_\mathrm{max} + |\mathcal{E}_\mathrm{f}|$. Using (7.169) we obtain at the recombination time t_rec for the return energy $\mathcal{E}_\mathrm{ret}$

$$\mathcal{E}_\mathrm{ret} = \frac{1}{2}p^2(t_\mathrm{rec}) = \frac{1}{2}[\boldsymbol{A}(t_\mathrm{rec}) - \boldsymbol{A}(t_\mathrm{ion})]^2 \tag{7.177}$$

where we have to impose [see (7.172)]

$$|\boldsymbol{r}(t_\mathrm{rec})| = |\boldsymbol{\alpha}(t_\mathrm{rec}) - \boldsymbol{\alpha}(t_\mathrm{ion}) - \boldsymbol{A}(t_\mathrm{ion})(t_\mathrm{rec} - t_\mathrm{ion})| \overset{!}{<} \epsilon. \tag{7.178}$$

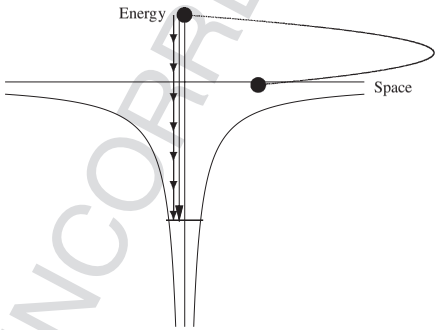

Fig. 7.15 Illustration of the three-step model for high harmonic generation. An electron is (i) released, (ii) accelerated in the laser field, and (iii) driven back to the ion. There it may recombine upon emitting a single photon which corresponds to a multiple of the photon energy of the incident laser light

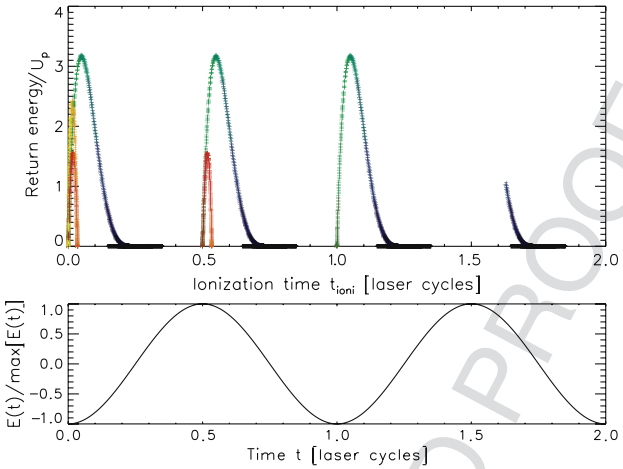

Fig. 7.16 Return energy as a function of the ionization time. The color coding indicates the time between ionization and recombination (the longer this time the lighter the color). The maximum return energy is $\simeq 3.17U_\mathrm{p}$. The course of the laser field is shown in the lower panel

Figure 7.16 shows the possible return energies fulfilling (7.177) and (7.178). We infer that the maximum return energy is around $\simeq 3.2$. Closer inspection shows that the number is 3.17 so that the cut-off law reads

$$\omega_\mathrm{max} = 3.17U_\mathrm{p} + |\mathcal{E}_\mathrm{f}|. \tag{7.179}$$

This celebrated $\approx 3\,U_p$ cut-off rule was first established empirically [94] and explained soon after within simple man's theory [95, 96].

Lewenstein and co-workers [97] showed that, more precisely, it reads $\omega_\mathrm{max} = 3.17U_\mathrm{p} + 1.32|\mathcal{E}_\mathrm{f}|$.

From simple man's theory one expects that harmonic generation should be much less efficient in elliptically polarized laser fields since, classically, the freed electron never comes back to its parent ion so that recombination can be considered unlikely. This indeed was confirmed experimentally (see [10], and references therein).

Harmonic generation in atoms, molecules and clusters has huge practical relevance as an efficient source of intense XUV radiation. This is because (i) the ponderomotive scaling of the cut-off allows to achieve high values of $\mathcal{E}_\mathrm{max}$ and thus high harmonic orders n, and (ii), fortunately, the strength of the harmonics does not decay exponentially with the order n but displays, after a decrease over the first few harmonics, an overall plateau (at least on the logarithmic scale) up to the cut-off energy $3.17\,U_\mathrm{p} + |\mathcal{E}_\mathrm{f}|$, allowing relatively high intensities at short wavelengths. In

fact, high-order harmonics below $\lambda = 4.4\,\mathrm{nm}$, the so-called water-window (between the K-edges of carbon and oxygen) have been observed experimentally [98, 99]. The intensity of the emitted radiation in the plateau region is about 10^{-6} of the incident laser intensity which is typically 10^{15}–$10^{18}\,\mathrm{Wcm}^{-2}$ in rare gas experiments. Therefore, the intensity of the high-order harmonics is sufficient for various kinds of applications, such as interferometry, for dense plasma diagnostics, holography, high-contrast microscopy of biological materials, and attosecond spectroscopy or metrology. Attosecond pulses are generated via harmonic generation. If the incoming pulse is already short (i.e., consists only of a few cycles) the harmonic emission is restricted to a narrow time window similar to the "double slit in time"-experiment mentioned above. As a consequence, the harmonic pulse has a duration that is short compared to the laser period of the incoming pulse (usually a few hundred attoseconds). If the incoming laser pulse is longer, one can construct attosecond pulse trains by selecting a few phase-locked harmonics. Attosecond pulses that are generated via harmonic generation have been used to probe the ionizing laser field itself [100] as well as fast atomic processes such as Auger decay [101].

For calculating the rate of harmonic emission one may follow the same route as in the SFA treatment of ionization. Harmonic generation and ATI are complementary to each other: while in harmonic generation the electron comes back to the ion and eventually recombines, upon emitting radiation, in high-order ATI it rescatters upon which it may gain additional energy. In harmonic generation one observes a plateau reaching up to photon energies $3.17\,U_\mathrm{p} + |\mathcal{E}_\mathrm{f}|$. In ATI a plateau is observed as well – this time with respect to the kinetic energy of the photo electrons – extending up to $10\,U_\mathrm{p}$ (for one rescattering event).

In classical electrodynamics, the total radiated power by a dipole of charge q is given by Larmor's formula

$$P = \frac{2q^2}{3c^3}\,|\ddot{\boldsymbol{r}}|^2. \tag{7.180}$$

Thus, in a semiclassical approach, it appears reasonable to replace the acceleration by its quantum mechanical expectation value and making use of Ehrenfest's theorem. One obtains

$$P = \frac{2q^2}{3c^3}\left|\frac{d^2}{dt^2}\langle\hat{\boldsymbol{r}}\rangle\right|^2 = \frac{2q^2}{3c^3}\left|\frac{1}{m}\left\langle -\frac{\partial\hat{H}}{\partial\hat{\boldsymbol{r}}}\right\rangle\right|^2. \tag{7.181}$$

The last expression on the right-hand side is particularly suited for the numerical evaluation of the harmonic spectra. In order to simplify even further we write the dipole as a Fourier-transform,

$$\boldsymbol{d}(t) = q\,\langle\hat{\boldsymbol{r}}\rangle = \frac{q}{\sqrt{2\pi}}\int_{-\infty}^{\infty} d\omega\,\exp(\mathrm{i}\omega t)\boldsymbol{d}(\omega). \tag{7.182}$$

The total emitted energy then is

$$\mathcal{E}_\mathrm{rad} = \int_{-\infty}^{\infty} dt\; P = \frac{2}{3c^3}\int_{-\infty}^{\infty} d\omega\,\omega^4\,|\boldsymbol{d}(\omega)|^2, \tag{7.183}$$

and we infer that the yield radiated into a spectral interval $[\omega, \omega + d\omega]$ is

$$\epsilon_{\mathrm{rad},\,\omega}\,d\omega \sim \omega^4\,|\boldsymbol{d}(\omega)|^2\,d\omega. \tag{7.184}$$

A full quantum mechanical treatment reveals that calculating the harmonic spectrum emitted by a single atom from the square of the dipole expectation value is actually incorrect [92, 102]. Since the expectation value of the number of photons in a mode $\omega, \boldsymbol{k}$ (with creation and annihilation operators $\hat{a}^\dagger$, $\hat{a}$, respectively) at time t is [103]

$$\begin{aligned}\langle\hat{a}^\dagger(t)\hat{a}(t)\rangle = {} & \langle\hat{a}^\dagger(t_\mathrm{i})\hat{a}(t_\mathrm{i})\rangle + 2C\Re\int_{t_\mathrm{i}}^{t} dt'\,\langle\hat{\boldsymbol{r}}(t')\hat{a}(t_\mathrm{i})\rangle\exp(-\mathrm{i}\omega t') \\ & + C^2\int_{t_\mathrm{i}}^{t} dt'\int_{t_\mathrm{i}}^{t} dt''\,\langle\hat{\boldsymbol{r}}(t'')\hat{\boldsymbol{r}}(t')\rangle\exp[\mathrm{i}\omega(t'-t'')],\end{aligned} \tag{7.185}$$

where C is a coupling constant, one sees that if the mode under consideration is not excited at the initial time $t = t_\mathrm{i}$, as it is the case here, only the third term survives. This term accounts for spontaneous emission and scattering. Hence, the harmonic spectrum of a single atom should be calculated from the two-time dipole-dipole correlation function $\langle\hat{\boldsymbol{r}}(t'')\hat{\boldsymbol{r}}(t')\rangle$ instead of the Fourier-transformed one-time dipole. However, if one considers a sample of N atoms

$$\langle\hat{a}^\dagger(t)\hat{a}(t)\rangle = C^2\sum_{k=1}^{N}\sum_{j=1}^{N}\int_{t_\mathrm{i}}^{t} dt'\int_{t_\mathrm{i}}^{t} dt''\,\langle\hat{\boldsymbol{r}}_k(t'')\hat{\boldsymbol{r}}_j(t')\rangle\exp[\mathrm{i}\omega(t'-t'')] \tag{7.186}$$

results and, by assuming that all these atoms are uncorrelated, that is $\langle\hat{\boldsymbol{r}}_k(t'')\hat{\boldsymbol{r}}_j(t')\rangle \simeq \langle\hat{\boldsymbol{r}}_k(t'')\rangle\langle\hat{\boldsymbol{r}}_j(t')\rangle$, one arrives at

$$\langle\hat{a}^\dagger(t)\hat{a}(t)\rangle \approx C^2\left|\sum_{k=1}^{N}\int_{t_\mathrm{i}}^{t} dt'\,\langle\hat{\boldsymbol{r}}_k(t')\rangle\exp(\mathrm{i}\omega t')\right|^2 \tag{7.187}$$

if $N \gg 1$ is assumed so that the self-interaction terms $\sim \langle\hat{\boldsymbol{r}}_k(t'')\rangle\langle\hat{\boldsymbol{r}}_k(t')\rangle$ contribute negligibly. Moreover, if all atoms "see" the same field one obtains simply the absolute square of N times the single dipole expectation value. Therefore, calculating the harmonic spectra from the Fourier-transformed dipole, although not correct in the single atom response case, is a reasonable method when comparison with HOHG experiments in dilute gas targets is made. Hence, for the study of macroscopic

UNCORRECTED PROOF

propagation effects the dipole expectation value may be inserted as a source into Maxwell's equations.

7.3.9 Strong Field Approximation for High-Order Harmonic Generation: the Lewenstein Model

The dipole expectation value of a single atom with one active electron ($q = -1$) is

$$\begin{aligned} \boldsymbol{d}(t) &= -\langle\Psi(t)|\hat{\boldsymbol{r}}|\Psi(t)\rangle \\ &= -\langle\Psi_0(t_\mathrm{i})|\hat{U}(t_\mathrm{i},t)\,\hat{\boldsymbol{r}}\,\hat{U}(t,t_\mathrm{i})|\Psi_0(t_\mathrm{i})\rangle, \end{aligned} \tag{7.188}$$

where we assumed again that at the initial time t_i the electron starts in the state $|\Psi_0(t_\mathrm{i})\rangle =: |\Psi_0\rangle$. Using (7.125) we obtain

$$\begin{aligned} \boldsymbol{d}(t) = &-\langle\Psi_0(t)|\hat{\boldsymbol{r}}|\Psi_0(t)\rangle \\ &-\mathrm{i}\int_{t_\mathrm{i}}^{t} dt'\,\langle\Psi_0(t')|\hat{W}(t')\hat{U}(t',t)\hat{\boldsymbol{r}}|\Psi_0(t)\rangle \\ &+\mathrm{i}\int_{t_\mathrm{i}}^{t} dt'\,\langle\Psi_0(t)|\hat{\boldsymbol{r}}\hat{U}(t,t')\hat{W}(t')|\Psi_0(t')\rangle \\ &-\int_{t_\mathrm{i}}^{t} dt'\int_{t_\mathrm{i}}^{t} dt''\,\langle\Psi_0(t')|\hat{W}(t')\hat{U}(t',t)\hat{\boldsymbol{r}}\hat{U}(t,t'')\hat{W}(t'')|\Psi_0(t'')\rangle. \end{aligned} \tag{7.189}$$

The first term vanishes for a spherically symmetric binding potential. The second and third term are complex conjugates of each other and describe ionization ($\hat{W}$), propagation ($\hat{U}$), and recombination ($\hat{\boldsymbol{r}}$) (i.e., the emission of harmonic radiation) in different time-ordering. The last term involves one additional interaction with the laser field. We will neglect it here (see [104]). As in the SFA for ionization we replace the full time evolution operator $\hat{U}$ by $\hat{U}^{(\mathrm{V})}$,

$$\boldsymbol{d}^{(\mathrm{L})}(t) = -\mathrm{i}\int_{t_\mathrm{i}}^{t} dt'\,\langle\Psi_0(t')|\hat{W}(t')\hat{U}^{(\mathrm{V})}(t',t)\hat{\boldsymbol{r}}|\Psi_0(t)\rangle + \mathrm{c.c.}, \tag{7.190}$$

we shall recover the Lewenstein-result [97]. In length gauge [$\hat{W}(t) = \boldsymbol{E}(t)\cdot\hat{\boldsymbol{r}}$] we obtain (suppressing the "+c.c.")

$$\boldsymbol{d}^{(\mathrm{L})}(t) = -\mathrm{i}\int_{t_\mathrm{i}}^{t} dt' \int d^3p\,\langle\Psi_0(t')|\boldsymbol{E}(t')\cdot\hat{\boldsymbol{r}}|\boldsymbol{p}+\boldsymbol{A}(t')\rangle\langle\boldsymbol{p}+\boldsymbol{A}(t)|\hat{\boldsymbol{r}}|\Psi_0(t)\rangle \mathrm{e}^{-\mathrm{i}S_p(t',t)} \tag{7.191}$$

where we used (7.123) and $\hat{U}^{(\mathrm{V})}(t',t)|\boldsymbol{p}+\boldsymbol{A}(t)\rangle = \mathrm{e}^{-\mathrm{i}S_p(t',t)}|\boldsymbol{p}+\boldsymbol{A}(t')\rangle$. With

$$S_{\boldsymbol{p},\mathcal{E}_0}(t,t') = \int_{t'}^{t} dt''\,\left(\frac{1}{2}[\boldsymbol{p}+\boldsymbol{A}(t'')]^2 - \mathcal{E}_0\right) \tag{7.192}$$

we can write (7.191) as

$$\boldsymbol{d}^{(\mathrm{L})}(t) = -\mathrm{i}\int_{t_\mathrm{i}}^{t} dt' \int d^3p\,\langle\Psi_0|\boldsymbol{E}(t')\cdot\hat{\boldsymbol{r}}|\boldsymbol{p}+\boldsymbol{A}(t')\rangle\langle\boldsymbol{p}+\boldsymbol{A}(t)|\hat{\boldsymbol{r}}|\Psi_0\rangle \mathrm{e}^{-\mathrm{i}S_{p,\mathcal{E}_0}(t',t)}. \tag{7.193}$$

Introducing the dipole matrix element

$$\boldsymbol{\mu}(\boldsymbol{p}) = \langle\boldsymbol{p}|\hat{\boldsymbol{r}}|\Psi_0\rangle = \frac{1}{(2\pi)^{3/2}}\int d^3r\,\mathrm{e}^{-\mathrm{i}\boldsymbol{p}\cdot\boldsymbol{r}}\boldsymbol{r}\Psi_0(\boldsymbol{r}) \tag{7.194}$$

we have

$$\boldsymbol{d}^{(\mathrm{L})}(t) = \mathrm{i}\int_{t_\mathrm{i}}^{t} dt' \int d^3p\,\mathrm{e}^{-\mathrm{i}S_{p,\mathcal{E}_0}(t,t')}\boldsymbol{\mu}^*[\boldsymbol{p}+\boldsymbol{A}(t)]\boldsymbol{E}^*(t')\cdot\boldsymbol{\mu}[\boldsymbol{p}+\boldsymbol{A}(t')] + \mathrm{c.c.}$$

The integration over momentum can be approximated using the stationary phase method again, i.e.,

$$\nabla_{\boldsymbol{p}} S_{\boldsymbol{p},\mathcal{E}_0}(t,t') \stackrel{!}{=} 0. \tag{7.195}$$

For a linearly polarized laser pulse with a slowly varying envelope we have

$$\boldsymbol{E}(t) = \hat{E}\boldsymbol{e}_z\cos\omega t, \qquad \boldsymbol{A}(t) = -\frac{\hat{E}}{\omega}\boldsymbol{e}_z\sin\omega t, \tag{7.196}$$

so that

$$\boldsymbol{\alpha}(t) - \boldsymbol{\alpha}(t') = \int_{t'}^{t} dt''\,\boldsymbol{A}(t'') = \frac{\hat{E}}{\omega^2}\boldsymbol{e}_z(\cos\omega t - \cos\omega t') \tag{7.197}$$

and

$$\frac{\partial S_{\boldsymbol{p},\mathcal{E}_0}(t,t')}{\partial p_z} = p_z(t-t') + \frac{\hat{E}}{\omega^2}(\cos\omega t - \cos\omega t') \stackrel{!}{=} 0 \tag{7.198}$$

$$\Rightarrow \qquad p_{z,\mathrm{s}}(t,\tau) = -\frac{\hat{E}[\cos\omega t - \cos\omega(t-\tau)]}{\omega^2\tau}, \qquad \tau = t - t'. \tag{7.199}$$

The transverse stationary momentum vanishes, $p_{x,\mathrm{s}} = p_{y,\mathrm{s}} = 0$. Plugging $\boldsymbol{p}_\mathrm{s}$ into (7.192) and integrating yield the stationary action

$$S_\mathrm{s}(t,\tau) = (U_\mathrm{p} - \mathcal{E}_0)\tau - 2U_\mathrm{p}\frac{1-\cos\omega\tau}{\omega^2\tau} - U_\mathrm{p}\frac{C(\tau)}{\omega}\cos[(2t-\tau)\omega] \tag{7.200}$$

with

$$C(\tau) = \sin\omega\tau - \frac{4}{\omega\tau}\sin^2\frac{\omega\tau}{2}. \tag{7.201}$$

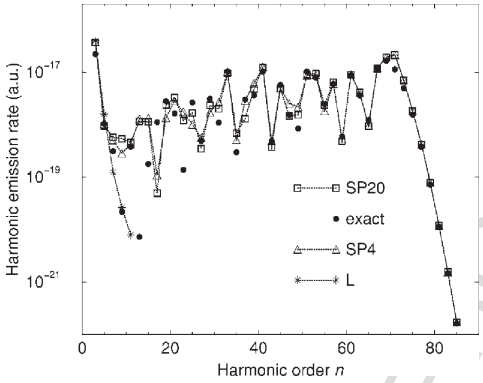

Fig. 7.17 Harmonic spectrum obtained using the SFA (Lewenstein model) for H(1s), 2×10^{14} Wcm^{-2}, and photon energy 1.17 eV. The time integral in (7.202) was calculated either directly (labeled "exact") or applying the saddle-point approximation. The expected cut-off at harmonic order $n = 72.3$ is confirmed (from [105])

In the original Lewenstein-paper [97] it is shown that the cut-off law $3.17U_\mathrm{p} + \mathcal{E}_\mathrm{ip}$ can be derived from the function $C(\tau)$. Setting $t_\mathrm{i} = 0$, the final result for the SFA dipole after saddle-point integration reads

$$\boldsymbol{d}^{(\mathrm{L})}(t) = \mathrm{i}\int_0^t d\tau \left(\frac{2\pi}{\mathrm{i}\tau}\right)^{3/2} \mu_z^*[p_{z,\mathrm{s}}(t,\tau) + A(t)] \times \mu_z[p_{z,\mathrm{s}}(t,\tau) + A(t-\tau)]\hat{E}\cos[\omega(t-\tau)]\mathrm{e}^{-\mathrm{i}S_\mathrm{s}(t,\tau)} + \mathrm{c.c.} \tag{7.202}$$

from which, via Fourier-transformation, the harmonic spectra $\epsilon_{\mathrm{rad},\,\omega}$ (7.184) can be calculated. Figure 7.17 shows an example for a harmonic spectrum calculated using the Lewenstein model.

7.3.10 Harmonic Generation Selection Rules

As the name "harmonics" suggests, the emission of laser-driven targets mainly occurs at multiples of the fundamental, incoming laser frequency ω_1, that is $\omega = n\omega_1$ with n the harmonic order. In the case of atoms in a linearly polarized laser field, for instance, only odd harmonics are emitted, i.e., $n = 1, 3, 5, \ldots$. One could think that this "quantized" emission is a quantum effect. However, this is not the case. Pure classical simulations also show harmonic generation and not just continuous spectra. The selection rules governing which harmonic orders n are allowed and which are forbidden are determined by the symmetry of the combined system target + laser field, i.e., the symmetry of the field-dressed target, also called dynamical

symmetry. We shall now employ the Floquet theory introduced in Sect. 7.3.1 to derive the selection rules for harmonic emission for a few exemplary systems.

Let $\hat{H}(t)$ be the Hamiltonian of an electron in a linearly polarized monochromatic laser field $E\cos(\omega_1 t)\boldsymbol{e}_z$ of amplitude E and an ionic potential $\hat{V}(\hat{\boldsymbol{r}})$,

$$\hat{H}(t) = \frac{\hat{p}^2}{2} + \hat{V}(\hat{\boldsymbol{r}}) + E\hat{z}\cos\omega_1 t. \tag{7.203}$$

The Schrödinger equation reads $\mathrm{i}\frac{d}{dt}|\Psi(t)\rangle = \hat{H}(t)|\Psi(t)\rangle$, and since the Hamiltonian is periodic in time,

$$\hat{H}(t + 2\pi/\omega_1) = \hat{H}(t), \tag{7.204}$$

from the Floquet theorem (cf. Sect. 7.3.1)

$$|\Psi(t)\rangle = \mathrm{e}^{-\mathrm{i}\epsilon t}|\Phi(t)\rangle, \qquad |\Phi(t + 2\pi/\omega_1)\rangle = |\Phi(t)\rangle \tag{7.205}$$

follows, and $|\Phi(t)\rangle$ fulfills the Schrödinger equation

$$\hat{\mathcal{H}}(t)|\Phi(t)\rangle = \epsilon|\Phi(t)\rangle, \qquad \hat{\mathcal{H}}(t) = \hat{H}(t) - \mathrm{i}\frac{d}{dt} \tag{7.206}$$

which looks like a stationary Schrödinger equation in an extended Hilbert space [106] with the time as an additional dimension and ϵ a quasi-energy. The scalar product in this extended Hilbert space reads

$$\langle\langle\Phi|\Phi'\rangle\rangle := \frac{\omega_1}{2\pi}\int_0^{2\pi/\omega_1} dt\,\langle\Phi(t)|\Phi'(t)\rangle. \tag{7.207}$$

For the derivation of the harmonic generation selection rules we consider an infinitely long laser pulse and assume that the system is well described by a single, nondegenerate Floquet state. The only nonvanishing dipole expectation value is in field-direction and then reads

$$d(t) = -\langle\Psi(t)|\hat{z}|\Psi(t)\rangle = -\langle\Phi(t)|\hat{z}|\Phi(t)\rangle. \tag{7.208}$$

We define the dipole strength of the harmonic n as

$$|d(n)|^2 = \left|\frac{\omega_1}{2\pi}\int_0^{2\pi/\omega_1} dt\,\exp(-\mathrm{i}n\omega_1 t)\,d(t)\right|^2 = \left|\langle\langle\Phi|\exp(-\mathrm{i}n\omega_1 t)\,\hat{z}|\Phi\rangle\rangle\right|^2, \tag{7.209}$$

which is proportional to the absolute square of the Fourier-transformed dipole. The squared, extended Hilbert space matrix element on the right-hand side of (7.209)

may be also interpreted as the probability for a transition from a Floquet state to itself, generated by the operator $\exp(-\mathrm{i}n\omega_1 t)\,\hat{z}$, accompanied by the emission of radiation of frequency $n\omega_1$.

The Floquet–Hamiltonian $\hat{\mathcal{H}}(t)$ is invariant under space inversion plus a translation in time by π/ω_1,

$$\hat{P}_{\mathrm{inv}} = (\boldsymbol{r} \to -\boldsymbol{r}, t \to t + \pi/\omega_1) \tag{7.210}$$

so that $\hat{P}_{\mathrm{inv}}|\Phi\rangle = \sigma|\Phi\rangle$, and σ is a phase, i.e, $|\sigma|^2 = 1$. Inserting the unity $\hat{P}_{\mathrm{inv}}^{-1}\hat{P}_{\mathrm{inv}}$ in the matrix element in (7.209) twice yields

$$\langle\langle\Phi|\exp(-\mathrm{i}n\omega_1 t)\,\hat{z}|\Phi\rangle\rangle = \underbrace{\langle\langle\Phi|\hat{P}_{\mathrm{inv}}^{-1}}_{\langle\langle\Phi|\sigma^*}\hat{P}_{\mathrm{inv}}\exp(-\mathrm{i}n\omega_1 t)\,\hat{z}\hat{P}_{\mathrm{inv}}^{-1}\underbrace{\hat{P}_{\mathrm{inv}}|\Phi\rangle\rangle}_{\sigma|\Phi\rangle\rangle}$$
$$= \langle\langle\Phi|\hat{P}_{\mathrm{inv}}\exp(-\mathrm{i}n\omega_1 t)\,\hat{z}\hat{P}_{\mathrm{inv}}^{-1}|\Phi\rangle\rangle = -\exp(-\mathrm{i}n\pi)\,\langle\langle\Phi|\exp(-\mathrm{i}n\omega_1 t)\,\hat{z}|\Phi\rangle\rangle.$$

It follows that n must be odd in order to fulfill

$$-\exp(-\mathrm{i}n\pi) = 1. \tag{7.211}$$

Hence, only odd harmonics are emitted in the case of linearly polarized laser pulses impinging on spherically symmetric systems such as atoms.

In the case of monochromatic circularly polarized laser light (with the electric field vector in the xy-plane) the Floquet–Hamiltonian may be written (using the cylindrical coordinates ρ and φ) as

$$\hat{\mathcal{H}}(t) = \hat{H}_{\mathrm{kin}} + \hat{V}(\hat{\boldsymbol{r}}) + \frac{E}{\sqrt{2}}\rho\cos(\varphi - \omega_1 t) - \mathrm{i}\frac{d}{dt}. \tag{7.212}$$

This expression is invariant under the continuous symmetry operation

$$\hat{P}_{\mathrm{rot}} = (\varphi \to \varphi + \theta, t \to t - \theta/\omega_1) \tag{7.213}$$

with θ an arbitrary real number. We thus have

$$\langle\langle\Phi|\exp(-\mathrm{i}n\omega_1 t)\,\rho\exp(\mp\mathrm{i}\varphi)|\Phi\rangle\rangle$$
$$= \exp(\mathrm{i}n\theta \mp \mathrm{i}\theta)\,\langle\langle\Phi|\exp(-\mathrm{i}n\omega_1 t)\,\rho\exp(\mp\mathrm{i}\varphi)|\Phi\rangle\rangle$$

where $\rho\exp(\mp\mathrm{i}\varphi)$ is the dipole operator for circularly polarized light (with the same helicity $(-)$ and the opposite helicity $(+)$ as the incident pulse, respectively). Hence, for all θ

$$\exp[\mathrm{i}\theta(n \mp 1)] = 1 \tag{7.214}$$

must hold, which cannot be fulfilled for any $n > 1$ so that no harmonics are emitted. However, circularly polarized harmonics may be emitted if bichromatic incident laser light is used [107–109]. With the two lasers polarized in opposite directions and frequencies ω_1 and $m\omega_1$, respectively, the interaction Hamiltonian reads

$$\hat{W}(t) = \frac{E_1}{\sqrt{2}}\rho\cos(\varphi - \omega_1 t) + \frac{E_2}{\sqrt{2}}\rho\cos(\varphi + m\omega_1 t). \tag{7.215}$$

E_1 and E_2 are the electric field amplitudes of the first and second laser, respectively. The symmetry operation under which the Floquet–Hamiltonian is invariant now reads

$$\hat{P}_{\mathrm{rot}}^{(m+1)} = \left(\varphi \to \varphi + \frac{2\pi}{m+1},\ t \to t - \frac{2\pi}{\omega_1(m+1)}\right). \tag{7.216}$$

In the same manner as in the two previous examples one arrives at the condition

$$1 = \exp\left(\mathrm{i}2\pi\frac{n \mp 1}{m+1}\right). \tag{7.217}$$

Hence, harmonics of order

$$n = k(m+1) \pm 1, \qquad k = 1, 2, 3, \ldots \tag{7.218}$$

are expected. The harmonics with $n = k(m+1) + 1$ have the same polarization as the incident laser, whereas those with $n = k(m+1) - 1$ are oppositely polarized. With increasing m more and more low order harmonics are suppressed.

The same selection rule (7.218) is obtained for a target having an M-fold discrete rotational symmetry axis parallel to the laser propagation direction [110]. An example for such a target is the benzene molecule with $M = 6$. The Floquet-Hamiltonian in this case may be written as

$$\hat{\mathcal{H}}(t) = \hat{H}_{\mathrm{kin}} + \hat{V}(\rho, \varphi, z) + \frac{E}{\sqrt{2}}\rho\cos(\varphi - \omega_1 t) - \mathrm{i}\frac{d}{dt}. \tag{7.219}$$

Owing to the discrete rotational symmetry C_M of $\hat{V}(\rho, \varphi, z)$ the symmetry operation of interest now is

$$\hat{P}_{\mathrm{rot}}^{(M)} = \left(\varphi \to \varphi + \frac{2\pi}{M},\ t \to t - \frac{2\pi}{\omega_1 M}\right), \tag{7.220}$$

from which the selection rule

$$n = kM \pm 1, \qquad k = 1, 2, 3, \ldots \tag{7.221}$$

follows, which is indeed of the same form as in the bichromatic, atomic case (7.218). Note that (7.219) is only a single active electron-Hamiltonian but sufficient for the purposes here because the electron-electron interaction term is invariant under the operation (7.220) anyway.

For deducing these selection rules one assumes that the incident laser pulse is infinitely long. This is required for (7.204) to be true. In finite laser pulses the simple selection rules above may be violated and one has to consider not only a single Floquet states but superpositions of them [111, 112].

7.4 Strong Laser–Atom Interaction Beyond the Single Active Electron

Since the early eighties sufficiently intense lasers were available to produce noncollisional multiple ionization of atoms [113]. A sequential viewpoint where at a certain intensity of the laser pulse envelope the currently outermost electron is released, leaving the remaining core essentially in the ground state, was successful in explaining most of the experimentally observed results [17]. Signatures of double-electron excitation were observed but simultaneous two-electron ejection was not detected. The situation changed when in 1992 Fittinghoff et al. [114] observed nonsequential double-ionization (NSDI) of helium at 614 nm in 120 fs laser pulses. This phenomenon will be discussed in more detail in Sect. 7.4.1.

The theoretical treatment of correlated multi-electron systems is a formidable task already in the stationary case. The direct solution of the Schrödinger equation is prohibitive because of the so-called "exponential wall" [115]: the dimension of the configuration space scales with the number of particles N so that the computational cost of the representation of the N-body wave function scales exponentially. Matters get worse for nonperturbative, time-dependent problems where the wave function must be propagated in time. In full dimensionality, the simulation of helium in strong laser fields is currently at the limit of feasibility [116].

A technique which allows to calculate nonperturbatively single (or, recently, also double) ionization but taking into account excitation of the other electrons is the R-matrix Floquet theory [117–119]. This method is a combination of the powerful and in the electron-atom collisions-community well-known R-matrix method [120, 121] and Floquet theory. Alternative methods for the study of ionization in two active electron systems are the complex scaling technique used in [48–50], and the state-specific approach [122, 123]. However, none of these methods so far reproduced, e.g., nonsequential double ionization. On the other hand, low-dimensional model systems [124–133] where the degrees of freedom of the two or more electrons is restricted, are rather inaccurate on a quantitative level but helped to identify, e.g., the nonsequential ionization mechanism and, moreover, serve as important test cases for approximative approaches [61, 124, 127, 128, 134–136].

Methods such as time-dependent Hartree-Fock (TDHF) and simple versions of time-dependent density functional theory (TDDFT) fail miserably in describing

laser-driven correlated electron dynamics [129, 137, 138]. This triggered strong interest in the multi-configurational TDHF (MCTDHF) approach [139–141] and in the improvement of TDDFT [134–136]. MCTDHF becomes exact if a sufficient number of configurations is taken into account but is very demanding computationally. TDDFT, on the other hand, is also – in principle – exact and numerically rather inexpensive as long as "standard" exchange-correlation functionals (such as the local density approximation, for instance) are used as an approximation. However, these standard functionals do not reproduce correlated strong-field phenomena such as NSDI or resonant interactions so that further improvements of the method are required [134–136].

7.4.1 Nonsequential Ionization

As already mentioned in the introduction of this chapter Fittinghoff et al. [114] found a signature of nonsequential ionization (NSDI) in the He ion yields after the interaction with a 614 nm, 120 fs laser pulses. A refined measurement at 780 nm with 160 fs pulses was presented by Walker et al. [142]. The main result is shown in Fig. 7.18. One sees that below $10^{15}\,\mathrm{Wcm}^{-2}$ the measured He^{2+} yield is many orders of magnitude greater than expected from a sequential "single active electron" (SAE) ionization scenario. The latter is sketched by the solid curves in the plot. At around $10^{15}\,\mathrm{Wcm}^{-2}$ the He^{2+} curve changes slope and tends to merge with the theoretical SAE prediction, forming the so-called NSDI "knee". This happens when the previous charge state saturates, indicating that the NSDI emission of the second electron is correlated with the dynamics of the first electron. The experimental ion yields continue to increase even after saturation because of the focal expansion $\sim I^{3/2}$ [143]. Obviously, the increased He^{2+} yield originates from the interaction of the two electrons in the laser field. NSDI was also observed in other rare gases and higher charge states [34, 144, 145], and in In^{+} [146].

Two possible mechanisms responsible for NSDI were suggested. Corkum proposed a rescattering scenario [96] where the electron released first is driven back to the ionic core by the laser and dislodges the second electron by a collision. Fittinghoff et al. [114] suggested a "shake-off" of the second electron due to the sudden loss of screening when the first electron is removed. Another mechanism one may think of is collective tunneling. However, the amplitude for such a process is too low for explaining NSDI [147, 148].

The measurement of strongly driven multi-particle dynamics received a new twist with the invention of the so-called reaction microscope (see Ref. [149] for a review): cold target recoil ion momentum spectroscopy (COLTRIMS) and electron momentum spectroscopy provide correlated momentum spectra containing much more information than just the total ion yields. For recent experiments using the new technique see, e.g., [150–159].

In sequential ionization the momentum distribution of the ion is centered at zero. Note that the ion momentum equals the sum of the electron momenta because the

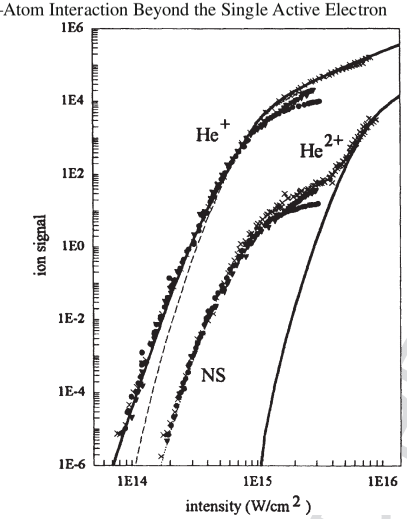

Fig. 7.18 Experimental ion yields for He^+ and He^{2+} after the interaction with a 160 fs 780 nm laser pulse. The solid lines are the theoretically expected yields when a sequential, single active electron ionization scenario is assumed. It is seen that below $10^{15}\,Wcm^{-2}$ the measured He^{2+} yield is many orders of magnitude greater before it merges with the theoretical prediction. The deviation from the sequential rate (*solid curve*) is the so-called nonsequential ionization (NSDI) "knee". From [142]

photon momentum can be neglected for laser wavelengths $\simeq$ 800 nm. In NSDI instead, the momentum distribution shows a clear double-peaked structure, as shown in Fig. 7.19. This is an indication that NSDI is not a pure "shake-off" effect because an isotropic momentum distribution is expected for the second electron in this case. Experimentally obtained differential momentum spectra show that the two electrons escape finally in almost the same direction [152, 153]. This is in contrast to double ionization with energetic photons where the two electrons are emitted "back to back" in opposite directions due to their mutual Coulomb repulsion. At low frequencies the electric field of the laser prevails, thus forcing the electrons to move in the same direction.

Theoretically, NSDI was successfully analyzed by solving the TDSE of low-dimensional two-electron model atoms [128–130, 133], by classical simulations [160–163], and simplified quantum models based on distinguishable electrons (i.e., an "inner" and an "outer" one) [164–166]. As in the case of high-order ATI and HOHG, the SFA treatment gives the deepest physical insight into the NSDI process, especially when interpreted in terms of quantum trajectories. The standard, single active electron SFA needs to be extended in order to allow for (laser field-dressed) collisional ionization by the rescattered electron [6, 157, 167–180]. Starting point is the still exact expression for the transition matrix element (7.129), but now formu-

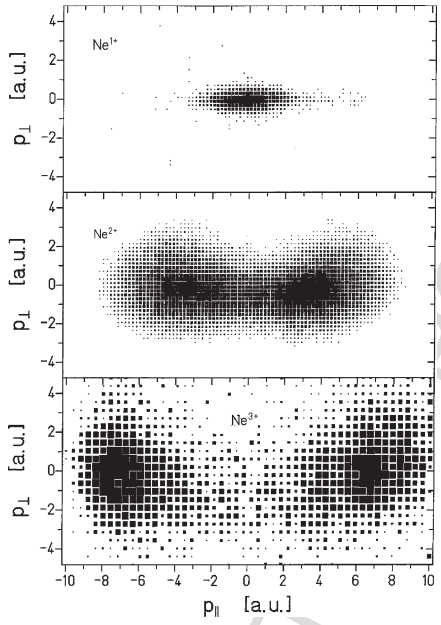

Fig. 7.19 Momentum distributions of Ne^{n+} ions at $1.3\,PWcm^{-2}$ (Ne^+, Ne^{2+}) and $1.5\,PWcm^{-2}$ (Ne^{3+}) after a 30 fs 795 nm laser pulse obtained with the COLTRIMS method. $p_\parallel$ is the momentum parallel to the laser polarization, $p_\perp$ perpendicular to it. The distribution for Ne^{2+} and Ne^{3+} shows a minimum at $p_\parallel$, indicating that NSDI is not a (pure) shake-off effect but relies on Coulomb interaction of the electrons. From [150]

lated for two electrons. In terms of Feynman diagrams, this matrix element contains all graphs with arbitrary large numbers of vertices. Without having a physical picture of the NSDI process in mind it is hard to extract the leading diagram describing the NSDI process. However, if rescattering of one of the electrons is crucial for NSDI, it is clear that the NSDI process is contained in the second term of (7.129). We assume that initial and final state correlations are unimportant. Moreover, we approximate the final states by plane waves, so that the matrix element of interest reads

$$M_{\boldsymbol{p}_1\boldsymbol{p}_2} = -\int_{t_i}^{t} dt' \int_{t_i}^{t'} dt'' \langle \boldsymbol{p}_1 + \boldsymbol{A}(t')|\langle \boldsymbol{p}_2 + \boldsymbol{A}(t')|\hat{V}\hat{U}(t', t'')\hat{W}(t'') \times |\Psi_{01}\rangle|\Psi_{02}\rangle \exp\left(-\mathrm{i}(\mathcal{E}_{01} + \mathcal{E}_{02})t'' - \mathrm{i}\sum_{i=1}^{2} S_{\boldsymbol{p}_i}(t, t')\right)$$

with $\mathcal{E}_{0i}$ the initial energies of the two electrons $i = 1, 2$. Here, we suppress an explicit antisymmetrization of the initial and final two-electron states as the tran-

sition matrix element with proper symmetry can easily be constructed a posteriori. The NSDI matrix element is obtained by selecting only a particular of the very many processes implicitly contained in the sequence of operators $\hat{V}\hat{U}(t',t'')\hat{W}(t'')$, namely $\hat{V}_{12}\{[\hat{U}_1^{(\mathrm{V})}(t',t'')\hat{W}_1(t'')]\otimes\hat{U}_{02}(t',t'')\}$. Here, $\hat{U}_{02}$ is the field-free time evolution operator $\hat{U}_0$ acting on electron 2, $\hat{U}_1^{(\mathrm{V})}$, $\hat{W}_1(t'')$ act on electron 1, and $\hat{V}_{12}$ governs the interaction between the two electrons (i.e., the collision). In length gauge we obtain

$$M^{\mathrm{NSDI}}_{\boldsymbol{p}_1\boldsymbol{p}_2} = -\int_{t_\mathrm{i}}^{t}dt'\int_{t_\mathrm{i}}^{t'}dt''\,\langle\boldsymbol{p}_1+\boldsymbol{A}(t')|\langle\boldsymbol{p}_2+\boldsymbol{A}(t')|\hat{V}_{12}\hat{U}_1^{(\mathrm{V})}(t',t'')\hat{W}_1(t'') \times|\Psi_{01}\rangle|\Psi_{02}\rangle\exp\left(-\mathrm{i}\mathcal{E}_{01}t''-\mathrm{i}\mathcal{E}_{02}t'-\mathrm{i}\sum_{i=1}^{2}S_{\boldsymbol{p}_i}(t,t')\right).$$

The interpretation is that at time t'' electron 1 is ionized by the field ($\hat{W}_1(t'')$) and propagates thereafter in the vacuum until time t' ($\hat{U}_1^{(\mathrm{V})}(t',t)$). Electron 2 meanwhile remains in its bound state ($\hat{U}_{02}(t',t'')$, which simply becomes $\exp[-\mathrm{i}\mathcal{E}_{02}(t'-t'')]$ when applied to $|\Psi_{02}\rangle$). At time t' the first electron returns to its parent ion and interacts via $\hat{V}_{12}$ with the second electron. The latter may be dislodged due to this interaction. NSDI thus may be viewed as laser-driven collisional ionization. In reality, the second electron may be excited instead of immediately ejected. It then may be freed later by the laser pulse, leading also to double ionization. This process was coined RESI (recollision-induced excitation followed by subsequent field ionization) [156]. Whether NSDI or RESI are dominant in an actual experiment is target-dependent and can be distinguished because both processes lead to different momentum spectra, as will become clear below. The SFA devised here does not include excited states so that RESI is not covered. Using (7.130) in length gauge for $\hat{U}_1^{(\mathrm{V})}(t',t'')$ yields

$$M^{\mathrm{NSDI}}_{\boldsymbol{p}_1\boldsymbol{p}_2} = -\int_{t_\mathrm{i}}^{t}dt'\int_{t_\mathrm{i}}^{t'}dt''\int d^3k_1\,\langle\boldsymbol{p}_1+\boldsymbol{A}(t')|\langle\boldsymbol{p}_2+\boldsymbol{A}(t')|\hat{V}_{12}|\boldsymbol{k}_1+\boldsymbol{A}(t')\rangle \times\langle\boldsymbol{k}_1+\boldsymbol{A}(t'')|\boldsymbol{r}_1\cdot\boldsymbol{E}(t'')|\Psi_{01}\rangle|\Psi_{02}\rangle \times\exp\left(-\mathrm{i}\mathcal{E}_{01}t''-\mathrm{i}\mathcal{E}_{02}t'-\mathrm{i}S_{\boldsymbol{k}_1}(t',t'')-\mathrm{i}\sum_{i=1}^{2}S_{\boldsymbol{p}_i}(t,t')\right).$$

Introducing the form factor

$$V_{\boldsymbol{p}_i\boldsymbol{k}_1}(t') = \langle\boldsymbol{p}_1+\boldsymbol{A}(t')|\langle\boldsymbol{p}_2+\boldsymbol{A}(t')|\hat{V}_{12}|\boldsymbol{k}_1+\boldsymbol{A}(t')\rangle|\Psi_{02}\rangle, \tag{7.222}$$

the matrix element

$$W_{\boldsymbol{k}_1}(t'') = \langle\boldsymbol{k}_1+\boldsymbol{A}(t'')|\boldsymbol{r}_1\cdot\boldsymbol{E}(t'')|\Psi_{01}\rangle, \tag{7.223}$$

and the total action

$$S_{\boldsymbol{p}_i\boldsymbol{k}_1}(t,t',t'') = \mathcal{E}_{01}t''+\mathcal{E}_{02}t'+S_{\boldsymbol{k}_1}(t',t'')+\sum_{i=1}^{2}S_{\boldsymbol{p}_i}(t,t') \tag{7.224}$$

the NSDI matrix element reads

$$M^{\mathrm{NSDI}}_{\boldsymbol{p}_1\boldsymbol{p}_2} = -\int_{t_\mathrm{i}}^{t}dt'\int_{t_\mathrm{i}}^{t'}dt''\int d^3k_1\,V_{\boldsymbol{p}_i\boldsymbol{k}_1}(t')W_{\boldsymbol{k}_1}(t'')\exp[-\mathrm{i}S_{\boldsymbol{p}_i\boldsymbol{k}_1}(t,t',t'')]. \tag{7.225}$$

Upon integration by parts and neglecting boundary terms (cf. [71]) one obtains the matrix element

$$M^{\mathrm{NSDI}'}_{\boldsymbol{p}_1\boldsymbol{p}_2} = -\int_{t_\mathrm{i}}^{t}dt'\int_{t_\mathrm{i}}^{t'}dt''\int d^3k_1\,V_{\boldsymbol{p}_i\boldsymbol{k}_1}(t')V_{\boldsymbol{k}_1}(t'')\exp[-\mathrm{i}S_{\boldsymbol{p}_i\boldsymbol{k}_1}(t,t',t'')] \tag{7.226}$$

is obtained, where

$$V_{\boldsymbol{k}_1}(t'') = \langle\boldsymbol{k}_1+\boldsymbol{A}(t'')|\hat{V}_1|\Psi_{01}\rangle. \tag{7.227}$$

The matrix element (7.226) is widely used in the literature (see, e.g., [179]). Assuming a monochromatic laser field and a contact-type interaction $\hat{V}_{12}\sim\delta(\boldsymbol{r}_1-\boldsymbol{r}_2)\delta(\boldsymbol{r}_2)$, all of the integrals in (7.226) apart from a single, remaining time integral can be solved. For few-cycle pulses the two time integrals remain to be evaluated numerically. This is nontrivial because of the highly oscillatory nature of the integrand. Alternatively, the saddle-point method (or refined versions of it) may be applied (see, e.g., [179]). Figure 7.20 shows results for correlated momentum spectra

$$P(p_{1\parallel},p_{2\parallel}) = \int d^2p_{1\perp}\int d^2p_{2\perp}\left|M^{\mathrm{NSDI}'}_{\boldsymbol{p}_1\boldsymbol{p}_2}\right|^2, \tag{7.228}$$

calculated for neon in a 4-cycle, linearly polarized laser pulse of the form $\boldsymbol{A}(t)=A_0\boldsymbol{e}_z\exp[-4(\omega t-\pi n)^2/(\pi n)^2]\sin[\omega t+\phi]$. The actual values of all the parameters are given in the figure caption. The momenta $p_{i\parallel}$ and $\boldsymbol{p}_{i\perp}$ are parallel and perpendicular to the laser polarization direction, respectively. The typical diagonal "double blob" structure in the $p_{1\parallel}$, $p_{2\parallel}$-plane is observed, indicating that the electrons are preferentially emitted in the same direction. In the case of phase-stabilized few-cycle laser pulses, the structure sensitively depends on the carrier-envelope phase ϕ, as was also demonstrated experimentally [181]. Integrating $P(p_{1\parallel},p_{2\parallel})$ for fixed sum momenta $p_\parallel=p_{1\parallel}+p_{2\parallel}$) (i.e., perpendicular to the diagonal $p_{1\parallel}=p_{2\parallel}$ in the plots in Fig. 7.20) a double-hump structure is obtained in the NSDI regime. In the case of few-cycle pulses the weights of the two humps depend sensitively on the carrier-envelope or absolute phase ϕ. Because of momentum conservation the double-hump in the electron sum momenta is reflected in the measured ion recoil

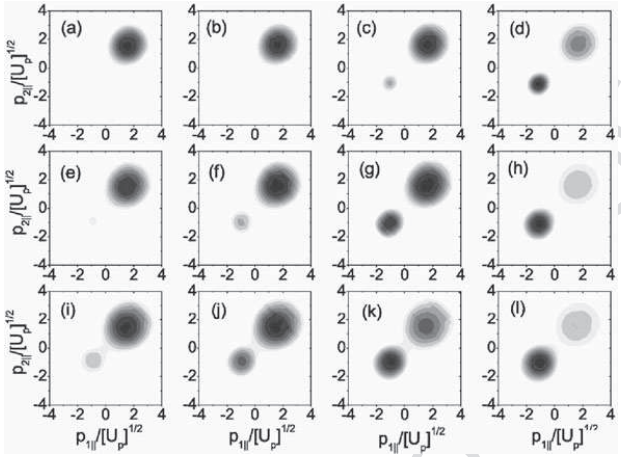

Fig. 7.20 Differential electron momentum distributions computed for neon ($\mathcal{E}_{01} = -0.79$ and $\mathcal{E}_{02} = -1.51$ a.u.) subject to a four-cycle pulse of frequency $\omega = 0.057$ (Ti:Sapphire, $\lambda \simeq 800$ nm) and various intensities and absolute phases. The upper, middle and lower panels correspond to $I = 4 \cdot 10^{14}\,\mathrm{Wcm}^{-2}(U_\mathrm{p} = 0.879)$, $I = 5.5 \cdot 10^{14}\,\mathrm{Wcm}^{-2}(U_\mathrm{p} = 1.2)$, and $I = 8 \cdot 10^{14}\,\mathrm{Wcm}^{-2}(U_\mathrm{p} = 1.758)$, respectively. The absolute phases are given as follows: Panels (a), (e), and (i): $\phi = 0.8\pi$; panels (b), (f), and (j): $\phi = 0.9\pi$; panels (c), (g), and (k): $\phi = \pi$; and panels (d), (h), and (l): $\phi = 1.1\pi$. Taken from [179]

momentum spectra (the momentum of the near infrared photons involved can be neglected).

As already demonstrated for ATI and HOHG, cut-offs in intense laser-atom interaction can always be explained by means of classical electron trajectories. The same holds true for the maximum electron sum momentum in NSDI. The link between classical trajectories and the SFA is formally established by the stationary phase approach already used in (7.160) and (7.195). To that end we seek those values of $\boldsymbol{k} = \boldsymbol{k}_1, t'$, and t'' such that $S = S_{\boldsymbol{p}_i \boldsymbol{k}}(t, t', t'')$ is stationary. The conditions $\partial_{t'} S = 0$, $\partial_{t''} S = 0$, and $\nabla_{\boldsymbol{k}} S = \boldsymbol{0}$ give

$$\sum_{i=1}^{2} [\boldsymbol{p}_i + \boldsymbol{A}(t')]^2 = 2\mathcal{E}_{02} + [\boldsymbol{k} + \boldsymbol{A}(t')]^2, \tag{7.229}$$

$$\big[\boldsymbol{k} + \boldsymbol{A}(t'')\big]^2 = 2\mathcal{E}_{01}, \tag{7.230}$$

$$\int_{t''}^{t'} dt\, [\boldsymbol{k} + \boldsymbol{A}(t)] = 0, \tag{7.231}$$

respectively. Equations (7.229) and (7.230) ensure energy conservation at the rescattering time t' and the emission time t'' of the first electron. Equation (7.231) restricts

the first electron's intermediate momentum such that rescattering occurs. Since $\mathcal{E}_{01} < 0$, (7.230) has only solutions for complex times t'' ($\boldsymbol{k}$ is kept real). The classical trajectories of simple man's theory are obtained for vanishing $\mathcal{E}_{01}$. Equation (7.230) then implies $\boldsymbol{k} = -\boldsymbol{A}(t'')$. Together with (7.231) we have

$$-\boldsymbol{A}(t'')(t' - t'') + \boldsymbol{\alpha}(t') - \boldsymbol{\alpha}(t'') = 0.$$

Comparison with (7.170) shows that this expression is indeed equivalent to $\boldsymbol{r}_1(t') = 0$ when electron 1 was emitted at time t''. If the second electron is dislodged with vanishing initial momentum at a time t' when the electric field of the laser vanishes, its kinetic energy will assume the maximum value $2U_\mathrm{p}$ so that $|p_{2\|}| = 2\sqrt{U_\mathrm{p}}$ is expected. This crude estimate is well confirmed by virtue of Fig. 7.20. If n electrons are involved in the multiple ionization process and all acquire this maximum momentum (in the same direction), the ultimate classical cut-off for the ion recoil momentum is $2n\sqrt{U_\mathrm{p}}$. Recoil ion spectra of neon confirm this estimate [156]. However, if the returning electron is likely to excite but not to directly free the second electron (i.e., the above mentioned RESI occurs), the delayed ionization occurs at high electric field values so that the drift momentum of the second electron will be much lower than $2\sqrt{U_\mathrm{p}}$. Whether collisional ionization or collisional excitation prevails strongly depends on the target.

References

1. Burnett, K., Reed, V.C., Knight, P.L.: J. Phys. B: At. Mol. Opt. Phys. **26**, 561 (1993)
2. Protopapas, M., Keitel, C.H., Knight, P.L.: Rep. Prog. Phys. **60**, 389 (1997)
3. Joachain, C.J., Dörr, M., Kylstra, N.J.: Adv. At. Mol. Opt. Phys. **42**, 225 (2000)
4. Brabec, Th. (ed.): Strong Field Laser Physics. Springer, New York (2008)
5. Popov, V.S.: Physics Uspekhi **47**, 855 (2004)
6. Becker, A., Faisal, F.H.M.: J. Phys. B: At. Mol. Opt. Phys. **38**, R1 (2005)
7. Brabec, T., Krausz, F.: Rev. Mod. Phys. **72**, 545 (2000)
8. Becker, W., et al.: Adv. At. Mol. Opt. Phys. **48**, 35 (2002)
9. Miloşević, D.B., Paulus, G.G., Bauer, D., Becker, W.: J. Phys. B: At. Mol. Opt. Phys. **39**, R203 (2006)
10. Salières, P., L'Huillier, A., Antoine, P., Lewenstein, M.: Adv. At. Mol. Opt. Phys. **4**, 83 (1999)
11. Mihai Gavrila: J. Phys. B: At. Mol. Opt. Phys. **35**, R147 (2002)
12. Becker, A., Dörner, R., Moshammer, R.: J. Phys. B: At. Mol. Opt. Phys. **38**, S753 (2005)
13. Agostini, P., DiMauro, L.F.: Rep. Prog. Phys. **67**, 1563 (2004); corrigendum in **67**, 1563 (2004)
14. Scrinzi, A., Ivanov, M.Yu., Kienberger, R., Villeneuve, D.M.: J. Phys. B: At. Mol. Opt. Phys. **39**, R1 (2006)
15. Krausz, F., Ivanov, M.: Rev. Mod. Phys. **81**, 163 (2009)
16. Paulus, G.G., Bauer, D.: Time in Quantum Mechanics II, Lecture Notes in Physics, p. 303. Springer, Berlin Heidelberg (2010)
17. Lambropoulos, P., Maragakis, P., Zhang, J.: Phys. Rep. **305**, 203 (1998)
18. Chu, S.-I., Telnov, D.A.: Phys. Rep. **390**, 1 (2004)
19. Keitel, C.H.: Contemp. Phys. **42**, 353 (2001)
20. Salamin, Y.I., Hu, S.H., Hatsagortsyan, K.Z., Keitel, C.H.: Phys. Rep. **427**, 41 (2006)
21. Marques, M.A.L., Gross, E.K.U.: Annu. Rev. Phys. Chem. **55**, 427 (2004)

22. Marques, M.A.L., Ullrich, C.A., Nogueira, F., Rubio, A., Burke, K., Gross, E.K.U. (eds.): Time-Dependent Density Functional Theory. Springer, Berlin (2006)
23. Bandrauk, A.D. (ed.): Molecules in Laser Fields. Marcel Dekker, New York (1993)
24. Posthumus, J. (ed.): Molecules and Clusters in Intense Laser Fields. Cambridge University Press, Cambridge (2001)
25. Lein, M.: J. Phys. B: At. Mol. Opt. Phys. **40**, R135 (2007)
26. Saalmann, U., Siedschlag, Ch., Rost, J.M.: J. Phys. B: At. Mol. Opt. Phys. **39**, R39 (2006)
27. Fennel, Th., Meiwes-Broer, K.-H., Tiggesbäumker, J., Reinhard, P.-G., Dinh, P.M., Suraud, E.: preprint arXiv:0904.2706 (to be published in Rev. Mod. Phys.)
28. Landau, L.D., Lifshitz, E.M.: Volume 3 of Course of Theoretical Physics: Quantum Mechanics. Pergamon, Oxford (1965)
29. Friedrich, H.: Theoretical Atomic Physics. Springer, Berlin (1998)
30. Bransden, B.H., Joachain, C.J.: Physics of Atoms and Molecules. Prentice Hall, Harlow (2003)
31. Kustaanheimo, P., Stiefel, E.: J. Reine Angew. Mathematik **218**, 204 (1965)
32. Bauer, D.: Phys. Rev. A **55**, 2180 (1997)
33. Shakeshaft, R., Potvliege, R.M., Dörr, M., Cooke, W.E.: Phys. Rev. A **42**, 1656 (1990)
34. Larochelle, S., Talebpour, A., Chin, S.L.: J. Phys. B **31**, 1201 (1998)
35. Gubbini, E., Eichmann, U., Kalashnikov, M., Sandner, W.: Phys. Rev. Lett. **94**, 053602 (2005)
36. Pitrelli, D., Bauer, D., Macchi, A., Cornolti, F.: J. Phys. B: At. Mol. Opt. Phys. **33**, 829 (2000)
37. Ammosov, M.V., Delone, N.B., Krainov, V.P.: Sov. Phys. JETP **64**, 1191 (1986)
38. Nikishov, A.I., Ritus, V.I.: Zh. Eksp. Teor. Fiz. **50**, 255 (1966) [Sov. Phys. JETP **23**, 162 (1966)]
39. Perelomov, A.M., Popov, V.S., Terent, M.V.'ev: Zh. Eksp. Teor. Fiz. 50 1393; 51 309 (1966) [Sov. Phys. JETP **23**, 924 (1966); 24, 207 (1967)]
40. Perelomov, A.M., Popov, V.S.: ZhÈ ksp. Teor. Fiz. **52**, 514 (1967) [Sov. Phys. JETP **25**, 482 (1967)]
41. Nikishov, A.I., Ritus, V.I.: Zh. Eksp. Teor. Fiz. **52**, 223 (1967) [Sov. Phys. JETP **25**, 145 (1967)
42. Keldysh, L.V.: Eksp. Teor. Fiz. **47**, 1945 (1964) [Sov. Phys. JETP **20**, 1307 (1965)]
43. Taïeb, R., Véniard, V., Maquet, A.: Phys. Rev. Lett. **87**, 053002 (2001)
44. Floquet, G.: Ann. Ecol. Norm. Sup. **12**, 47 (1883)
45. Potvliege, R.M.: Comput. Phys. Comm. **114**, 42 (1998)
46. Scully, M.O., Zubairy, M.S.: Quantum Optics. Cambridge University Press, Cambridge (1997)
47. Siegert, A.J.F.: Phys. Rev. **56**, 750 (1939)
48. Armin Scrinzi and Bernard Piraux: Phys. Rev. A **58**, 1310 (1998)
49. Scrinzi, A., Geissler, M., Brabec, T.: Phys. Rev. Lett. **83**, 706 (1999)
50. Scrinzi, A.: Phys. Rev. A **61**, 041402(R) (2000)
51. Potvliege, R.M., Robin Shakeshaft: Phys. Rev. A **40**, 3061 (1989)
52. Freeman, R.R., Bucksbaum, P.H., Milchberg, H., Darack, S., Schumacher, D., Geusic, M.E.: Phys. Rev. Lett. **59**, 1092 (1987)
53. Pauli, W., Fierz, M.: Nuovo Cimento **15**, 167 (1938)
54. Kramers, H.A.: Collected Scientific Papers. North-Holland, Amsterdam (1956)
55. Henneberger, W.C.: Phys. Rev. Lett. **21**, 538 (1968)
56. Pont, M., Walet, N.R., Gavrila, M., McCurdy, C.W.: Phys. Rev. Lett. **61**, 939 (1988)
57. Bauer, D., Ceccherini, F.: Phys. Rev. A **66**, 053411 (2002)
58. Pont, M., Gavrila, M.: Phys. Rev. Lett. **65**, 2362 (1990)
59. Lambropoulos, P.: Phys. Rev. Lett. **55**, 2141 (1985)
60. de Boer, M.P., Hoogenraad, J.H., Vrijen, R.B., Noordam, L.D., Muller, H.G.: Phys. Rev. Lett. **71**, 3263 (1993)
61. Bauer, D., Ceccherini, F.: Phys. Rev. A **60**, 2301 (1999)
62. Gaier, L.N., Keitel, C.H.: Phys. Rev. A **65**, 023406 (2002)
63. Staudt, A., Keitel, C.H.: Phys. Rev. A **73**, 043412 (2006)

64. Faisal, F.H.M.: J. Phys. B: Atom. Molec. Phys. **6**, L89 (1973)
65. Reiss, H.R.: Phys. Rev. A **22**, 1786 (1980)
66. Faisal, F.H.M.: Theory of Multiphoton Processes. Plenum Press, New York (1987)
67. Fick, E.: Einführung in die Grundlagen der Quantentheorie. Aula-Verlag, Wiesbaden (1988)
68. Göppert-Mayer, M.: Ann. Phys. **9**, 273 (1931)
69. Gordon, W.: Z. Phys. **40**, 117 (1926)
70. Volkov, D.V.: Z. Phys. **94**, 250 (1935)
71. Lohr, A., Kleber, M., Kopold, R., Becker, W.: Phys. Rev. A **55**, R4003 (1997)
72. Bauer, D., Miloşević, D.B., Becker, W.: Phys. Rev. A **72**, 023415 (2005)
73. Becker, W., Chen, J., Chen, S.G., Miloşević, D.B.: Phys. Rev. A **76**, 033403 (2007)
74. Bergues, B., Ansari, Z., Hanstorp, D., Kiyan, I.Yu.: Phys. Rev. A **75**, 063415 (2007); see also Comment by Reiss, H.R.: Phys. Rev. A **77**, 067401 (2008)
75. Paulus, G.G., Grasbon, F., Walther, H. H, Kopold, R., Becker, W.: Phys. Rev. A **64**, 021401 (2001)
76. Kopold, R., Becker, W., Kleber, M., Paulus, G.G.: J. Phys. B: At. Mol. Opt. Phys. **35**, 217 (2002)
77. Agostini, P., Fabre, F., Mainfray, G., Petite, G., Rahman, N.: Phys. Rev. Lett. **42**, 1127 (1979)
78. Freeman, R.R., Bucksbaum, P.H.: J. Phys. B: At. Mol. Opt. Phys. **24**, 325 (1991)
79. Bleistein, N., Handelsmann, R.A.: Asymptotic Expansions of Integrals. Dover Publications, New York (1986)
80. Salières, P., et al.: Science **292**, 902 (2001)
81. Miloşević, D.B., Bauer, D., Becker, W.: J. Mod. Opt. **53**, 125 (2006)
82. Bauer, D., Miloşević, D.B., Becker, W.: J. Mod. Opt. **53**, 135 (2006)
83. Faisal, F.H.M., Schlegel, G.: J. Phys. B **38**, L223 (2005); J. Mod. Opt. **53**, 207 (2006)
84. Smirnova, O., Spanner, M., Ivanov, M.: Phys. Rev. A **77**, 033407 (2008)
85. Arbó, D.G., et al.: Phys. Rev. A **77**, 013401 (2008)
86. Popruzhenko, S.V., Bauer, D.: J. Mod. Opt. **55**, 2573 (2008)
87. Popruzhenko, S.V., Paulus, G.G., Bauer, D.: Phys. Rev. A **77**, 053409 (2008)
88. Blaga, C.I., et al.: Nature Physics **5**, 335 (2009)
89. Lindner, F., et al.: Phys. Rev. Lett. **95**, 040401 (2005)
90. Arbó, D.G., Persson, E., Burgdörfer, J.: Phys. Rev. A **74**, 063407 (2006)
91. Gopal, R., et al.: Phys. Rev. Lett. **103**, 053001 (2009)
92. Sundaram, B., Milonni, P.W.: Phys. Rev. Lett. **41**, 6571 (1990)
93. Di Piazza, A., Fiordilino, E., Mittleman, M.H.: J. Phys. B: At. Mol. Opt. Phys. **34**, 3655 (2001)
94. Krause, J.L., Schafer, K.J., Kulander, K.C.: Phys. Rev. Lett. **68**, 3535 (1992)
95. Kulander, K.C., Schafer, K.J., Krause, J.L.: In: Piraux, B., et al. (eds.) Super-Intense Laser–Atom Physics, NATO ASI series B, vol. 316, p. 95. Plenum Press, New York (1993)
96. Corkum, P.B.: Phys. Rev. Lett. **71**, 1994 (1993)
97. Lewenstein, M., Balcou, Ph., Ivanov, M.Yu., L'Huillier, A., Corkum, P.B.: Phys. Rev. A **49**, 2117 (1994)
98. Spielmann, Ch., et al.: Science **278**, 661 (1997)
99. Chang, Z., Rundquist, A., Wang, H., Murnane, M., Kapteyn, H.: Phys. Rev. Lett. **79**, 2967 (1997)
100. Goulielmakis, E., et al.: Science **305**, 1267 (2004)
101. Drescher, M., et al.: Nature **419**, 803 (2002)
102. Eberly, J.H., Fedorov, M.V.: Phys. Rev. A **45**, 4706 (1992)
103. Knight, P.L., Milonni, P.W.: Phys. Rep. **66**, 21 (1980)
104. Becker, W., Lohr, A., Kleber, M., Lewenstein, M.: Phys. Rev. A. **56**, 645 (1997)
105. Miloşević, D.B., Becker, W.: Phys. Rev. A **66**, 063417 (2002)
106. Sambe, H.: Phys. Rev. A **7**, 2203 (1973)
107. Eichmann, H., Egbert, A., Nolte, S., Momma, C., Wellegehausen, B., Becker, W., Long, S., McIver, J.K.: Phys. Rev. A **51**, R3414 (1995)

108. Becker, W., Chichkov, B.N., Wellegehausen, B.: Phys. Rev. A **60**, 1721 (1999)
109. Milosevic, D.B., Becker, W., Kopold, R.: Phys. Rev. A **61**, 063403 (2000)
110. Averbukh, V., Alon, O.E., Moiseyev, N.: Phys. Rev. A **60**, 2585 (1999)
111. Ceccherini, F., Bauer, D.: Phys. Rev. A **64**, 033423 (2001)
112. Ceccherini, F., Bauer, D., Cornolti, F.: J. Phys. B: At. Mol. Opt. Phys. **34**, 5017 (2001)
113. Luk, T.S., Pummer, H., Boyer, K., Shakidi, M., Egger, H., Rhodes, C.K.: Phys. Rev. Lett. **51**, 110 (1983)
114. Fittinghoff, D.N., Bolton, P.R., Chang, B., Kulander, K.C.: Phys. Rev. Lett. **69**, 2642 (1992)
115. Kohn, W.: Rev. Mod. Phys. **71**, 1253 (1999)
116. Smyth, E.S., Parker, J.S., Taylor, K.T.: Comput. Phys. Comm. **114**, 1 (1998)
117. Burke, P.G., Francken, P., Joachain, C.J.: Europhys. Lett. **13**, 617 (1990)
118. Burke, P.G., Francken, P., Joachain, C.J.: J. Phys. B: At. Mol. Opt. Phys. **24**, 761 (1991)
119. Feng, L., van der Hart, H.W.: J. Phys. B: At. Mol. Opt. Phys. **36**, L1 (2003)
120. Wigner, E.P.: Phys. Rev. **70**, 15 (1946)
121. Burke, P.G., Robb, W.D.: Adv. At. Mol. Opt. Phys. **11**, 143 (1975)
122. Themelis, S.I., Mercouris, T., Nicolaides, C.A.: Phys. Rev. A **61**, 024101 (2000)
123. Mercouris, T., Themelis, S.I., Nicolaides, C.A.: Phys. Rev. A **61**, 013407 (2000)
124. Pindzola, M.S., Griffin, D.C., Bottcher, C.: Phys. Rev. Lett. **66**, 2305 (1991)
125. Grobe, R., Eberly, J.H.: Phys. Rev. Lett. **68**(2), 905 (1992)
126. Haan, S.L., Grobe, R., Eberly, J.H.: Phys. Rev. A **50**, 378 (1994)
127. Pindzola, M.S., Robicheaux, F., Gavras, P.: Phys. Rev. A **55**, 1307 (1997)
128. Bauer, D.: Phys. Rev. A **56**, 3028 (1997)
129. Lappas, D.G., van Leeuwen, R.: J. Phys. B: At. Mol. Opt. Phys. **31**, L249 (1998)
130. Lein, M., Gross, E.K.U., Engel, V.: Phys. Rev. Lett. **85**, 4707 (2000)
131. Roso, L., et al.: Laser Phys. **15**, 1393 (2005)
132. Ruiz, C., Plaja, L., Roso, L.: Phys. Rev. Lett. **94**, 063002 (2005)
133. Ruiz, C., Plaja, L., Roso, L., Becker, A.: Phys. Rev. Lett. **96**, 053001 (2006)
134. Lein, M., Kümmel, S.: Phys. Rev. Lett. **94**, 143003 (2005)
135. Wilken, F., Bauer, D.: Phys. Rev. Lett. **97**, 203001 (2006)
136. Ruggenthaler, M., Bauer, D.: Phys. Rev. Lett. **102**, 233001 (2009)
137. Petersilka, M., Gross, E.K.U.: Laser Physics **9**, 105 (1999)
138. Bauer, D., Ceccherini, F.: Optics Express **8**, 377 (2001)
139. Zanghellini, J., Kitzler, M., Brabec, T., Scrinzi, A.: J. Phys. B: At. Mol. Opt. Phys. **37**, 763 (2004)
140. Kitzler, M., et al.: Phys. Rev. A **70**, 041401 (2004)
141. Caillat, J., et al.: Phys. Rev. A **71**, 012712 (2005)
142. Walker, B., Sheehy, B., DiMauro, L.F., Agostini, P., Schafer, K.J., Kulander, K.C.: Phys. Rev. Lett. **73**, 1227 (1994)
143. Cervenan, M.R., Isenor, N.R.: Opt. Comm. **13**, 175 (1975)
144. Talebpour, A., Chien, C.-Y., Liang, Y., Larochelle, S., Chin, S.L.: J. Phys. B **30**, 1721 (1997)
145. Maeda, H., Dammasch, M., Eichmann, U.: Phys. Rev. A **62**, 035402 (2000)
146. Maeda, H., Dammasch, M., Eichmann, U.: Phys. Rev. A **63**, 025401 (2001)
147. Zon, B.: J. Exp. Theor. Phys. **89**, 219 (1999)
148. Eichmann, U., Dörr, M., Maeda, H., Becker, W., Sandner, W.: Phys. Rev. Lett. **84**, 3550 (2000)
149. Ullrich, J., et al.: Rep. Prog. Phys. **66**, 1463 (2003)
150. Moshammer, R., et al.: Phys. Rev. Lett. **84**, 447 (2000)
151. Weber, Th., et al.: Phys. Rev. Lett. **84**, 443 (2000)
152. Weber, Th., et al.: Nature **404**, 658 (2000)
153. Dörner, R., Giessen, H., Moshammer, R., Rottke, H.: Phys. Bl. **57**, 49 (2001) (in German)
154. Moshammer, R., et al.: J. Phys. B: At. Mol. Opt. Phys. **36**, L113 (2003)
155. Weckenbrock, M., et al.: Phys. Rev. Lett. **92**, 213002 (2004)
156. Rudenko, A., et al.: Phys. Rev. Lett. **93**, 253001 (2004)
157. Liu, X., et al.: Phys. Rev. Lett. **93**, 263001 (2004)

158. Böttcher, M., et al.: J. Phys. B: At. Mol. Opt. Phys. **38**, L389 (2005)
159. Zrost, K., et al.: J. Phys. B: At. Mol. Opt. Phys. **39**, S371 (2006)
160. Fu, L.-B., Liu, J., Chen, S.-G.: Phys. Rev. A **65**, 021406(R) (2002)
161. Haan, S.L., Wheeler, P.S., Panfili, R., Eberly, J.H.: Phys. Rev. A **66**, 061402(R) (2002)
162. Panfili, R., Haan, S.L., Eberly, J.H.: Phys. Rev. Lett. **89**, 113001 (2002)
163. Ho, P.J., Panfili, R., Haan, S.L., Eberly, J.H.: Phys. Rev. Lett. **94**, 093002 (2005)
164. Watson, J.B., Sanpera, A., Lappas, D.G., Knight, P.L., Burnett, K.: Phys. Rev. Lett. **78**, 1884 (1997)
165. Tolley, A.J.: J. Phys. B: At. Mol. Opt. Phys. **32**, 3449 (1999)
166. Prager, J., Keitel, C.H.: J. Phys. B: At. Mol. Opt. Phys. **35**, L167 (2002)
167. Becker, A., Faisal, F.H.M.: Phys. Rev. A **50**, 3256 (1994)
168. Becker, A., Faisal, F.H.M.: J. Phys. B: At. Mol. Opt. Phys. **29**, L197 (1996)
169. Becker, A., Faisal, F.H.M.: Phys. Rev. Lett. **84**, 3546 (2000)
170. Becker, A., Faisal, F.H.M.: Phys. Rev. Lett. **89**, 193003 (2002)
171. Kopold, R., Becker, W., Rottke, H., Sandner, W.: Phys. Rev. Lett. **85**, 3781 (2000)
172. Heinrich, A., Lewenstein, M., Sanpera, A.: J. Phys. B **37**, 2087 (2004)
173. Goreslavskii, S.P., Popruzhenko, S.V., Kopold, R., Becker, W.: Phys. Rev. A **64**, 053402 (2002)
174. Goreslavskii, S.P., Popruzhenko, S.V., Kopold, R., Becker, W.: Phys. Rev. A **64**, 053402 (2002)
175. Popruzhenko, S.V., Korneev, Ph.A., Goreslavskii, S.P., Becker, W.: Phys. Rev. Lett. **89**, 023001 (2002)
176. Figueira de Morisson Faria, C., Becker, W.: Laser Phys. **13**, 1196 (2003)
177. Figueira de Morisson Faria, C., Liu, X., Becker, W., Schomerus, H.: Phys. Rev. A **69**, 021402(R) (2004)
178. Figueira de Morisson Faria, C., Schomerus, H., Liu, X., Becker, W.: Phys. Rev. A **69**, 043405 (2004)
179. Figueira de Morisson Faria, C., Liu, X., Sanpera, A., Lewenstein, M.: Phys. Rev. A **70**, 043406 (2004)
180. Figueira de Morisson Faria, C., Lewenstein, M.: J. Phys. B: At. Mol. Opt. Phys. **38**, 3251 (2005)
181. Liu, X., Figueira de Morisson Faria, C.: Phys. Rev. Lett. **92**, 133006 (2004)